Advanced Modelling and Control of Wind Power Systems

Adrian Constantin

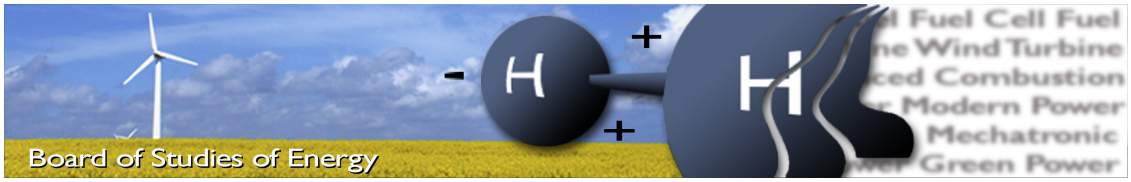

Title:	Advanced Modelling and Control of Wind Power Systems
Semester:	10
Semester theme:	Master Thesis - Control of Wind Power Systems
Project period:	4.02.2009 to 3.06.2009
ECTS:	30
Supervisor:	Florin Iov
Project group:	WPS4 - 1051

Adrian Constantin

Copies:	2
Pages, total:	126
Appendix:	11
Supplements:	

SYNOPSIS:

Nowadays, the Transmission System Operators are dealing with an increasing share of wind power, thus issuing new grid requirements in order to maintain power system stability. The Wind Farms must provide grid support capabilities similar with conventional power plants. The purpose of this project is the implementation of a wind power control system in accordance with the grid regulations in Denmark. Modelling of the wind power system, grid connection techniques and the Wind Farm control architecture have been performed and analyzed. The active and reactive power control functions implemented in the model verify the powerful grid support that a Wind Farm can provide to the stability of the power system. A dynamic RMS simulation platform including a reduced model of a Wind Farm, a VSC-HVDC transmission system and a Wind Farm controller, has been implemented in Power Factory DIgSILENT and is available for future studies.

By signing this document, each member of the group confirms that all participated in the project work and thereby all members are collectively liable for the content of the report.

Preface

The present project entitled "Advanced Modelling and Control of Wind Power Systems" is made by group WPS4-1051 formed by one degree student in the 4th Master semester at the Institute of Energy Technology, Aalborg University, Denmark. The project period is from February 4th until June 3rd 2009. Literature references are mentioned in square brackets by numbers (Vancouver style). The appendices are assigned with letters and are arranged in alphabetical order. Equations are numbered in format (X.Y) and Figures are numbered in format Figure X.Y, where X is the chapter number and Y is the number of the item. The enclosed CD-ROM contains the project report written in Lyx and Adobe PDF format, the documentation from the Internet the developed model as a DIgSILENT dz library type file and several Matlab scripts used throughout the report.

The author would like to thank the supervisor Florin Iov for the support and ideas provided throughout the entire project period.

The report is conducted by:

Adrian Constantin

Contents

Nomenclature

AC Alternating Current

CHP Combined Heat and Power

DC Direct Current

DER Distributed Energy Resources

DFIG Doubly Fed Induction Generator

DSL DIgSILENT Simulation Language

EMT Electromagnetic Transients

FACTS Flexible AC Transmission System

GTO Gate Turn Off transistor

HAWT Horizontal Axis Wind Turbine

HV High Voltage

HVAC High Voltage AC

HVDC High Voltage DC

IEEE Institute of Electrical and Electronics Engineers

IGBT Insulated Gate Bipolar Transistor

P Electrical Active Power

PCC Point of Common Coupling

PI Proportional - Integral

PM Permanent Magnet

PSD Power Spectra Density

PWM Pulse Width Modulation

Q Electrical Reactive Power

RMS Root Mean Square

RMS Root Mean Square

SCIG Squirel Cage Induction Generator

SCIG Squirrel Cage Induction Generator

SCR Short Circuit Ratio

STATCOM Static VAr Compensation - IGBT based

SVC Static VAr Compensation - thyristor based

THD Total Harmonic Distortion

TSOs Transmission System Operator

VPP Virtual Power Plants

VSC Voltage Source Converter

WFs Wind Farm

WPS Wind Power System

WPS Wind Power System

WRIG Wound Rotor Induction Generator

WT Wind Turbine

List of Figures

List of Tables

1. Introduction

This chapter is intended to provide the reader an overview of Wind Power Systems from an electrical engineering perspective. In Section 1.1, the current status of the wind power development is briefly reviewed and introductory information regarding the wind power transmission into the main electrical grid are provided. Section 1.2, presents the state of the art in wind turbine and transmission system technologies. Section 1.3 presents the grid code requirements in Denmark with small comparisons to another grid utility in Germany, E.ON, that is also dealing with a high share of wind power in the total spectrum of power generation. A description of the specific problem being dealt with in this project is described in Section 1.4. Basically, there is an increasingly number of grid support requirements for Wind Power Systems that need to be fulfilled in order to connect larger Wind Farms into the main power grid. Also, the WFs must play an active role in the power system stability issues, being able to provide full grid support. Finally, in Section 1.5, the project objectives and research approach are detailed. A simulation platform for power system stability studies is also proposed containing a large WF and an VSC HVDC transmission system. All the analyzes that are performed in this project are based on the fore mentioned simulation platform.

1.1. Background

The continuous development of the renewables industry in the last decade had its basis on the need of diversifying the energy sources from which electricity is being generated and also on the unique opportunity that renewable energy sources has to offer for sustainability and a healthier climate. The evolution of wind power has taken big steps when considering the total amount of wind power installed worldwide (see Figure 1.1) as well as the Wind Turbine technologies involved.

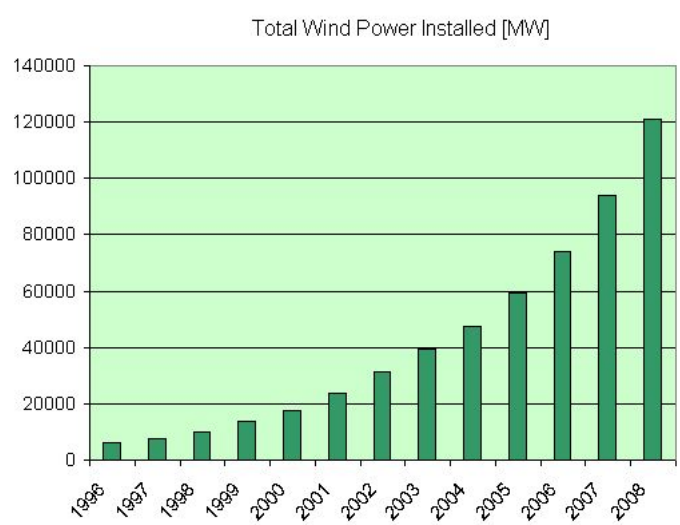

Figure 1.1.: Total installed wind power worldwide[1]

In the past, since the influence of small WTs was insignificant to the national power system, there was no need for special regulations on distributed generation of wind power. The Danish WT concept with the WT's Squirrel Cage Induction Generator connected directly to the grid emerged and proved to be reliable, efficient and economical. Few power regulation functions were available to this WT concept and therefore, almost all WTs were connected to the Distribution System. The grid balance and system stability were entirely the responsibility of large conventional power stations. In 1988, IEEE Standard 1001 - "IEEE Guide for Interfacing Dispersed Storage and Generation Facilities with Electric Utility Systems"[2] was the only guidance for deployment of new renewable energy sources including wind energy conversion systems[3]. As the wind industry increased its share in power generation compared to the conventional plants, it was necessary to control the power output and the power factor in the connection point of the WTs. Nowadays, the connection point of modern large scale WFs is usually located on the transmission level of the power system. Only recently, in 2003's IEEE Standard 1547, advanced guidelines are detailed for wind power system developers to meet grid requirements[8]. Better controllability and reliable operation of these systems are the main issues being dealt with in the latest grid codes issued by the Transmission System Operators that are confronting with high penetration of wind power[4]-[6].

The share of wind energy in the total electrical generation system is approximately 20 per cent in Denmark. For this level of wind energy, the main problems regarding power system stability and further integration of large scale wind power are divided in three groups[9]:

- Global Power System issues: frequency and voltage regulation, stationary and transient stability and low frequency oscillations;
- Regional Transmission System issues: thermal capacity, power losses, installation of new lines;
- Local Transmission Systems events: voltage collapse, flicker and system stability.

The Grid Codes formulated by Energinet.dk [4, 5] are designed to cover the previously mentioned aspects. In Germany, the TSO E.ON Netz requires all generation units to comply with the standard grid code [6] and has already defined specific rules for offshore wind installations[7]. Usually, each grid code specifically requires the WF owner to provide simulation models of the plant in order for the TSO to perform analyses on the impact of the WF on the electrical power grid. It is therefore essential to develop reliable and accurate models of the wind power system and study its impact on the main grid. The TSO's acceptance of the project is depending on the validation of the simulation study with real measurements performed on the system[4, 5].

1.2. State of the Art in Wind Power Systems

Wind power has evolved rapidly in the last two decades with regards to the WT power rating and consequently to the rotor diameter of the WT as it can be seen in Figure 1.2. 3.6 MW and 6 MW prototype WTs are being tested for commercial production[10].

In the past few years a different type of development has taken place: instead of a continuous increase in WT rated power, the wind turbine manufacturers focused on developing WTs that are more reliable, grid code compliant and suitable for different installation environments - onshore and offshore, as it can be seen in the commercial offer of the wind industry, with the main WTs being rated around 2 to 3 MW [58, 59].

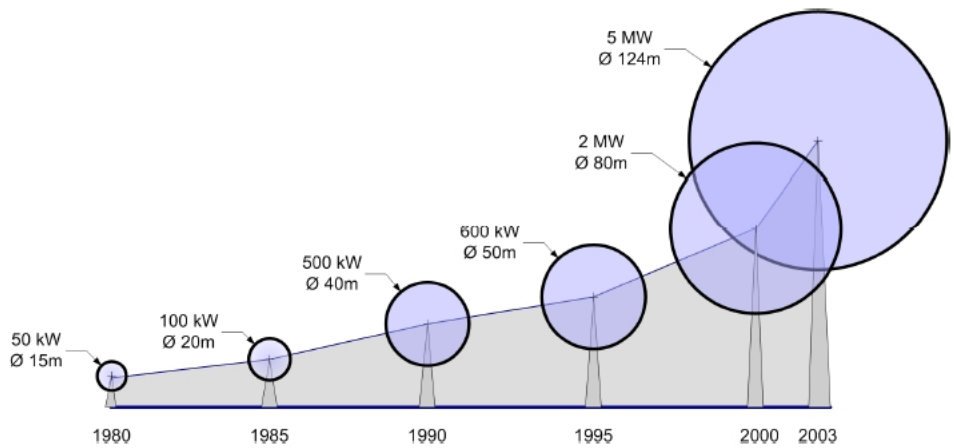

Figure 1.2.: Wind Turbine Rated Power Increase[10]

1.2.1. Wind Turbine Technologies

A number of WT types have proved their reliability along time, therefore, these ones will be further on reviewed. The most commonly known WT design is the HAWT with three blades. The WT concepts are divided according to the speed of the WT's rotor: fixed and variable speed WTs. The following types have been developed[11]:

- Danish WT concept - fixed speed WT;
- Partially variable speed WT with WRIG;
- Variable speed WT with full rating power converter (PM or SCIG);
- Variable speed WT with DFIG.

Currently, the fixed and partially variable speed types are becoming less marketed, while the last two although more expensive, are performing much better in terms of grid support functions, lower mechanical stress on the WT's structure and energy extraction efficiency. In [34] a comparison between the fixed and variable speed types of WTs is made. Ideally, an energy capture gain of 5.2% is obtained in variable speed operation compared to the fixed speed alternative having the same generator type.

From the point of view of WF design, there are several solutions for choosing the WT type. The state of the art is the use of WFs that have turbines with SCIGs - resulting in fixed speed operation of the WF or, WTs with DFIGs that may vary the speed of the WT rotor - therefore obtaining variable speed operation. In all cases a constant grid frequency is present (50 Hz in Europe). The usual grid connection technology adopted in these cases is the HV/MV AC due to the low initial investment costs. Nowadays, the evolution of power electronics and specifically of the HV switching valves with turn off capability (GTOs and IGBTs), made possible another solution: the variable speed operation of the entire WF at variable internal grid frequency. The advantage is that no PWM converter is necessary on each of the WTs in order to obtain variable speed operation, as it is the case in DFIGs. The variable internal grid frequency must be set by the power converter of an VSC HVDC transmission system. Therefore, by implementing an HVDC system, the WTs are operating at a variable frequency different from the one of the grid. An energy yield gain compared to the fixed speed operation tied to the grid frequency can be studied.

1.2.2. Grid Connection Technologies for Wind Farms

The standard approach when connecting WFs consists on using HVAC connections. All WFs built until now are using this grid connection type for several reasons:

- HVAC is a proved and reliable technology;
- currently developed WFs are located close to shore and a PCC to the transmission voltage level of the power grid;
- smaller investment costs compared to the alternative solution - HVDC;
- smaller power losses for small transmission distances.

The HVAC solution performs very well coupled with a very strong power system but has limitations with respect to the transmission distances and the grid support capabilities e.g. full reactive power control, black-start capability. The VSC-HVDC transmission system is one possible solution to fulfill the requirements of TSOs.

In [12], a study on the energy production costs of WFs with different AC and DC layouts is performed. It concludes that for large wind power applications for distances higher than 120 km, the DC connected WFs with an AC internal bus is the best option, while for medium distances between 20 and 120 km either AC WFs or DC connected WFs with series connected WTs are worth taking into consideration.

1.3. Grid Code Requirements of Wind Power Systems

The Danish TSO, Energinet, provides grid code requirements defined specifically for WTs and WFs connected at voltage levels below and above 100 kV. More interest is nowadays being given to the development of large scale wind power plants with power ratings of hundreds of MW. Such WFs are usually connected to the high and extra high voltage levels of the transmission grid. It is therefore the purpose of this project to review the requirements of the grid connection to these voltage levels of the transmission system.

The power grid requirements are generally designed with focus on the “n-1” contingency concept (see Appendix A.1).

1.3.1. Active Power Regulation

In Denmark, with respect to the active power requirements of WFs connected to voltage levels above 100 kV, a number of regulation techniques have been defined in [5], with the following priority order:

- System protection - downward regulation of the power generated by the WF in order to maintain the power system in normal operating conditions;
- Frequency control - when the frequency of the power system modifies, the WF must control actively the power production in order to participate in the frequency stability efforts (see Figure 1.3);

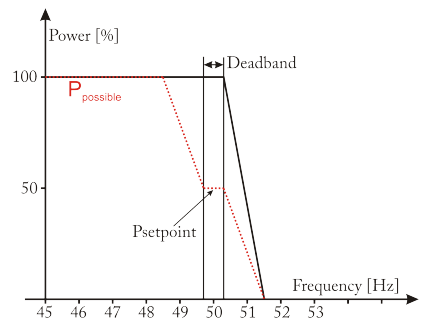

Figure 1.3.: Active power regulation - frequency control

- Stop regulation - in case the wind speed increases, the WF must be able to maintain the current production due to certain production constraints (see Figure 1.4);

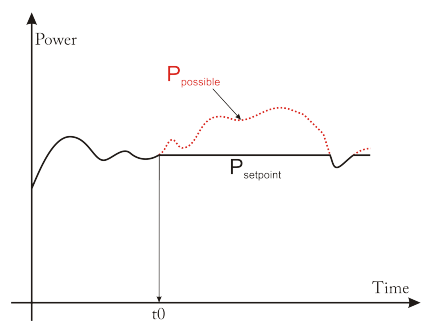

Figure 1.4.: Active power regulation - stop regulation

- Balance regulation - downward and upward regulation correlated with the power balance of the responsible market player (see Figures 1.5 and 1.6);

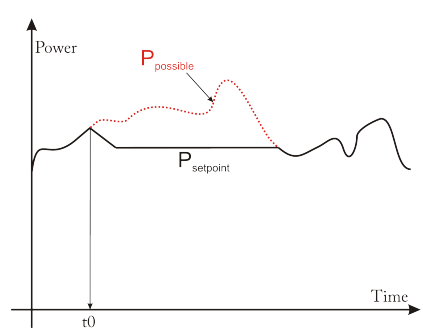

Figure 1.5.: Active power regulation - balance regulation

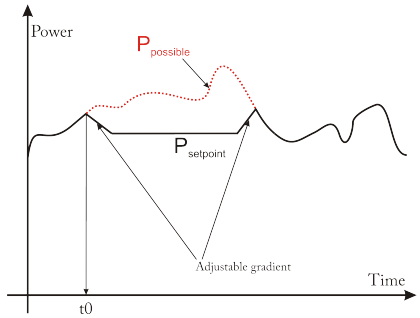

Figure 1.6.: Active power regulation - downward and upward balance

- Power gradient constraint - limitting the maximum speed with which the power output changes due to fast wind speed variations (see Figure 1.7);

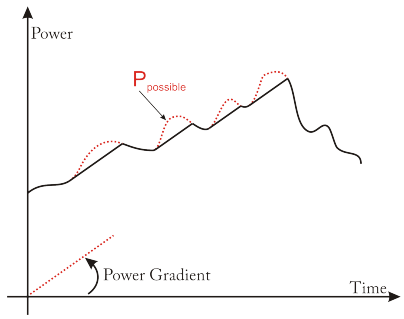

Figure 1.7.: Active power regulation - power gradient constraint

- Absolute production constraint - this control algorithm will limit the power production to a set maximum reference point (see Figure 1.8);

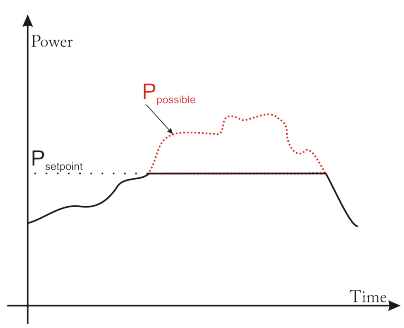

Figure 1.8.: Active power regulation - Absolute production constraint

- Delta production constraint - this control technique ensures that regulating power reserves are allocated, the power production being less than what it could have been possible at present (see Figure 1.9). This is similar with the spinning reserve in large power plants with synchronous machines.

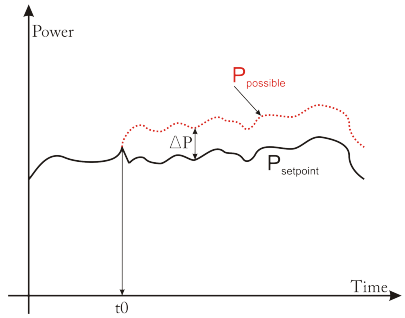

Figure 1.9.: Active power regulation - Delta production constraint

The public utility company in Germany, E.ON requires in the grid code [6], that generating plants with a capacity higher than 100 MW will necessarily provide primary control power.

1.3.2. Reactive Power Regulation

According to the Danish grid code, the WF must be equipped with reactive power compensation devices in such a manner that Q and P of the WF in the PCC will result in operating points always located in the control band interval in Figure 1.10.

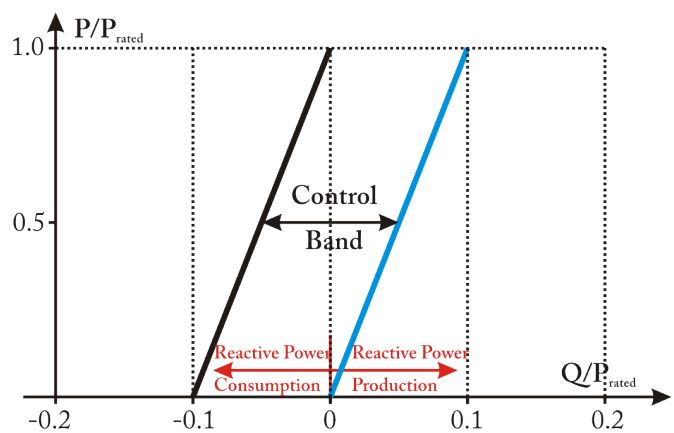

Figure 1.10.: Control band for the reactive power control in the PCC

In the Danish grid code, the plant owner has to provide the P-Q diagram of the WF in the PCC. If the amount of reactive power in the PCC can be controlled in specific intervals then Figure 1.10 may not be taken in consideration and a special agreement of the reactive power exchange will be submitted. Three types of regulation are mentioned in [5]:

- Mvar regulation;
- Voltage regulation;
- Reactive power regulation according to minimum requirements.

E.ON mentions as a standard in [6] only the interval of the power factor $cos(\varphi) = 0.95 \div 1$ located in Quadrant I for the PCC. A P-Q diagram is additionally provided in [7] for offshore wind installations as in Figure 1.11.

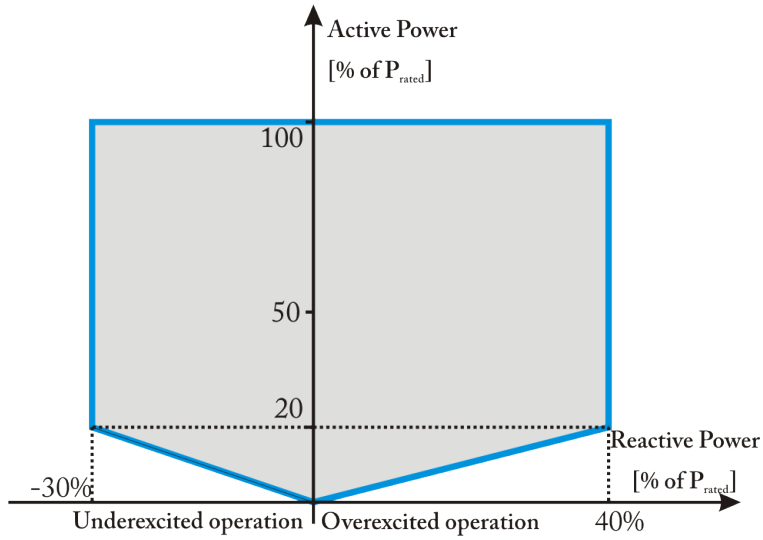

Figure 1.11.: P-Q diagram for offshore WFs in the E.ON grid code

1.3.3. Voltage Quality

Usually, the utility companies are setting requirements for the transmission power system regarding voltage quality aspects that include three main topics [5]:

- voltage fluctuations and flicker;
- harmonic currents; and
- rapid voltage changes or voltage jumps.

The flicker contributions, denoted with P_{st} and P_{lt} in IEC/TR 61000-3-7 must not exceed certain limits:

$$\begin{cases} P_{st} < 0.3 \\ P_{lt} < 0.2 \end{cases} \tag{1.1}$$

The flicker coefficient P_{st} is determined as a weighted average of the flicker contribution calculated on a ten minutes basis, while P_{lt} is calculated on a two hours or bigger time frame.

Rapid voltage changes occur for example due to breaker switching in the wind power system and are corresponding to changes in the RMS value of the voltage. The limits are expressed in per cent of the RMS rated value [5]:

General constraint	<3.0%
Until a frequency of 10 per hour	<2.5%
Until a frequency of 100 per hour	<1.5%

For harmonic disturbances, the indicator D_n related to each individual harmonic is defined in Equation 1.2:

$$D_n = \frac{U_n}{U_l} \times 100\% \tag{1.2}$$

Harmonic effects are commonly measured using the total harmonic effective distortion, defined as in Equation1.3:

$$THD = 100\sqrt{\sum_{n=2}^{50}(\frac{U_n}{U_l})^2}\% \tag{1.3}$$

A main requirement in [5] is that the THD must be smaller than 1.5 %, while in the E.ON network IEC regulations 61000 and standards series DIN EN 61000 are mentioned as a standard.

1.3.4. Operation during Disturbances of Wind Power Systems

In [5] a description of the events for which WFs must remain connected to the grid and not disconnect is enumerated. One Three-phase short circuits below 100ms, cascaded two two-phase short circuits with durations of 100 ms and single-phase short circuit of 100 ms are events that must not trigger the disconnection of the WF. The WTs must be tested for the above kind of faults and if central installations are included in the WF design then a verification of the stability using a simulation model must be carried out for a symmetric three-phase short circuit to the power grid. Asymmetrical faults are to be successfully overridden as well.

WT tests are to be performed using the voltage profile detailed in Figure 1.12. Parameters of interest are mentioned in [5] to be RMS values of current, active and reactive power in the PCC and the voltage variations.

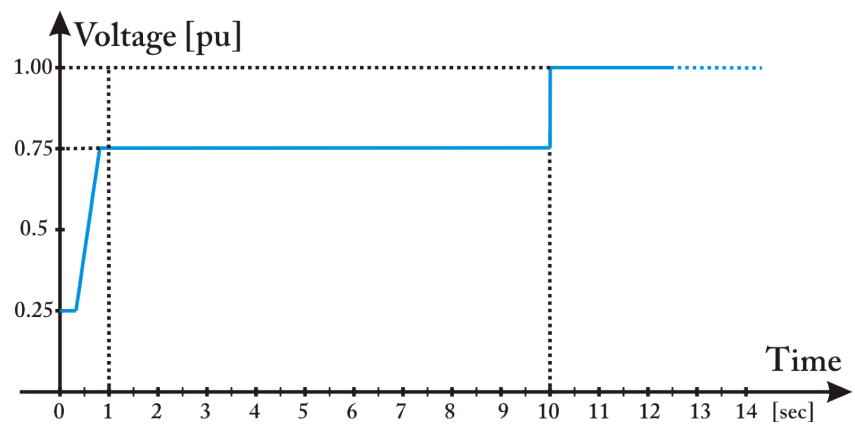

Figure 1.12.: Symmetric three-phase faults - Voltage profile

Certain criteria are also set for the successful operation of the WF and WT during grid faults. Worth mentioning is the requirement for the reactive power regulation system to change from normal to maximum voltage support during the voltage dip.

As a comparison, in the E.ON grid code, two voltage profiles are described depending on the generating station type:

- power station with synchronous generator(s) connected directly to the grid (Type 1);
- all other types of generating power station (Type 2) - the case of WFs.

The voltage profile for three phase faults in the case of Type 2 generating plants have the shape as in Figure 1.13.

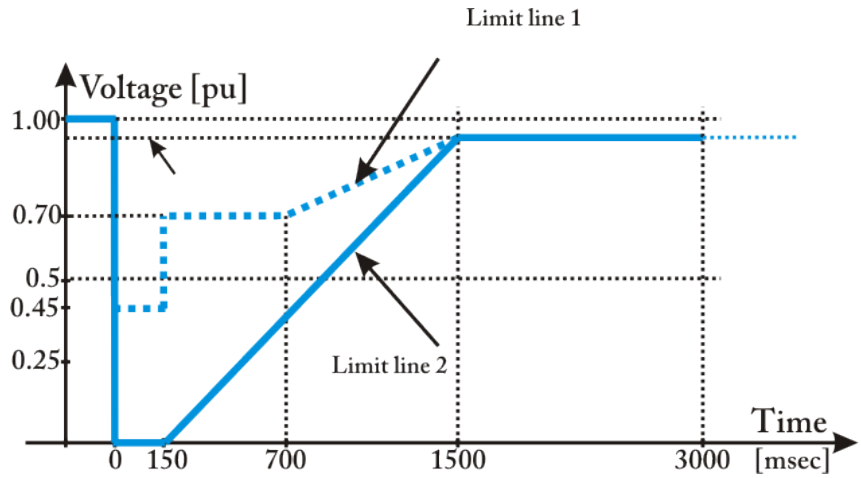

Figure 1.13.: Voltage profile of faults in E.ON grid code for grid connected synchronous generators

As in the Danish grid code, E.ON requires during voltage dips full voltage support of the generating power plant by providing additional reactive current. A distinction is made in the case of offshore wind installations, mentioning that full voltage support is to be triggered in the event of a voltage dip higher than 5% compared to normal generating power plants which are activating the control at 10% or more.

1.3.5. Future Trends

In the past the focus on installing new wind power was on installing individual or several wind turbines, while nowadays, the wind projects are usually oriented on the development of large onshore and offshore wind parks. In the long run, the diversification of energy sources and moreover, the development of dispersed power generation in the main electrical system will continue to have a direct influence over the grid requirements of utility companies.

In order to comply with the grid code, a number of new electrical components have emerged under the generic name of FACTS: VSC-HVDC, SVC, STATCOM.

The current grid codes previously discussed require the concentration of WTs in large WFs that are able to support the power grid and co-operate with the conventional power plants. In [14], this aspect is reiterated with emphasis on the use of power electronics including VSC-HVDC, which, in combination with fixed speed WTs, could provide a solution for cost efficient design and full compliance of the grid code.

Also, the concept of VPP has been recently introduced for describing the aggregation of DER[13]. Integrating VPPs in the Electrical Market and Grid implies that small renewable energy sources will be integrated in larger entities, being thus able to participate actively to the power system stability in the case of high penetration levels.

Also, another future direction is to empower the WFs with islanding operation capabilities, thus keeping the WFs on line even in the case of a power system shutdown. An overview in this direction has been performed in order to analyze to possible implications and advantages that result[16].

1.4. Problem Statement

The grid integration of large wind power systems is one of the main objectives of utility companies. Power system stability depends highly on the behaviour of such large WFs

connected to the Transmission System. Active and reactive power control, fault-ride through capability, power reserve capacity, voltage support during faults are among the features that WFs must provide nowadays, as can be seen in Figure 1.14. The red marked blocks are of particular interest in this project. By using power electronics, the total spectrum of functions of WFs can highly expand: virtual inertia may provide instantaneous power reserve, optimal production control can be used to minimize certain cost functions, and finally, island operation capability combined with black-start support is actively participating to the power system's stability.

Analyzing the advantages and disadvantages of each WF control function implies the development of simulation models of WFs connected to specific power grid structures. Models for wind speed fluctuations, WT mechanical and electrical components, WF grid electrical components, transmission system and main power grid are required. The control system for the WT, WF and transmission system are also necessary. Consequently, it is of great interest the operation of the developed system for certain operation conditions e.g. normal operation, faults in the PCC, etc.

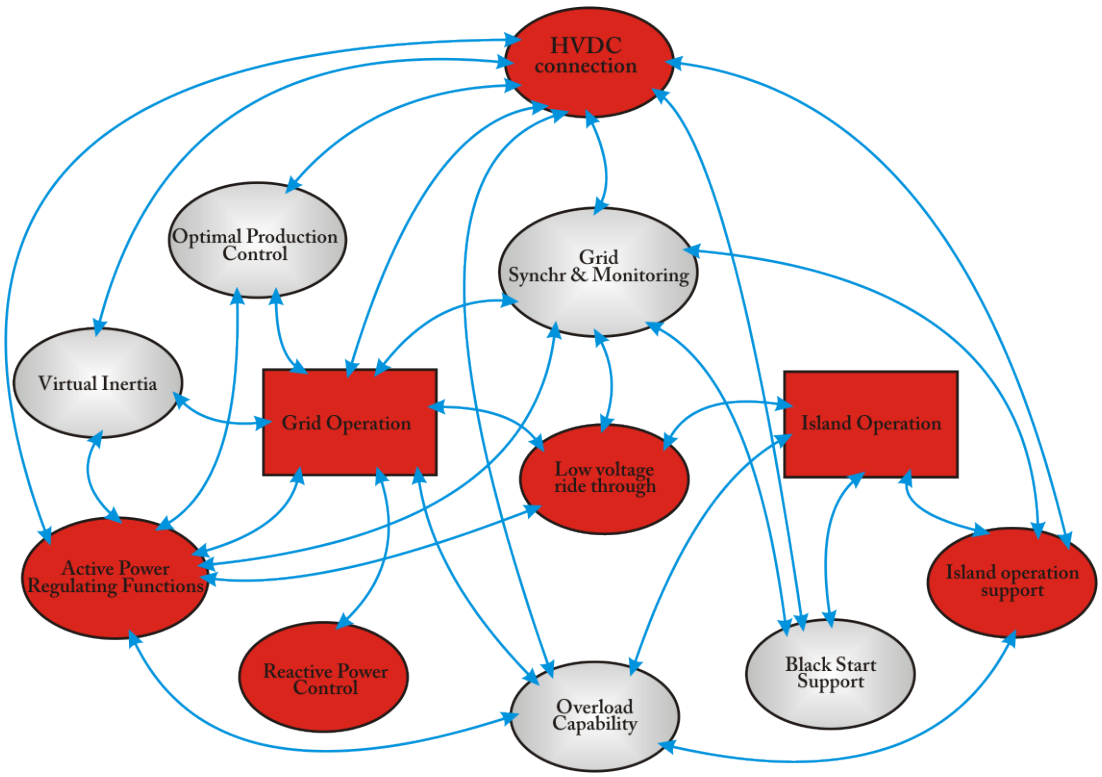

Figure 1.14.: Wind Farm Control Functions[15]

1.5. Project Goals and Research Approach

The main goal of this Master Thesis is study on and comprehension of dynamic modelling and analysis of modern wind power systems. Usually, power system analysis and modelling software is used rather than general purpose modelling applications such as Matlab. The advantage of using a dedicated power system software is that the model developing process is straightforward, allowing the user to focus specifically on the subject of study. Taking advantage of this fact, the modelling and simulation work is done mainly in PowerFactory DIgSILENT, and secondly in Matlab/Simulink.

For the purpose of exemplifying, a relatively large WF connected through an VSC HVDC transmission system to the PCC as it is presented in Figure 1.15 has been considered to study in this project. The simulation platform is intended to apply successfully to other similar configurations as well (number of WT, voltage and power ratings). It contains 30 WTs, each rated at 2.3 MW, therefore, with a WF rated active power of 69 MW. The WTs are pitch-controlled, fixed-speed equipped with induction generators. A power transformer is connected at the terminals of each WT and rises the voltage to medium voltage distribution levels. A collecting grid with a defined length connects to another power transformer and afterwards to the WF side converter. A VSC HVDC sending end station transmits power to the other "receiving end" station which will finally inject the WF power in the PCC of the main power grid. Consider also that the PCC is a HV or extra HV transmission node of the power system. The voltage ratings have been chosen so as to fulfill the DC voltage requirements of the power converter modules, as stated in [35] and typical modulation index values[34].

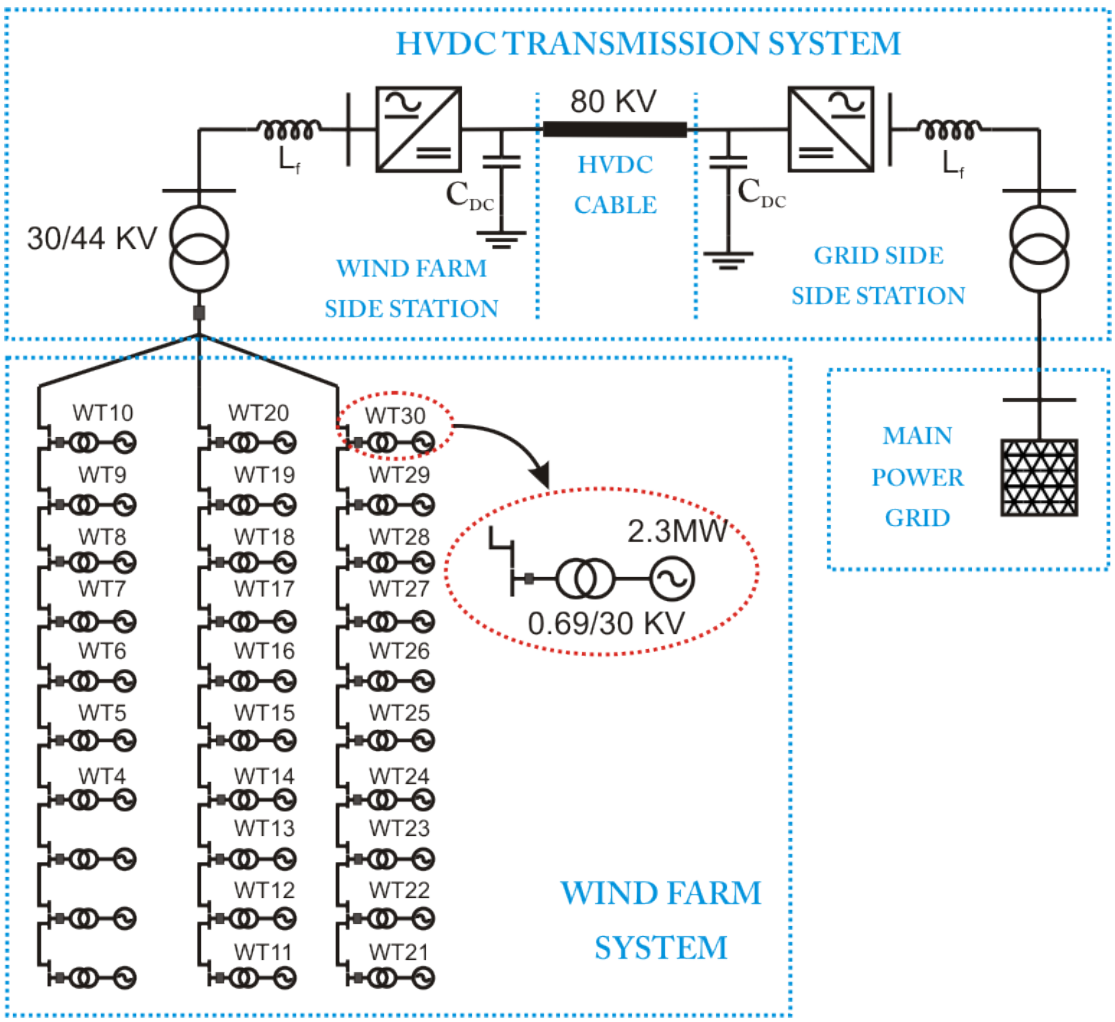

Figure 1.15.: Proposed Wind Power System

The analysis of the proposed WF system represents one method to accomplish the main goal of the thesis. Therefore, this generic study case is intended to provide a simulation platform for power system stability (RMS) analyses with focus on the fulfillment of the grid code requirements.

Within this project, WT and wind speed models developed in [11] will be adapted and further on used throughout the modelling work. In order to model a large scale WF, methods of simplifying the complexity of the system are required. Namely, a reduced model of the WF is implemented, as discussed in Section 2.3.1.

The WF's internal electrical grid and the transmission system connecting the WF to the main power grid require modelling and design efforts. By using Power Factory DIgSILENT, build-in models for PWM converter, grid infrastructure (AC and DC lines, line reactors, AC filters, DC capacitors, power transformers) are directly available. Therefore, in this project, setting of the datasheet parameters, where available, and proper sizing of the build-in models is done.

The decision of using an VSC HVDC transmission system is taken since most of the grid support functions are implemented through the use of such a connection. This HVDC link is coordinated by the overall WF controller. Design of the WF and HVDC control system is taken into consideration. The WF controller contains power (active and reactive) regulation functions which send reference setpoints to the corresponding controllers in the system e.g. pitch controllers, PWM converter control. The HVDC control system is split into the "receiving" and "sending" end station controllers acting on their associated converters.

Developing this simulation platform provides the possibility of analyzing the performance of the system under different operating conditions. Specifically, in this project it is of interest the analysis of the WF's active and reactive power control functions, low voltage ride through capability and island operation of the WF. In Figure 1.14, the red marked function blocks have been studied/developed.

As a conclusion, the scope of the dynamic (stability) simulations for Wind Power Systems is:

- investigation of the grid support functions,
- assessment of power system stability,
- a limited number of scenarios to be studied.

1.6. Report Structure

The report is organized in the following parts:

- Chapter 1 represents an introductory chapter describing the state of the art in wind power systems, the current WT technologies and grid code specifications for WFs in Denmark (Energinet.dk) and Germany(EON.Net). The problem statement, project goals and research approach are detailed.
- Chapter 2 contains most of the project's modelling work. The WT model with its components is presented in Section 2.2. The method for modelling a relatively large WF for grid interaction and cumulative response studies is detailed in Section 2.3.1. The main electrical components (AC and DC) used in the WF, transmission and power grid systems are properly sized for correct operation of the system under study in Section 2.4.
- Chapter 3 is dedicated to the design of the control systems used in the WF and transmission system models. Basically, the control system is split in two hierarchical levels: the user and the equipment control levels. The user control level, described in Section

3.1, is represented by the WF controller. It is responsible with the management the interface between the TSO and the WPS. Also, active and reactive power setpoints are calculated in this block and sent to the specific controllers. The equipment control level presented in Section 3.2, contains all the controllers for their associated equipment e.g. pitch, pwm converters. Control design of the WF and Grid side converters is detailed further on.

- Chapter 4 describes all the study cases performed on the simulation platform previously developed. It deals with the stability analysis of the proposed WPS. Study cases include analysis of fixed speed operation of the WF and assessment of the V/f control system in variable speed operation. Active and reactive power control capability of the WF is performed in order to analyze the grid support in terms of voltage and frequency.
- Chapter 5 draws the conclusions for the entire work performed in this thesis and proposes future developments that may be of interest.

2. System modelling

2.1. System Overview

The analysis of large power systems is strictly related to the development of accurate simulation models of the components involved. Specifically, in this project, the main parts of the studied system are:

- the WF containing a number of WTs and the collecting internal grid;
- the power transmission system transferring the power from the remote WF site to the PCC; and
- the main power grid.

Therefore, this chapter describes the models required for the stability (RMS) analysis of a large WF connected to the transmission system of the main power grid. Such a system, detailed in Figure 2.1, contains both electrical and mechanical components that must be modelled: WT generators, power electronics of the HVDC transmission system, power lines, transformers, line reactors, AC filters and others. Also, several mechanical models of components of the WT e.g. the drive train, are modelled. These mechanical parts are required because of their direct influence on the WF's performance e.g. during power system transients[17].

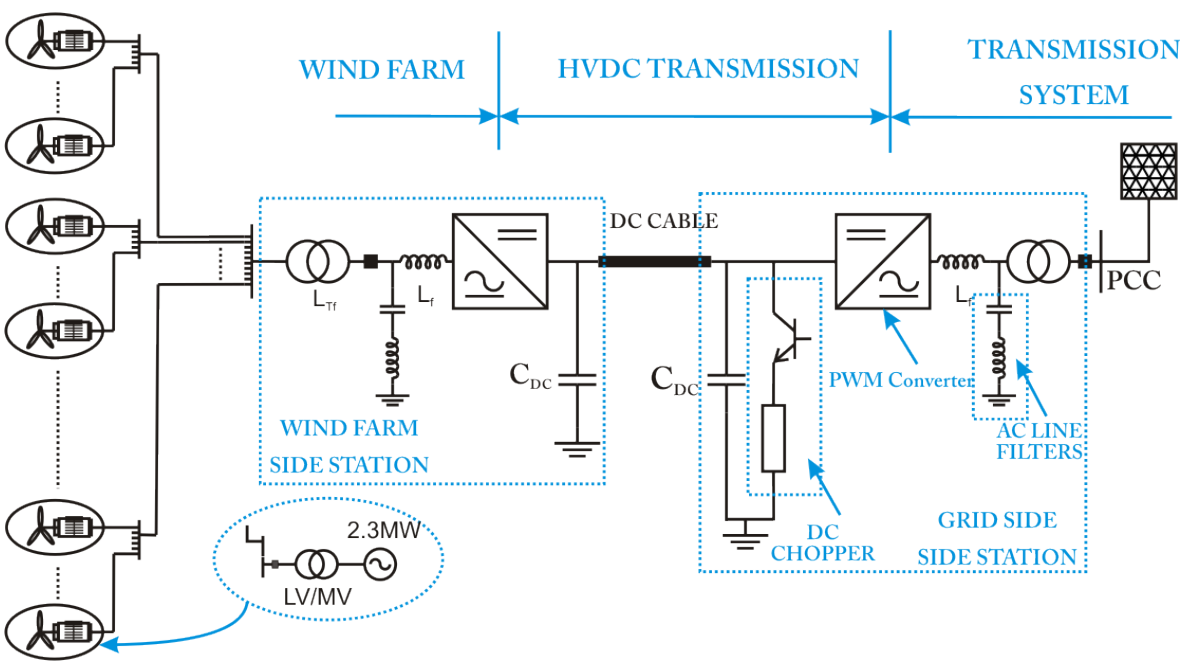

Figure 2.1.: WF System overview

Large WFs may contain tens or hundreds of WTs, each of them being made of many more individual elements that require modelling efforts in order to be able to analyze the entire system. It is therefore practically impossible to simulate in a reasonable time frame the whole system without having to perform simplification steps. Two main options are available[18]:

- The concept of WF system aggregation represents a solution to the analysis of large wind power systems. Using this method implies the implementation of each WT and the corresponding electrical components connecting the WT to the common WF grid e.g. AC transformer, no-load capacitor, power converter;
- The solution in which the WF is represented using reduced models: similar components of the WTs are aggregated into one cumulative model e.g. electrical generators, aerodynamic and mechanical models. Certain assumptions must be taken as it is explained in detail in Section 2.3.1.

As argumented in [18], for studies of power system stability where the overall response of the WF is of interest, the latter solution is reasonable, thus obtaining valid results. A reduced model is implemented in the simulation model of the WF. The assumption of identity between the response of a specific number of WTs and their reduced model response is verified in Section 2.3.

The structure of the WF system implemented in the power system simulation tool Power Factory DIgSILENT is presented in Figure 2.2.

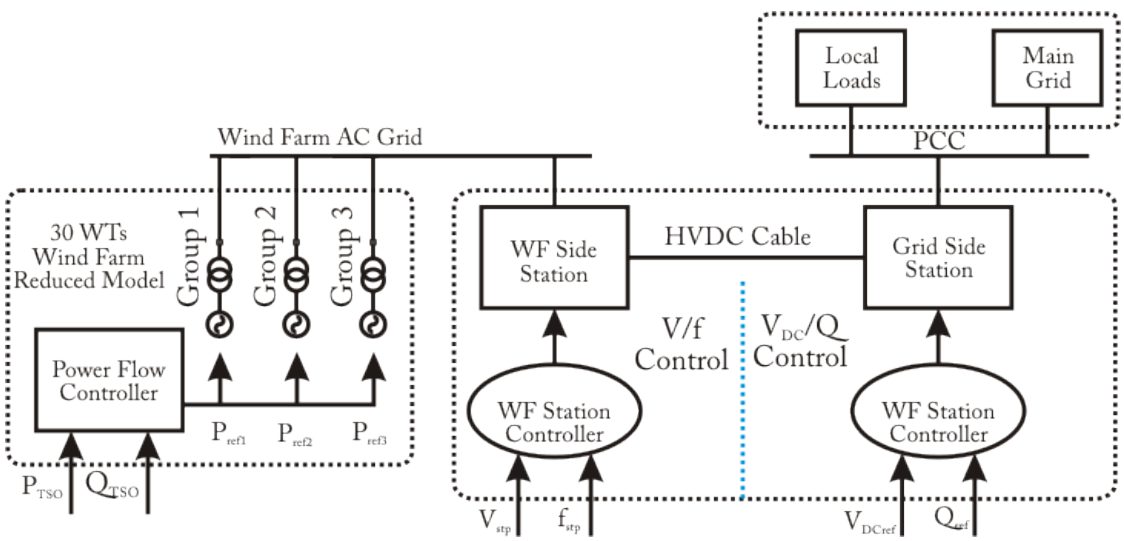

Figure 2.2.: Wind Power System control diagram

2.2. Wind Turbine Model

The block diagram and the signal transfer between each system component of one WT is sketched in Figure 2.3. The wind turbine model is based on [21] and [17] and previously developed in [11]. It is intended to model a variable speed variable pitch WT. Several additional modifications are made to the system as presented throughout the chapter with the purpose of adapting the one turbine model to a higher number of WTs. The WT system has been chosen to represent a commonly found, modern, 2.3 MW WT. The ratings of each of the components are listed in Appendix B.1.

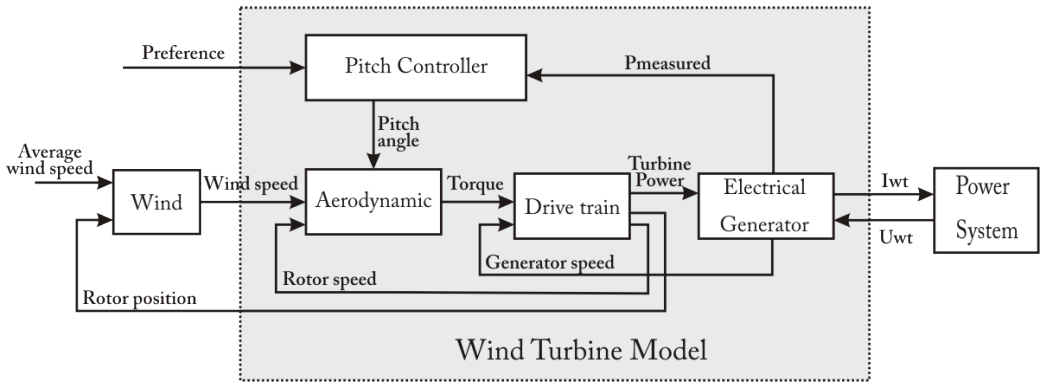

Figure 2.3.: Block diagram of Wind Turbine system

The wind model is based on [17] and is presented in Section 2.2.1. Using measurement data from a specific site in Denmark as the average wind speed, the model generates time series wind speed values depending on wind turbine's characteristics e.g. blade radius, rotor position and on environment characteristics e.g. turbulence intensity, terrain's scale etc. This block is essential for simulating realistic power fluctuations occurring in WTs due to variations in the wind speed at WT's hub. The WF smoothing effect that characterizes the power output and discussed in [23] is also analyzed and additional modifications to the wind model are performed.

The aerodynamic model converts the wind energy into mechanical rotor low speed torque fed to the drive train. It is built around the power coefficient dependence, $C_p(\lambda, \theta)$, which is characteristic for the studied type of wind turbine. It is detailed in Section 2.2.2.

The pitch control system of the WT basically is one PI controller that receives the error signal based on the difference between the power reference received from the WF controller and the WT power. The electrical active power, $P_{measured}$ is controlled by setting the pitch angle reference to the aerodynamic model. This model is described in Section 2.2.4.

The mechanical model of the WT represents the drive train as a two mass model, adequate for power system stability and transients studies[18]. It is presented in Section 2.2.3.

The electrical model comprises a squirrel cage induction generator, typically found in WT installations. A build-in model of the asynchronous machine, available in the simulation software used in this project, DIgSILENT Power Factory, has been used. No induction machine modelling is therefore required. In Section 2.2.4, dimensioning of the parameters of the electrical generator is presented. The WT/WF system interacts with the rest of the power system through the generator model by means of the generator's stator current I_{gen} and voltage U_{gen}.

2.2.1. Wind Model

The wind model is based on the Matlab model developed by RISØ and Aalborg University [17]. The model is implemented in Power Factory DIgSILENT using DSL and has the block diagram as in Figure 2.4. The model generates for each simulation time step the wind speed depending on the average wind speed and the rotor's instantaneous position. The average wind speed can be defined by the user with a specified time profile or recorded wind speed average values from measurement masts can be also provided to the model. The position of the rotor is necessary to model the so called "3p effect", which represents power fluctuations due to the passing of each of the WT's three blades next to the WT's tower. The frequency

of these power fluctuations is evidently equal to three times the rotational frequency of the rotor.

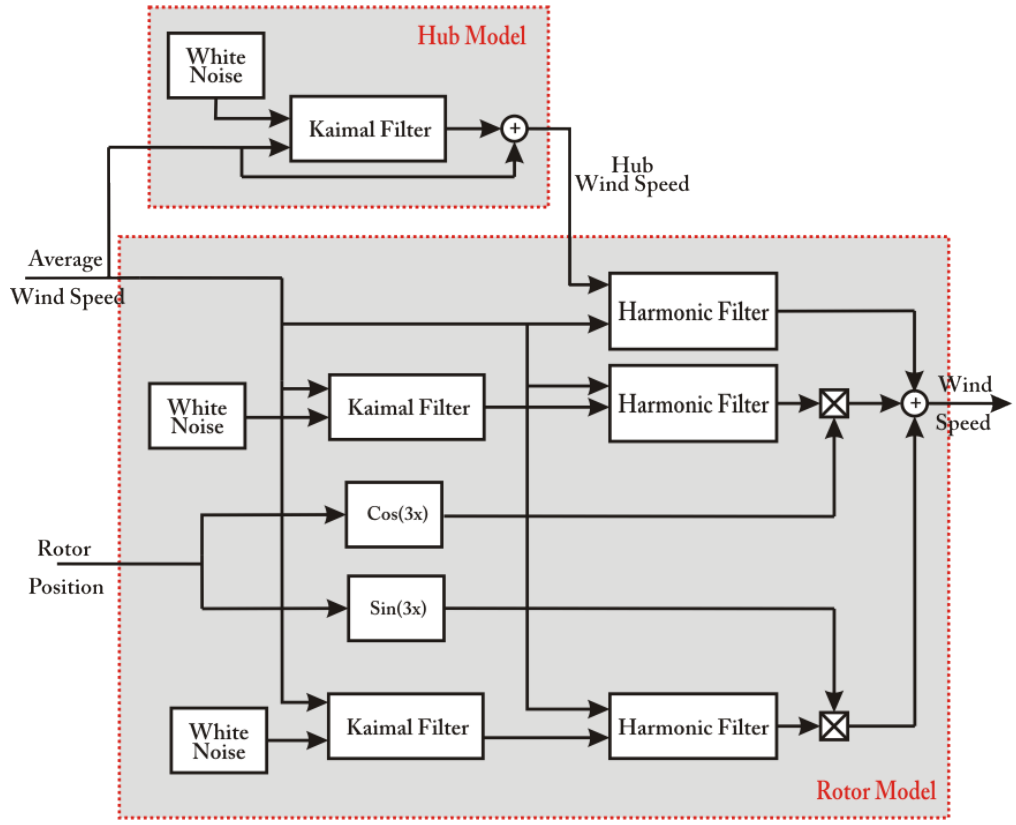

Figure 2.4.: Wind Model block diagram

The wind model consists of two main blocks representing the hub and the rotor. These are modelled using a series of Kaimal and Harmonic filters as described in [17]. Build-in Power Factory model of the noise generator with Gaussian distribution has been used for the white noise block. The sampling frequency of each noise signal is 20 Hz, high enough to model random turbulences that appear in the wind spectrum.

The parameters of the wind model are:

- Sample time step t_s;
- WT blade radius R, defined in the WT datasheet;
- Length scale L;
- Turbulence intensity σ.

The length scale and the turbulence intensity are the characterizing parameters of the area where the WT is located. The wind turbulence is modelled using the transfer function of a Kaimal filter:

$$H_{KF}(s) = K_K \frac{s^2 T_4^2 + sT_3 + 1}{s^2 T_2^2 + sT_1 + 1} \tag{2.1}$$

where K_K, T_1, T_2, T_3, T_4 are time varying parameters calculated based on the turbulence intensity, length scale and the average wind speed, as detailed in Appendix B.2.

The wind model for one WT has been also verified in [11]. In this project, instead of testing on WT wind model, the WF implementation of the wind model has been the main focus. For verification of the WT model several analyses have been made. A simple wind profile that starts from rated wind speed and is varied in the entire wind speed interval can be observed in Figure 2.5. The power spectra density of the associated generated wind power is shown in Figure 2.6. The PSD of the simulated wind is similar with the results in [17] and [25] with smaller power contents at higher frequencies with one exception corresponding to the 3p effect.

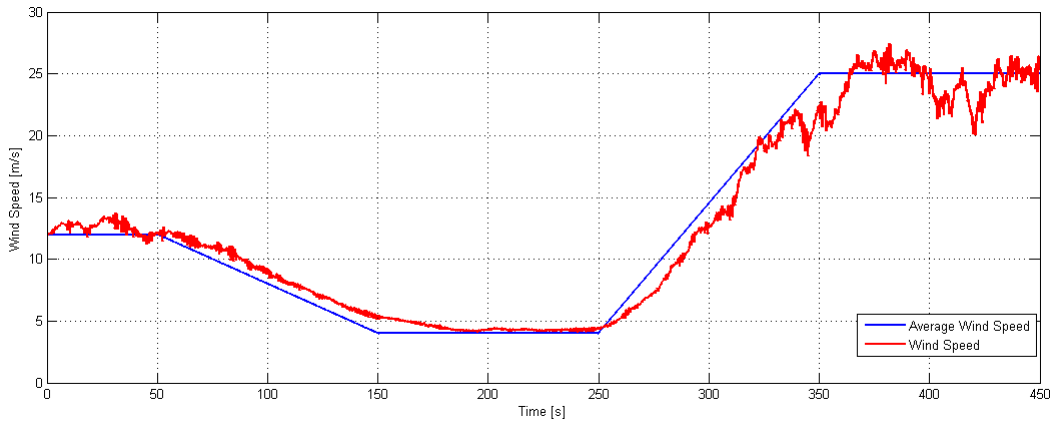

Figure 2.5.: Simulated wind speed profile for one WT system

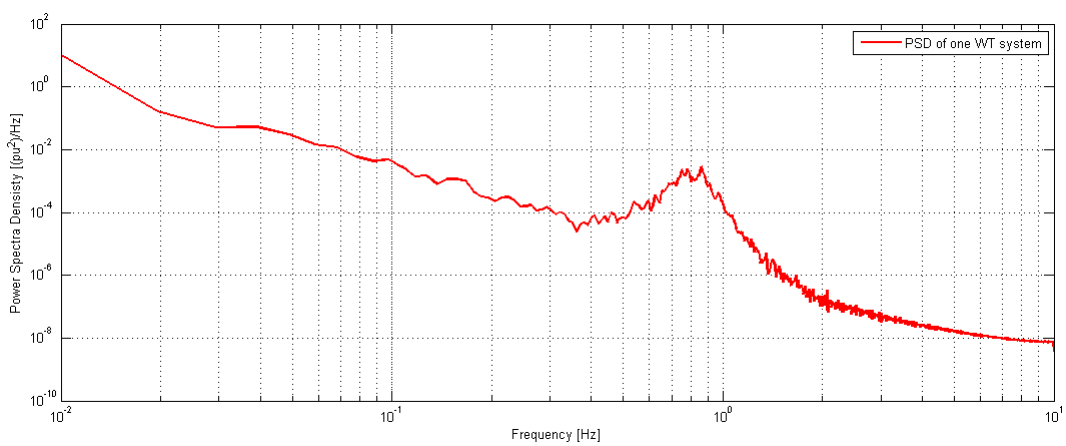

Figure 2.6.: Power Spectra Density for simulated wind for one WT

From the point of view of WF modelling the standard solution for representing the wind speed coherence between the WTs in the same WF is presented in detail in [25] and consists of developing a wind park model that outputs individual correlated wind speeds to each WT in the WF. This approach implies large computing efforts but outputs also very accurate wind power fluctuations. Also, in [24] it is mentioned that a characteristic of WF power output is the smoothing effect that takes place with the increasing number of WTs in the plant. In [23] a comparison of this power smoothing effect is being made between the power output of one, 30, 150 and 300 WTs. In general, the turbulence induced in the power output by the wind variations decreases with the number of WTs in the WF. In order to verify the possibility of using the one turbine wind model in a reduced WF, a comparison between the

power spectra of the reduced WF and the entirely simulated WF must be made. For this purpose, the study in [22] is relevant and can be also applied to this wind model. Similarly, the combined effect of 10 wind models of a small generic WF (thus containing 10 WTs) is studied and compared with the wind model of one WT system. A constant average wind speed of 10 m/s, a turbulence intensity of 10 per cent and a simulation time frame of 100 seconds are set. Figure 2.7 shows the per unit power output of each of the 10 WTs with green and the cumulative per unit power output of this small WF. It is obviously that the power output of the WF has a smoother characteristic than the one of a single WT system.

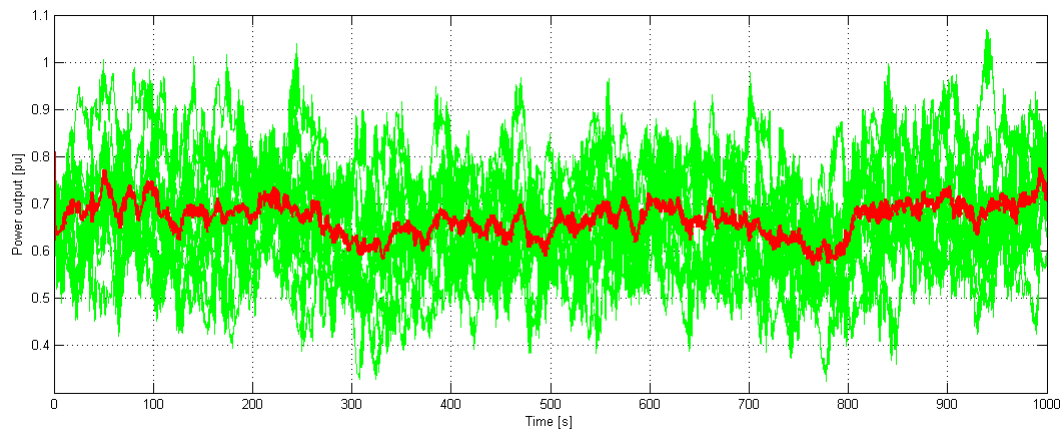

Figure 2.7.: Power output of each of the 10 WTs (green) and WF cumulative power output (red)

Figure 2.8 plots the cumulative power output of the 10 WTs and the power output of one WT for a 100 seconds time interval. Although the shape of the waveform is similar, in the case of a one WT system can be observed higher perturbances. From this observation appears the necessity of analyzing the power spectrum of the two types of signal.

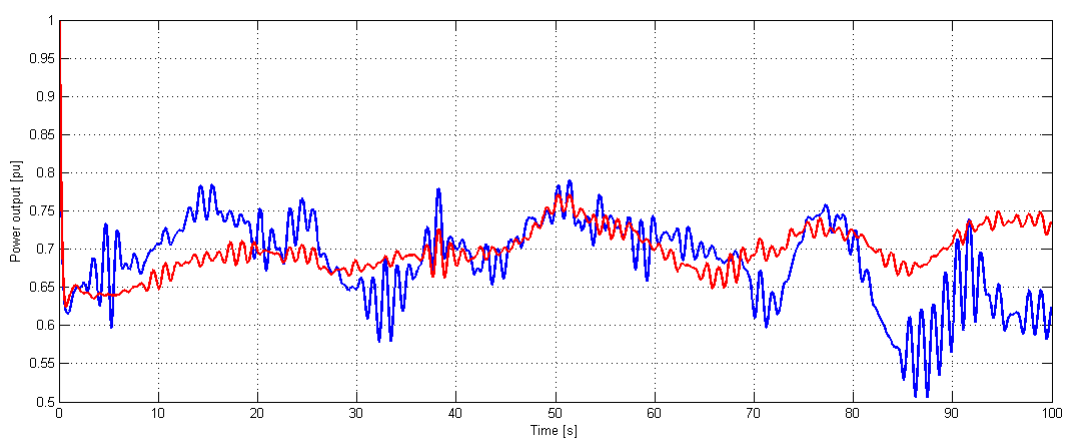

Figure 2.8.: Power output of one WT and of WF with 10 WTs at average wind speed 10 m/s

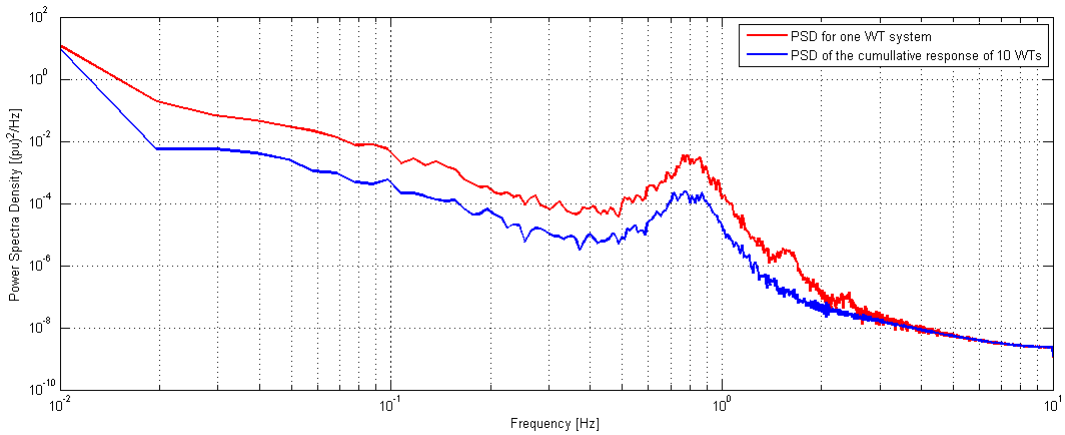

Figure 2.9.: Power spectra density for WT and WF with 10 WTs

In Figure 2.9, the PSD of the WF (blue) and one WT system (red) is plotted. The simulation time frame has been long, 1000 seconds. A higher damping of the WF power contents is observed compared to the single WT model case. This is normal considering the smoothing effect previously mentioned. In this project, further adaptations to the parameters corresponding to the turbulence effect have been made in order to match the power spectrum of a WF with a single wind model. The number of wind turbines being modelled in one reduced model has been chosen to be 10 as it is further explained in Section 2.3.1. Therefore, for a tuned set of wind model parameters, the PSD of the reduced WF wind model is overlapping the PSD of the separately simulated 10 WTs as it can be observed in Figure 2.11. Although for higher frequencies than the corresponding frequency for $3 \cdot \Omega_r$, the power spectrum contents might differ slightly between each other, the overall power contributions from these high frequencies is negligible when considering power system stability analyses. The power output of the two simulated systems is shown in Figure 2.10 for a 100 seconds simulation time frame.

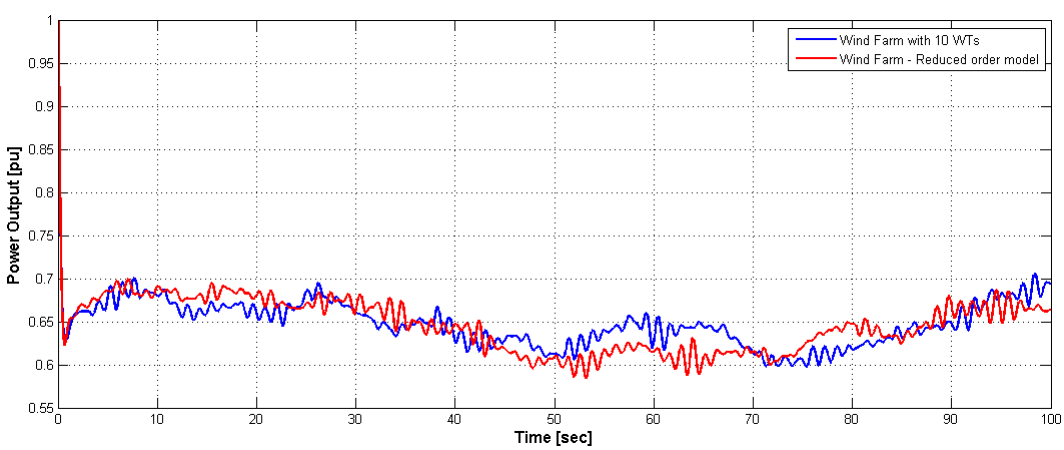

Figure 2.10.: Power output of reduced model WF and of WF with 10 WTs at average wind speed 10 m/s

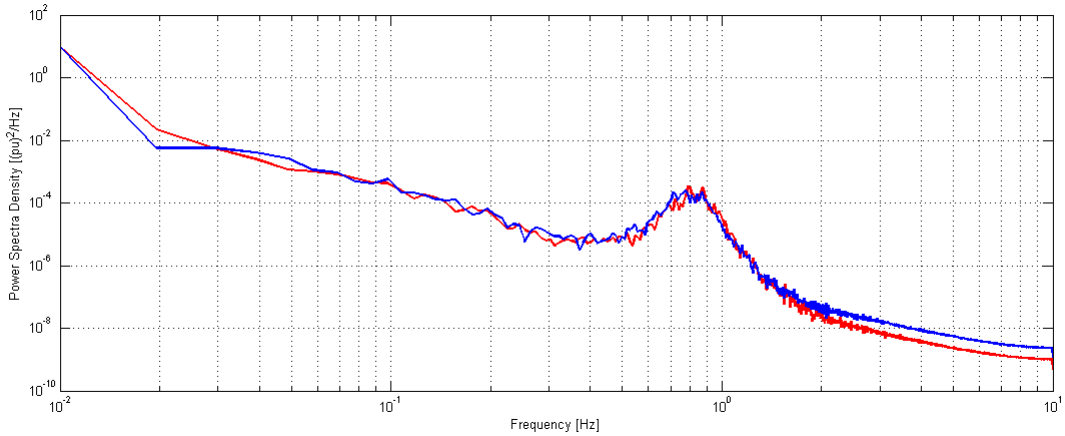

Figure 2.11.: Power spectra density for reduced WF and WF with 10 WTs

Histograms for the wind speed and power output of the reduced model are presented in Figures 2.12 and 2.13. Although in the power spectrum the gaussian distribution of the noise generators cannot be observed straightforward, this error is due to the small time frame of simulation. For exemplification, in Appendix B.2 a simulation with a larger time frame of 1000 seconds yields relevant results in Figures B.1 and B.2.

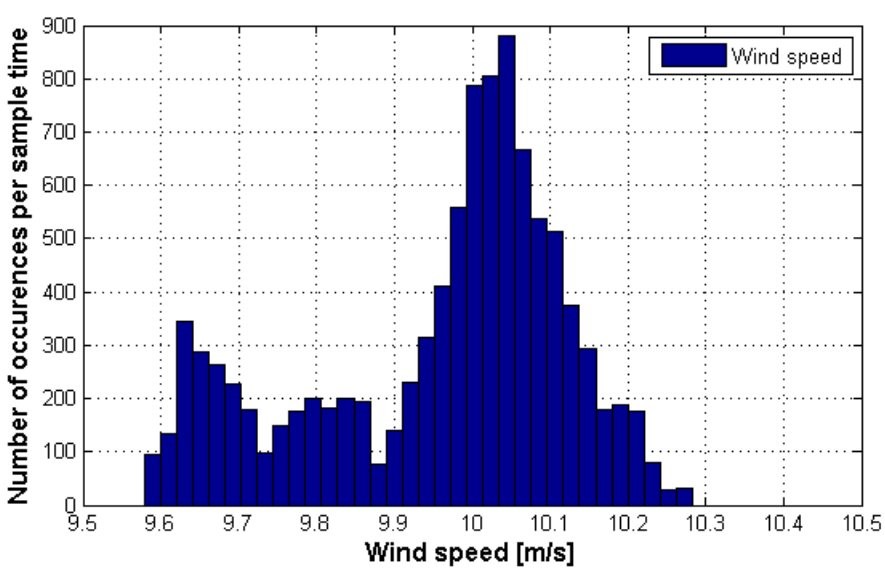

Figure 2.12.: Wind Speed Histogram for 10 m/s average wind speed

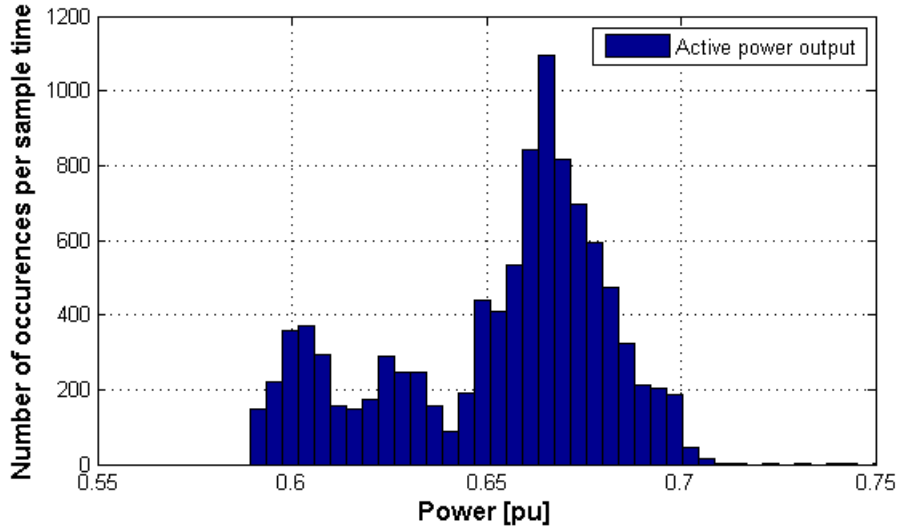

Figure 2.13.: Power output histogram for 10 m/s average wind speed

2.2.2. Aerodynamic Model

The capability of the WT system to extract power available in the wind and transfer it to the rotor shaft is modelled by the Aerodynamic model. The block diagram of this model is presented in Figure 2.14. This simple model is built around a WT aerodynamic measurement data set of the power coefficient $C_p(\lambda, \theta)$ which is specific for each WT type. Therefore, this data set models a two variable dependent function and it is implemented in Power Factory DIgSILENT as a look up table with λ, the tip speed ratio, and θ, the pitch angle, as inputs. The "Aerodynamic Torque" block models the transformation of energy at the WT rotor shaft using Equation 2.6, which was obtained through the definitions below.

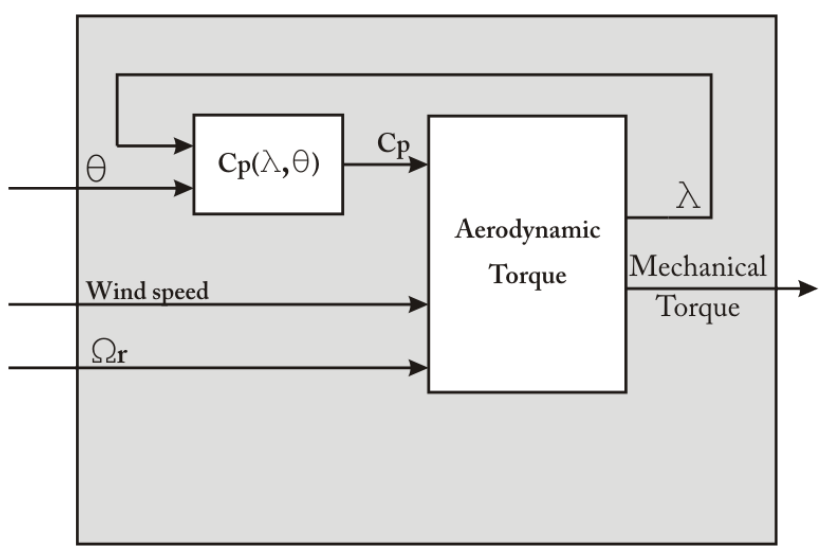

Figure 2.14.: Aerodynamic model block diagram

The power that the WT can absorb from the wind is proportional with the rotor aria πR^2, the air density at normal conditions ρ, the power coefficient C_p and the cubic of the wind speed v_∞, as described in Equation 2.2 [45]:

$$P = \frac{1}{2}\rho\pi R^2 C_p(\lambda,\theta)v_\infty^3 \tag{2.2}$$

The aerodynamic torque is expressed as in Equation 2.3 [45]:

$$T = \frac{1}{2}\rho\pi R^3 C_q(\lambda,\theta)v_\infty^2 \tag{2.3}$$

where $C_q(\lambda,\theta)$ represents the torque coefficient and is given in Equation 2.4:

$$C_q(\lambda,\theta) = \frac{C_p(\lambda,\theta)}{\lambda} \tag{2.4}$$

The tip speed ratio, λ, depends on the blade radius R, the wind speed v_∞, and the rotor angular speed Ω_r, as in Equation 2.5:

$$\lambda = \frac{\Omega_r R}{v_\infty} \tag{2.5}$$

Therefore, including Equations 2.4 and 2.5 into Equation 2.3, the following relation results (Equation 2.6):

$$T = \frac{P}{\Omega_r} = \frac{1}{2}\rho\pi R^2 \frac{C_p(\lambda,\theta)}{\Omega_r} v_\infty^3 \tag{2.6}$$

The "Aerodynamic Torque" block in the Aerodynamic model implements Equation 2.6 and uses as input the measurement file for the power coefficient. The influence of the air density variations are shown in Figure B.4 of the Appendix B.3. As a comparison, analytical methods for calculating the power coefficient are available. In [26], the power coefficient C_p is expressed using Equation 2.7:

$$C_p(\lambda,\theta) = 0.22(\frac{116}{\lambda_i} - 0.4\theta - 5)e^{\frac{-12.5}{\lambda_i}} \tag{2.7}$$

The tip speed ratio equivalent λ_i is calculated using Equation 2.8:

$$\lambda_i = \frac{1}{\lambda + 0.08\theta} - \frac{0.035}{\theta^3 + 1} \tag{2.8}$$

Figure 2.15 shows with continuous lines the measured power coefficient and the calculated torque coefficient (Equation 2.4) versus the tip speed ratio λ at zero pitch angle θ. Also, with dashed lines, the analytical torque and power coefficients are displayed. One observation would be that the maximum values for power and torque are obtained at different wind speeds. Since the main goal is the maximization of power output, the optimized variable will be the power coefficient. The noticeable difference between the measured, turbine specific power coefficient and the analytically calculated solution prove the importance of selecting a proper $C_p(\lambda,\theta)$ specifically chosen for the studied WT system in order to obtain valid results.

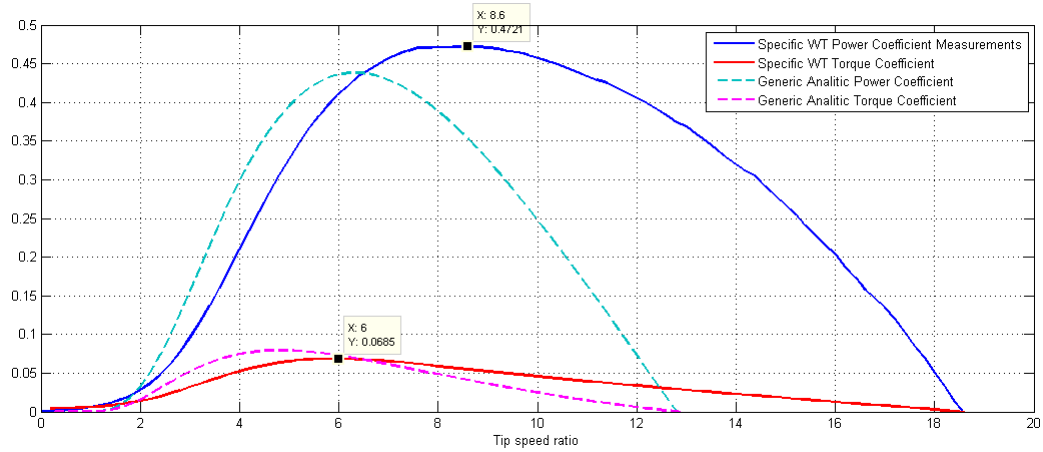

Figure 2.15.: Power C_p and torque C_q coefficients variation at zero pitch angle θ

Varying the wind speed while the pitch angle remains zero determines the power characteristic from Figure B.4 from Appendix B.3. The dependence of the power on the tip speed ratio λ and the pitch angle is presented in Figure 2.16. It can be seen that when designing the Pitch controller, the pitch angle can be maintained in a relatively small interval and still to be able to control the power output as required. As it was expected, for small tip speed ratios, and consequently, high wind speeds, the absorbed power increases considerably. The plot analyzes only tip speed ratios corresponding to wind speeds smaller than the cut-out wind speed v_{cut}.

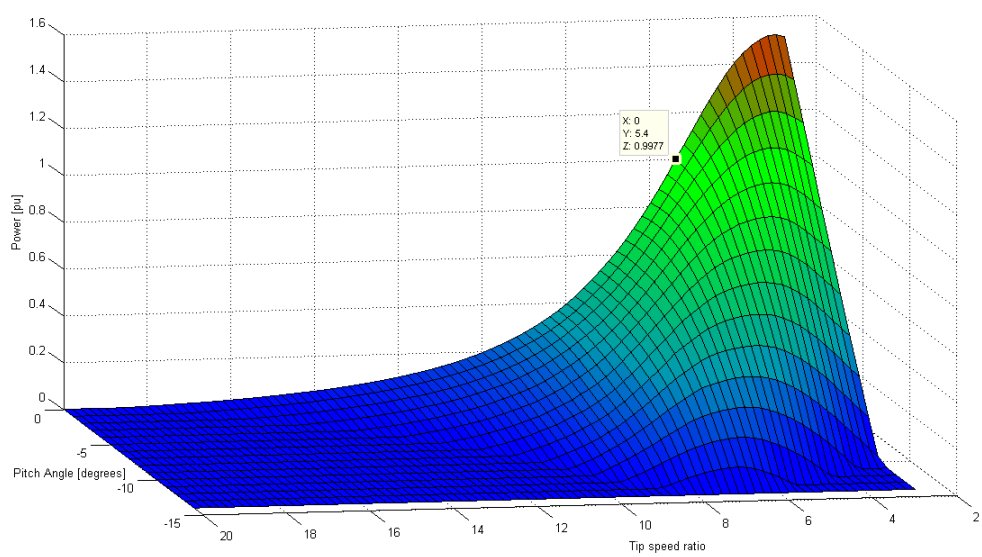

Figure 2.16.: Turbine Power related to θ and λ

The dependence of the output power on the rotor speed for different wind speeds while keeping the pitch angle zero is graphically shown in Figure 2.17. It is important to observe that the power output can be maximized by changing the turbine's rotor speed correlated with the wind speed. The goal of changing the WT generator's synchronous speed emerges from this observation, since this action will modify accordingly the rotor speed Ω_r.

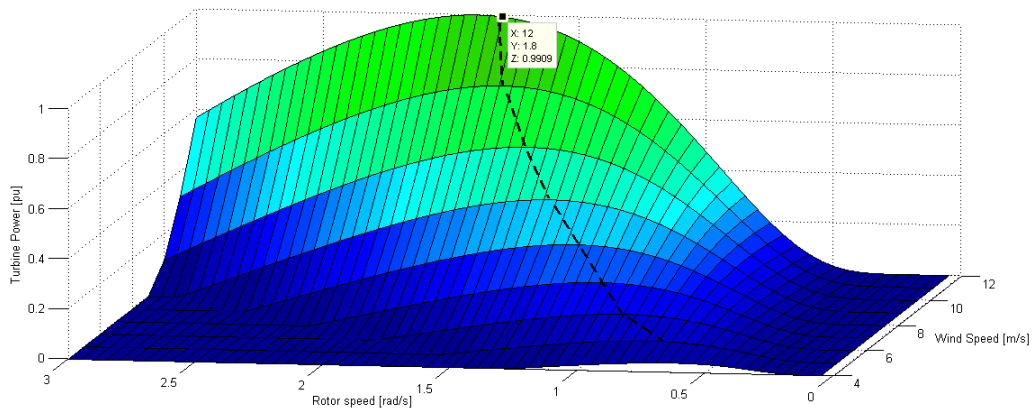

Figure 2.17.: Turbine power for different WT rotor and wind speeds

2.2.3. Mechanical Model

The mechanical system of the WT has important effects on the power system when load and torque transients appear at the shaft of the electrical generator [27, 28]. It is therefore necessary to dynamically model these interactions at a highly enough level of complexity. In [27] and [29] the WT drive train is represented as six mass model and analyzed for grid disturbances. Three, two and one mass models are developed in [17], while in [28] two mass models of the mechanical system are analyzed also for transient stability analysis. In [30] the one and two mass models are compared with measurement data and it is concluded that one mass models are not suitable for dynamic simulation of WTs in power system studies. A two mass mechanical model has been implemented in this project, this solution being the best trade-off between accuracy of results and simulation time. The mechanical effects of the turbine tower, flap bending and similar are neglected since they have negligible influence on the WT's power fluctuations. In [18] a detailed analysis regarding the modelling of the mechanical system for WFs is performed. Further details on the assumptions taken to the drive train in order to model a group or all of the correspondent mechanical system of the WTs in the WF are presented in Section 2.3.1.

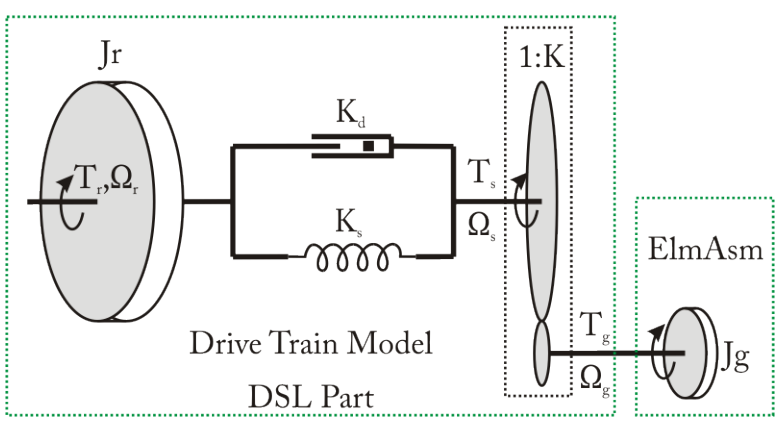

Figure 2.18.: WT Drive train as a two mass model

Figure 2.18 presents the concept of the mechanical two mass model. It is based on the model developed in [31], designed specifically for the simulation software used, Power Factory DIgSILENT. The masses of the WT blades, hub and rotor shaft are combined in one generic

rotor mass with its corresponding rotor inertia parameter J_r. The rotor torque T_r, acts as the driving force of the system providing momentum to a damper-spring block characterized by the damping coefficient K_d and the stiffness coefficient K_s. An ideal gearbox is modelled by a constant gearbox ratio K, which converts the torque from the low speed shaft T_s, Ω_s to the high speed shaft T_g, Ω_g. The asynchronous machine model in Power Factory DIgSILENT is designed to have as input variable the per unit turbine power Pt. Therefore, the torque T_g is further on used to obtain the turbine power Pt.

As described in [31], the state space equations of the two mass model implemented in DSL are shown in Equation 2.9 and 2.10:

$$\dot{\bar{x}} = \begin{pmatrix} 0 & 0 & 1 \\ 0 & 0 & 1 \\ \frac{-K_s}{J_r} & 0 & \frac{-K_d}{J_r} \end{pmatrix} \cdot \bar{x} + \begin{pmatrix} \frac{-1}{K} & 0 \\ 0 & 0 \\ \frac{K_d}{K \cdot J_r} & \frac{1}{J_r} \end{pmatrix} \cdot \bar{u} \tag{2.9}$$

$$\bar{y} = \begin{pmatrix} \frac{K_s}{K} & 0 & \frac{K_d}{K} \\ 0 & 1 & 0 \\ 0 & 0 & 1 \end{pmatrix} \cdot \bar{x} + \begin{pmatrix} \frac{-K_d}{K^2} & 0 \\ 0 & 0 \\ 0 & 0 \end{pmatrix} \cdot \bar{u} \tag{2.10}$$

where $\bar{u}$ denotes the input variables, $\bar{y}$ - the output variables and $\bar{x}$ - the state variables and relate to the two mass model variables as in Equation 2.11.

$$\bar{u} = \begin{pmatrix} \Omega_g \\ T_r \end{pmatrix}, \bar{y} = \begin{pmatrix} T_g \\ \theta_r \\ \Omega_r \end{pmatrix}, \bar{x} = \begin{pmatrix} \theta_k \\ \theta_r \\ \Omega_r \end{pmatrix} \tag{2.11}$$

The angular difference between the two ends of the flexible low speed shaft is denoted by θ_k and is expressed in Equation 2.12:

$$\theta_k = \theta_r - \theta_s \tag{2.12}$$

where θ_r represents the position of the rotor side shaft and θ_s represents the position of the gearbox side shaft.

The diagram block of the Mechanical model is shown in Figure 2.19. The "Drive Train Model - DSL Part" block is user programmed and implements the drive train equations except the Generator inertia. The build-in asynchronous generator models also the generator inertia, thus calculating the generator's speed and providing it to the DSL model.

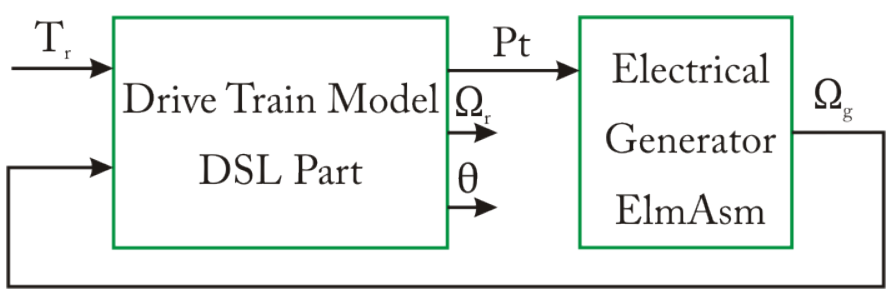

Figure 2.19.: Diagram block of the WT Mechanical Model

2.2.4. Generic Pitch Controller

The pitch controller has the purpose of keeping the power output to a set value by pitching the WT blades. In [33] the pitch controller is implemented using a proportional and satu-

ration/rate limiter. In [32] another solution has been used, the main difference being that the error signal is calculated based on the generator's speed and not on the measured power. A simple pitch controller has been implemented using a PI controller similar with [32] and [33]. The block diagram of the controller is shown in Figure 2.20. The power reference P_{ref} is being received from the WF power flow controller while the feedback power signal P_{meas} is being measured in the electrical connection point of the WT system. The error between the measured and reference power is the input signal for a PI controller $K_\theta(1+\frac{1}{sT_\theta})$. The output variable is the pitch angle referenceθ_{ref}, which controls the servo mechanism of the blades.

In [45] a model of the pitch angle actuator is presented. This model is also adopted in the pitch controller model as described in Figure 2.20, where the output of the pitch controller, the pitch angle reference θ_{ref} is fed to the actuator system. In the tuning of the PI parameters, the actuator must also be taken into consideration, as it has been done in Section 3.2.1.

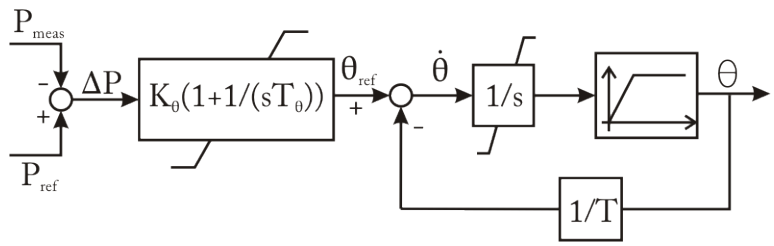

Figure 2.20.: Block diagram of pitch control system

Squirrel Cage Induction Generator Model

The model used in this project for the SCIG is a build-in model[36] directly available in Power Factory DIgSILENT. The electrical parameters of the machine must be set in the model's mask window. The block diagram of the machine with its corresponding inputs and outputs, as it is used in the project is shown in Figure 2.21. This model includes the generator inertia parameter J_g, therefore will participate also in calculating the generator speed Ω_g required in the Drive Train model. The active power required by the pitch controller is directly measured at the terminals of the generator, the signal *pgt* accounting for these measurement. Since the machine is in generating mode, *pgt* will be always negative.

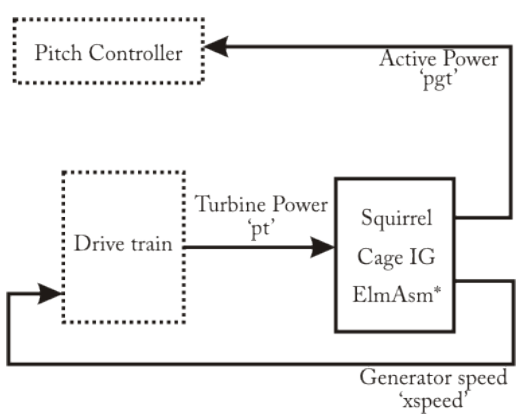

Figure 2.21.: WT Asynchronous Machine model block diagram

The specifications of the Asynchronous Machine build-in model can be defined by two methods:

- by setting the electrical parameters of the machine (rotor, stator resistances and reactances), or
- by describing the slip-torque and slip-current characteristic (mechanical steady-state characteristic) of the generator.

Having one of the two sets of parameters, the other one can be calculated. The nominal operating point is determined by the following parameters:

- rated mechanical power P_n;
- rated power factor $cos\varphi_n$;
- efficiency η_n;
- nominal speed Ω_{gn};

The stability model of the Asynchronous Machine build-in model is based on the steady state equations of the equivalent circuit from Figure 2.22:

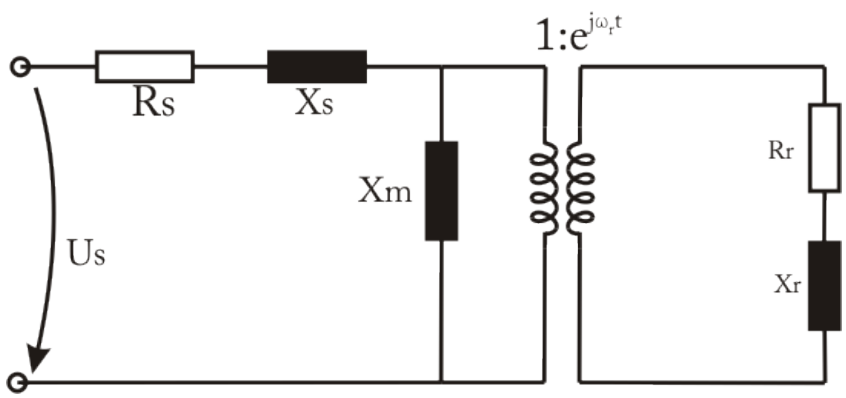

Figure 2.22.: Asynchronous machine - equivalent circuit

The voltage Equations 2.13 and 2.14 of the induction machine for stability (RMS and EMT) simulations in Power Factory DIgSILENT[36] are:

$$u_s = R_s \cdot i_s + j \cdot \omega_s \cdot \psi_s + \frac{d\psi_s}{dt} \tag{2.13}$$

$$0 = R_r \cdot i_r + j(\omega_s - \omega_r)\psi_r + \frac{d\psi_r}{dt} \tag{2.14}$$

where ω_s - synchronous speed, ω_r - angular speed of the rotor, $\psi_s, \psi_r, i_s, i_r, u_s$- space vectors for flux, current and voltage of the stator and the rotor respectively. For stability (RMS) simulations further simplifications are required. The stator voltage equation is further on reduced to its steady state equivalent. In Appendix B.4 the electrical datasheet parameters are transformed into their per unit equivalents. These values are required by the Power Factory DIgSILENT build-in induction generator model for its correct definition.

2.3. Wind Farm Modelling

Many WF models have been developed for power systems studies e.g. [18, 21, 22, 24, 31]. For transient voltage stability, most of the models can be divided into two main groups[18]:

- aggregated WF models;
- reduced WF models.

An aggregated WF model requires modelling of every WT system and its corresponding electrical e.g. power transformer, no-load capacitor, cables. Therefore, a WF consisting of n WTs will be modelled with n WT systems. The implementation of the aggregated model requires high computing efforts when the number of WTs in the WF is increasing. This model allows WF simulations which include the effect of distributed wind speeds across the plant.

If the collective response of the WF is of interest and the difference in power production among the WTs is not required, then a reduced model of a group or all the WTs in the wind power plant can be developed with no significant errors in the results.

As detailed in [18], the aggregated models can be used for investigation on the mutual interaction between the WTs of the same WF and response of the WTs of the same WF when subjected to a fault located in the internal grid. On the other hand, the reduced model can be successfully used in studies of the collective response of the WF when subjected to a fault in the main power system and voltage stability studies of the power grid with a large WF connected to the transmission system.

A reduced model of a relatively large WF consisting of 30 WTs of 2.3 MW has been implemented in this project as presented in 1.5. In Subsection 2.3.1, design considerations of the WF model have been made with focus on the chosen WF layout. Section 3.1 describes the WF controller, the control system responsible with active and reactive power regulation of the WF.

2.3.1. Reduced Model of a WF

Consider the WF described in Section 1.5, Figure 1.15. The WTs are marked by their position in the WF grid as $WT_{i,j}$, where i denotes the row and j, the column of the WF layout. By identical WTs, it is understood that the electrical and mechanical parameters of the WT are the same in all WTs. The reduced model of the WF takes into account the collective response of all identical WTs by grouping them into one rescaled model as it is shown in Figure 2.23. Modelling the WF by several reduced models of groups of WTs in the respective WF is called multi-machine equivalent model, as shown in Figure 2.24.

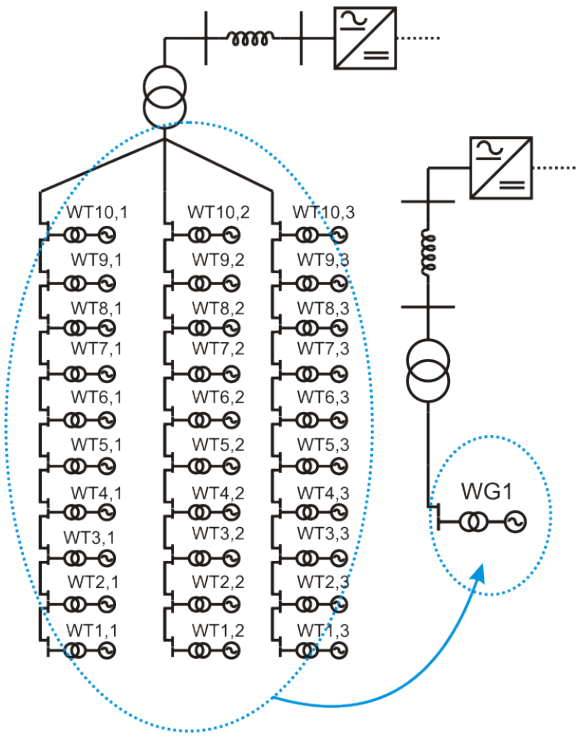

Figure 2.23.: Model reduction in WF

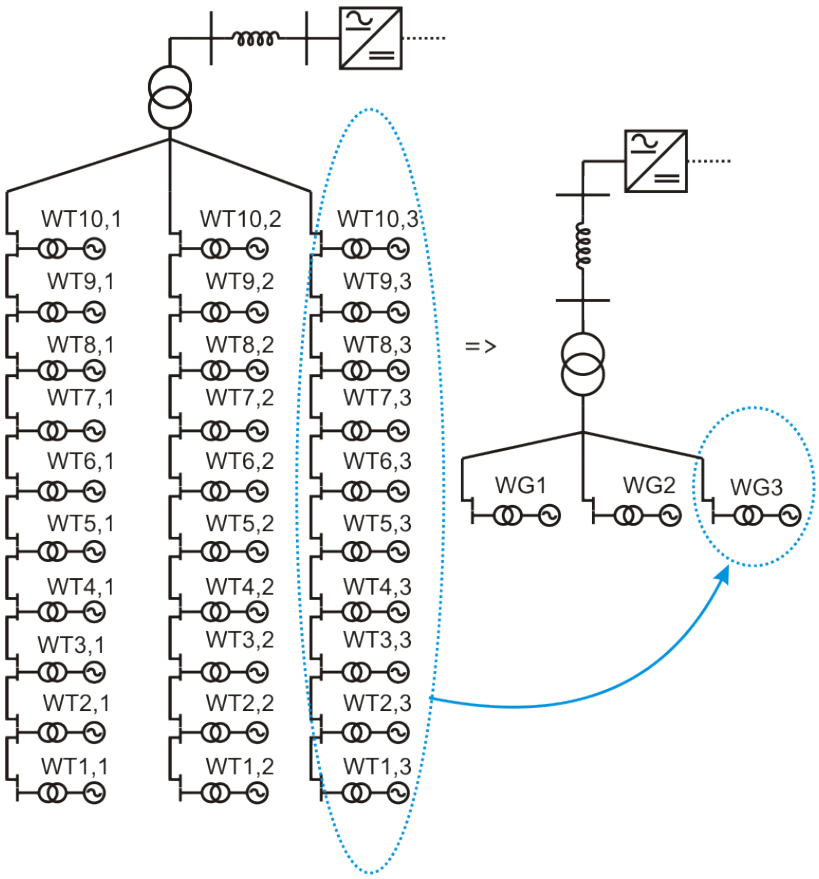

Figure 2.24.: Multi-machine equivalent

The following equalities and assumptions are mentioned in [18] for being applied to the reduced model of the WF. For a reduced model of a WF, the total power capacity and the active power produced are defined by Equations 2.15:

$$\begin{cases} S_{WF} = \sum_{i=1}^{n} \sum_{j=1}^{m} S_{i,j} \\ P_{WF} = \sum_{i=1}^{n} \sum_{j=1}^{m} P_{i,j} \end{cases} \tag{2.15}$$

The reduced large WF model can be applied if the following assumptions are met:

- With respect to voltage transients, in [18] the conclusion is that rated operation of the WF is necessary in order to obtain valid results. In the case of the proposed WF, since the VSC HVDC transmission system decouples the WF from the external grid, the previous condition applies only to faults in the internal AC grid of the WF.
- The differences between the operating points of each of the WTs are not very large. If there are such differences, but the wind speed follows a pattern, a multi machine equivalent can be applied with good enough accuracy.

In this project, the multi-machine equivalent has been adopted for the WTs placed on each column. For the 30 WTs WF results, therefore, three reduced models for 10 WTs. A characteristic of this model are the fast simulation time and good accuracy of the results.

More simplification assumptions have been adopted for the WF model:

- the wind direction is always normal on the WFs columns, therefore, each WT in the same column will operate with the same power output.
- the wind correlation between the rows of the WF is only a lagging factor; more advanced models have been developed in order to simulate the relationship between WTs' power output and the wind speed, but it is not an essential requirement in this project.

2.4. Design and Dimensioning Aspects of VSC Transmission Components

The transmission system is chosen and built with two main design aspects being taken into consideration:

- efficiency of transmission and economically related aspects such as investment costs, and
- grid support functions

The transmission solution that greatly improves the WF performance with respect to most requirements of grid codes is the VSC HVDC transmission although this may come with an extra initial investment cost. For this reason, the option of implementing the VSC HVDC system has been adopted.

For the purpose of dynamic stability simulation, which is the case in this project, Power Factory requires setting up a valid load flow model of the power grid which will determine a steady state operating point. From this equilibrium point the dynamic/stability simulation will proceed. As it is the case for all dynamic models included in the simulation, valid initial conditions (load flow calculation) are required. In other words, a successful load flow analysis

must be performed in the initial moment of the stability simulation. Special care must be addressed to the DSL models which are entirely developed by the simulation tool user. These include the WT model, the wind model and the control blocks for WF and PWM converters at the receiving and sending end stations. The build-in models such as electrical generators, PWM converters, synchronous generators and loads must be initialized accordingly to the load flow rules that apply in the node of connection of each component.

2.4.1. PWM Converter Model

The PWM Converter build-in model in Power Factory DIgSILENT is designed for all commonly used types of analyses: load flow, short circuit and stability (EMT and RMS) models are developed[37]. It models a self-commutated, voltage sourced AC/DC converter with turn off capability (GTO or IGBT) with the equivalent circuit in Figure 2.25.

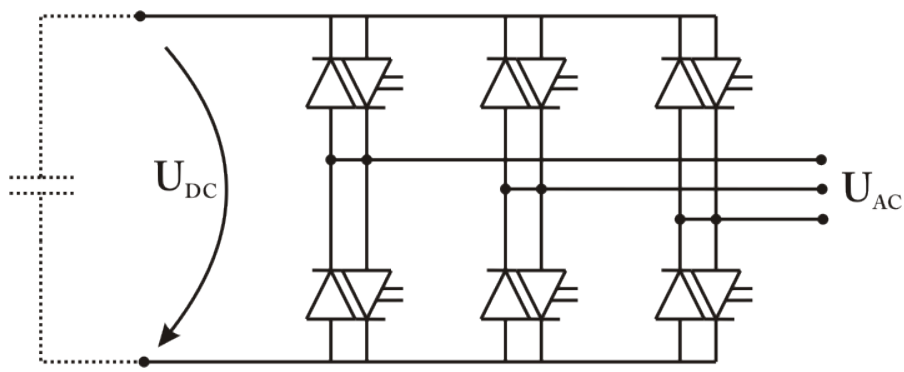

Figure 2.25.: PWM Converter with turn-off capability switches - equivalent circuit

The PWM converter is governed at the fundamental frequency by Equation 2.16:

$$\begin{cases} U_{ACr} = K_0 Pm_r U_{DC} \\ U_{ACi} = K_0 Pm_i U_{DC} \end{cases} \tag{2.16}$$

where K_0 represents the modulation factor depending on the modulation method used, Pm_r,Pm_i represent the PWM modulation index U_{ACr},U_{ACi} - real and imaginary AC voltage components and U_{DC} - the DC voltage RMS value.

Normal operation of the PWM converter implies that the modulation index P_m must satisfy Equation 2.17:

$$\mid P_m \mid < 1 \tag{2.17}$$

The PWM Converter model assumes ideally, loss-less operation, thus resulting the active power conservation between the AC and DC side in Equation 2.18:

$$P_{AC} = Re(\underline{U}_{AC}\underline{I}^*_{AC}) = U_{DC}I_{DC} = P_{DC} \tag{2.18}$$

In Power Factory DIgSILENT there are two types of modulation strategies: square-wave and sinusoidal. No space vector modulation is available. Therefore, the type of modulation that the PWM converter uses in this project has been selected to be sinusoidal for the harmonics introduced in the power system are considerably lower compared to rectangular modulation. Consequently, as stated in [37], the modulation factor is:

$$K_0 = \frac{\sqrt{3}}{2\sqrt{2}} \tag{2.19}$$

Equation 2.18 assumes that no power losses occur in the PWM converter. An additional parallel DC resistance accounting for the switching losses of the valves and a series resistance on the AC side have been modelled in order to accurately simulate the power losses in the PWM converter.

Regarding load flow analysis, the control modes of the PWM converter are of interest for the correct set up of the initial conditions. From the available options, two modes have been selected for the WF and grid side converter respectively:

- $V_{AC} - phi$: This type of load flow control mode is well suited for the WF side converter, where the converter must control both the AC voltage and the phase angle in order to obtain power flow balance. Also, variable speed operation can be performed in the WF[34];
- $V_{DC} - Q$: This mode is suitable for the grid side converter, for it provides DC voltage control and reactive power balance in the PCC.

As mentioned previously, the RMS stability model is developed on the fundamental frequency equation 2.16 and 2.18. The control options in dynamic simulation of the PWM converter are:

- Pm_r, Pm_i
- 'Pm_in', $dphiu$
- 'Pm_in', $f0$
- Pmd, Pmq, $cosref$, $sinref$

The control system for the WF and grid side converters is detailed in Chapter 3, Section3.3.

Consider the WF presented in Section 1.5. Dimensioning of each of the WF and grid side converters for the rated power defined in the proposed WF has been made.

For a given apparent power S_b and AC line voltage U_l, the following Equations apply:

$$U_b = \frac{U_l}{\sqrt{3}} \tag{2.20}$$

$$Z_b = 3\frac{U_b^2}{S_b} \tag{2.21}$$

$$I_b = \frac{S_b}{3U_b} \tag{2.22}$$

where, U_b , I_b and Z_b represent the base values for voltage, current and impedance, respectively. Voltage levels have been chosen based on [35], the technical description documentation for VSC HVDC solutions from ABB AB Sweden. The selection process is straightforward depending on the power ratings of the power plant. To further on ease the design, ABB

provides modularized stations based on voltage and current ratings. A guiding observation is that the economical solution is to choose the module that has the minimum voltage rating at the desired power capability[35]. A description of the selection process and base value parameters calculus used for the WF and grid side converters is detailed in Appendix C.1. Using the base values for the converters, calculation of all other AC and DC components can be performed.

2.4.2. AC Components

Further on, the main AC components that must be properly sized in order to achieve correct operation of the VSC transmission system are presented. The ratings of the line reactors, transformers, AC filters and loads are having the biggest impact on the system's performance.

Electrical Grid Build-in Model

The main power system comprises all the components in the power grid beyond the PCC of the WF. It can be modelled as a voltage source behind an impedance[44].

For modelling the main power system several options are available in Power Factory DIgSILENT:

- fully modelled power system;
- power grid build-in model;
- synchronous generator model;
- different combinations, e.g. IEEE 5 bus model.

In this project, an external grid build-in model has been used for its simplicity as well as for the flexibility in defining the type of grid under study. Two main parameters are available in the grid model:

- Acceleration time constant (in seconds) - this parameter relates to the system's inertia and basically dictates the voltage angle stability characteristic in the PCC; in DIgSILENT the default value for a stiff grid is 100 seconds [55].
- Short Circuit Power (in MVA) - this parameter is strictly related to the Short Circuit Ratio - SCR. It is defined by Equation [6].

$$SCR = \sqrt{3} \cdot U_{grid_{rated}} \cdot I_{scc} \tag{2.23}$$

where $U_{grid_{rated}}$is the nominal grid voltage, I_{SCC} the symmetrical short circuit current. The SCR is used as a reference calculation for three phase faults. For short circuit ratios higher than 10[5], the external grid is commonly known as a "stiff and strong" grid. For smaller values the grid is weaker.

Line Reactor

The line or phase reactors are positioned between the PWM converter and the power transformer. This component is essential for VSC converter operation, its function being of current regulation. Proper dimensioning is required for the total line reactance, including the line reactor.

The impedance values are calculated as follows:

$$\begin{cases} X_l = x_l \cdot Z_b \\ L_l = \frac{X_l}{2\pi f} \\ R_l = r_l \cdot Z_b \end{cases} \tag{2.24}$$

where, r_l is the resistance of the line reactor, Z_b is the base impedance of the line, X_l is the reactance of the inductive filter.

As a guiding value, in [34] and [43], the reactance of the phase reactor has been chosen to be 0.14 pu, while in [42] the inductance of the line reactor was 0.15 pu. A similar value is to be adopted in this project also, as in [34].

The resistance of the line reactor accounts for its internal resistance and also it can model the power losses of the PWM converter. As it is to be expected the per unit value is small compared to its reactance e.g. in [42] the reactor's p.u. resistance is 0.005.

The line reactor model used in this project is the build-in Series Reactor 'ElmSind', which has the following parameters:

- Reactance, X_L
- Resistance, R_L.

Power Transformers

Consider the proposed WF with the internal electrical grid as described in Figure 1.15 from Section 1.5. Depending on the position of each power transformer, several types of transformers are used. In all situations, the power transformer's main function is voltage level conditioning and galvanic insulation of the two connected circuits (if two winding three phase transformers are used). In this project, the build-in model power transformer[38] available in Power Factory DIgSILENT has been used.

The grid side and WF side PWM converters are connected to the AC system through a line reactor and a power transformer which transforms the voltage level to a suitable value required in the PCC and the common WF AC grid terminal, respectively. As mentioned before, the transformer has an important role in galvanic insulation of the WF system from the power grid and viceversa. Moreover, the reactance of the power transformer connecting the VSC - HVDC system must be taken into account when designing the control structure for the PWM converter. It is therefore, of interest to compute the total impedance, resistance and inductance of these two transformers, based on datasheet information as in Equations 2.25:

$$\begin{cases} Z_t = \frac{\Delta U_{uk} \cdot U_{rated}^2}{100 \cdot S_{rated}} \\ R_t = \frac{\Delta P_{CU} \cdot U_{rated}^2}{1000 \cdot S_{rated}} \\ X_t = \sqrt{Z_t^2 - R_t^2} \end{cases} \tag{2.25}$$

where ΔU_{uk} represents the short circuit voltage in per cent, ΔP_{CU} represents the copper losses in [KW], S_{rated} is the nominal apparent power of the power transformer in [KVA], U_{rated} is the nominal RMS voltage of the transformer in [V].

Regarding the power transformers situated in each of the WT systems, a special winding topology is always adopted in order to cope with voltage disturbances that may appear on the internal AC grid. In [41] a detailed study on the propagation of voltage sags and the influence

of the type of transformer winding is performed. As a conclusion, the power transformer type for WTs is usually $Y_n\Delta\angle 11$, the same configuration being selected in this project also. The transformer type for the grid side converter is a standard ΔY transformer.

AC Filters

The PWM converter used in this project is known to have unwanted harmonic currents injection in the power grid due to the switching of the valves and the 2 level architecture. It is therefore required the use of high pass AC filters for power quality conditioning. The AC filters are located on the AC side of each of the PWM converters as described in Figure 2.26.

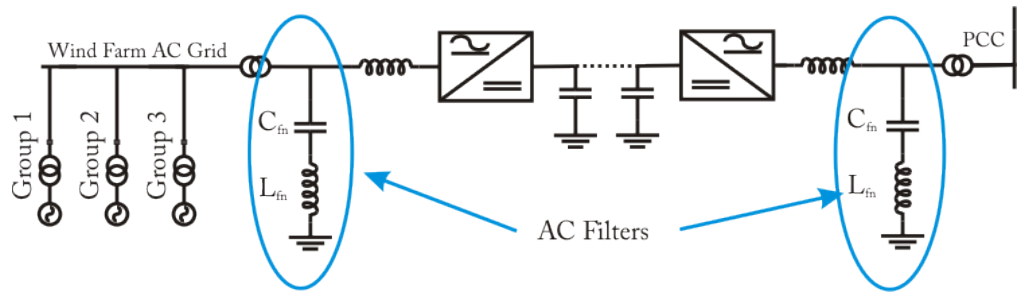

Figure 2.26.: AC Filters' positioning in WF

Therefore, tuning of these filters on the switching frequency and on multiples of this frequency is necessary. The filter's impedance associated for filtering the switching frequency and its close multiples is:

$$Z_0 = z_0 \cdot Z_b \tag{2.26}$$

where, z_0 is the impedance of the filters and Z_b is the base impedance of the line.
The converters inject harmonic currents of order:

$$n = k \cdot p \pm 1 \tag{2.27}$$

where, p is the number of pulses of the converter, $k = 1, 2, 3, \ldots$.
The harmonic frequency corresponding for each order is:

$$f_n = n \cdot f_{sw} \tag{2.28}$$

where, f_{sw} is the PWM switching frequency of the converter.
The design parameters for the AC filters are given below:

$$\begin{cases} L_{fn} = \frac{Z_0}{2\pi f_n} \\ C_{fn} = \frac{L_{fn}}{Z_0^2} \end{cases} \tag{2.29}$$

In the actual model, the first, second and third order harmonic filters have been implemented. In Appendix C.1 the calculus corresponding for each order AC filter is detailed.

Dynamic and Static Loads

In this project, for modelling various types of loads, the build-in 'General Load Model' has been used[39] and shown in Figure 2.27. In the case of high voltage transmission the

load concept represents entire MV-feeders or a combination of dynamic and static loads. In stability simulations, a three phase load is modelled using a constant impedance for the static load and a linear or non-linear dependency for the dynamic load.

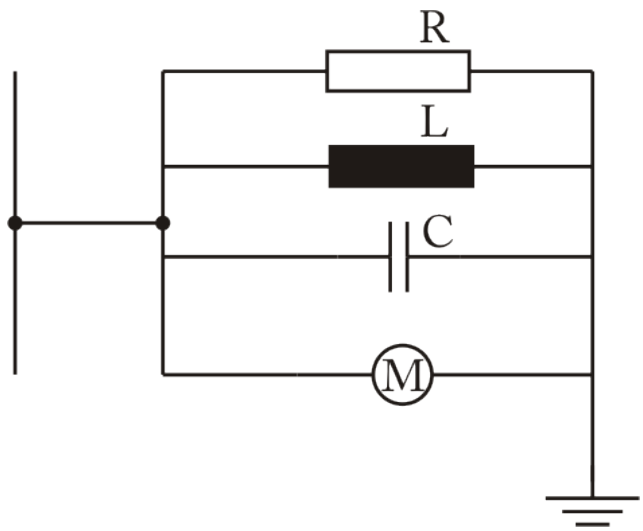

Figure 2.27.: General load model (as described in [39])

2.4.3. DC Components

The DC components of the HVDC transmission system are briefly discussed. Build-in models available in Power Factory DIgSILENT have been used for each of the components: DC link capacitors and DC cable. Dimensioning and proper sizing details are discussed in the following subsection.

DC Link Capacitors

The DC capacitors have an active role in keeping the DC link at constant voltage, acting as energy storage devices that regulate the power flow. Two DC capacitors are installed usually on the DC line, one at the 'sending end' station and another one at the 'receiving end' station. A balanced DC line implies the use of capacitors with the same capacitance at both ends. The size of these capacitors is related to the rated DC line voltage and the accepted ripple level on the line caused by the PWM switching pattern. The dimensioning of the DC bus capacitance has been performed as in [43] and follows.

The DC link voltage controller bandwidth is calculated based on :

$$\omega_l = 2 \cdot \pi \cdot 30 \backsimeq 188[rad/sec] \tag{2.30}$$

The nominal damping for ripple has been selected to be:

$$\zeta_n = \frac{\sqrt{2}}{2} \tag{2.31}$$

The relative converter voltage drop at rated power:

$$\delta_n = 0.05 \tag{2.32}$$

The DC link total required capacitance for stable operation of the HVDC system is calculated on the basis of the parameters previously mentioned in 2.30, 2.31, 2.32:

$$C_{DC} = \frac{P_{rated}}{V_{DC}^2} \cdot \frac{2 \cdot \zeta_n^2}{\omega_n} \cdot \frac{1}{(1-\delta_n) \cdot \delta_n} \tag{2.33}$$

where V_{DC} is the rated DC voltage.

This capacitance will be split in two, each of the 'sending end' and 'receiving end' capacitors having the following capacitance:

$$C_{DCr} = C_{DCs} = \frac{C_{DC}}{2} \tag{2.34}$$

where C_{DCr} and C_{DCs} are the 'receiving end' and 'sending end' capacitances respectively.

In this project, the DC capacitors have been implemented using the build-in model available in DIgSILENT - 'ElmShnt' [40].

HVDC Cable

The DC cable model in Power Factory DIgSILENT allows modelling the line as a Π model (Figure 2.28) or a series of Π models (Figure 2.29). In the single Π line model, R_s is the total line resistance, L_s is the total line inductance, C_s and C_r are the equivalent line capacitances at the beginning and at the end of the line. In Power Factory DIgSILENT, when considering more Π sections, it is assumed that the segments are equivalent e.g. length and line parameters. From the point of view of calculating the power losses on the DC cable and its overall dynamic performance, as it is the case in this project, the single Π line model is sufficient.

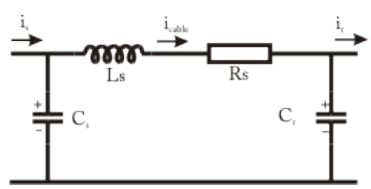

Figure 2.28.: Standard Π line model

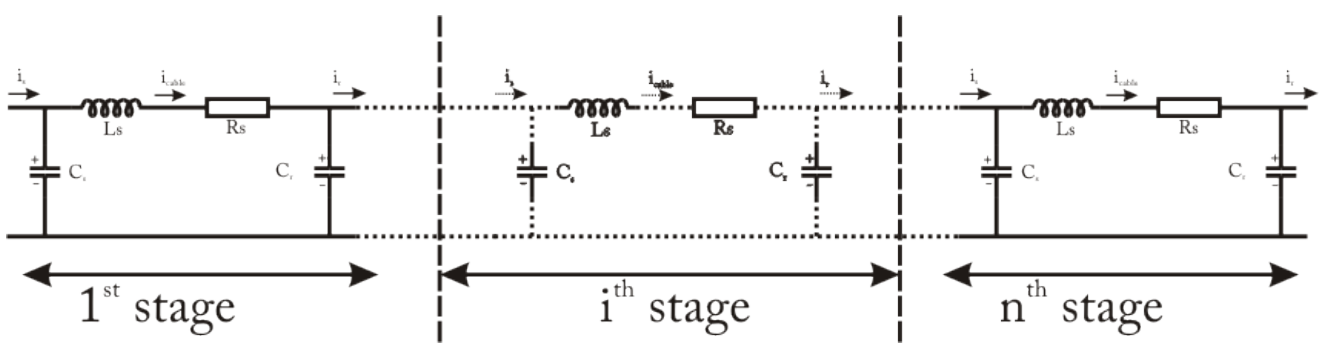

Figure 2.29.: Π line model with n sections

The parameters of the DC line have been set based on DC voltage and current ratings and chosen from datasheet catalogs (see Appendix C.1). The cable parameters must fulfill

certain requirements, as explained in [43], and defined by Equations 2.35:

$$\begin{cases} R_s < \frac{V_{DC}^2}{4P_n} \\ R_s > \sqrt{\frac{L_s}{C_s}} \end{cases} \tag{2.35}$$

DC Chopper Implementation

The use of a DC chopper on the DC bus system is commonly used as an emergency solution when certain amounts of wind power cannot be transferred any more into the main power grid. Such is the case also for large scale wind farms connected through VSC HVDC systems[53]. One possible scenario is the low voltage grid fault that, depending on the voltage level will seriously affect the grid side converter's ability to transfer power into the main power grid. Dangerous DC voltage levels may be expected if the power in excess is not redirected.

The DC Chopper is located in the grid side converter station and is designed to provide DC power evacuation into so called dumping resistors, which are specifically designed to withstand easily the rated DC current for a certain amount of time. The resistors can absorb the rated power of the WF for a specified period. Typical values for this time interval are in the order of seconds, long enough to permit the WF controllers to reduce its output power to zero. Safe operation of the WF system is thus achieved in the case of faults in the main power grid. A simple diagram of the DC Chopper is depicted in Figure 2.30. In this project, the main purpose has been to create a simple emergency DC voltage regulation system that consequently regulates the DC power and transfers it into an ideal power sink. Therefore, since the purpose of the project is not in depth modelling of the DC chopper, a similar, yet more simple to implement, system has been implemented in this project.

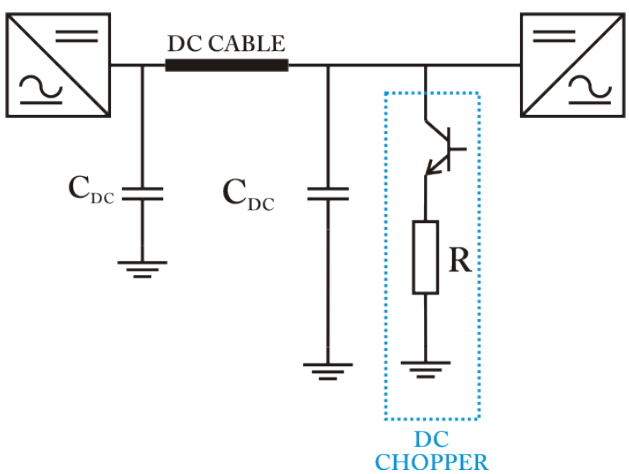

Figure 2.30.: Ideal DC Chopper model

Power Factory does not provide dynamic loads that can be connected on the DC bus, therefore the only available solution is to transfer the DC power through a converter into AC and only then use a AC power consumption model. For simplifying the design, the DC power evacuation model implemented in DIgSILENT has been made using a PWM DC/AC converter having the same power and voltage ratings as the other two converters and designed with the following considerations:

- the DC power evacuation model is regulating the DC power only when the DC voltage

exceeds 1.1 pu, therefore only in case of faults;

- the power flow on the AC side is balanced by an ideal energy absorption system e.g. dynamic AC load or very stiff AC grid build-in model.
- there is a linear dependency on the voltage at the AC mains of the converter and the dynamic load;

A simple ideal energy sink system has been connected on the AC side of the PWM converter with a voltage dependency as in Figure 2.31.

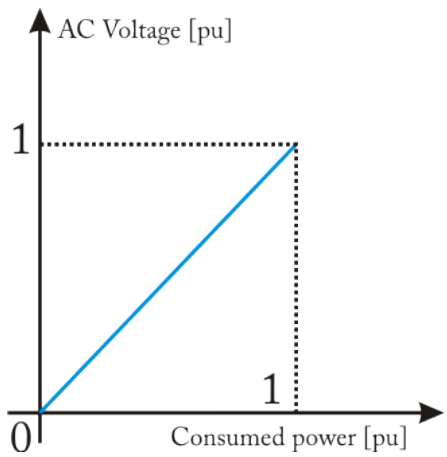

Figure 2.31.: Voltage dependency of the dynamic load

Voltage dependency in DIgSILENT can using a potential approach[39] as in Equation :

$$P = P_0(\frac{V}{V_0})^{kpu} \tag{2.36}$$

where P_0 and V_0 are the initial operating values as defined in the dialog box of the element, P and V the current values in the simulation and kpu the exponential coefficient.

By using this simple system, all the excess energy from the DC side is transferred directly in the "dump load" (the stiff external grid) with virtually infinite capacity. Therefore, for modelling more realistically this system, a time utilization limit of the DC power evacuation system has been set.

2.5. Summary

An overview of the main blocks used in the modelling process and a brief description of the chosen wind farm layout and of the HVDC transmission system has been presented in this chapter. A detailed description of the models that have been developed is also present. Brief simulation results are shown in order to provide more understanding on the behaviour of each developed block. The models defined in this chapter are used throughout the report, the information presented being the knowledge base of the modelling and dimensioning of the proposed WF system. The developed models correspond to a simulation platform that can be used for stability (RMS) analysis.

3. Control Architecture and Design

This chapter is focused on describing the control techniques implemented in DIgSILENT Power Factory. The first part presents the control of one wind turbine - the pitch control and also the wind turbine side of the full scale power converter. The second part of this chapter describes the control elements modeled for the transmission system, from the wind farm part to the onshore side. Several simulations are performed in order to verify and validate the models.

A two level control system is implemented in this project as described in Figure 3.1. The WF controller is at the user control level, thus all external or manually set references in the Power Plant are integrated in this block. The lower level controllers, called the equipment controllers are mainly consisting of the pitch angle controller corresponding to each reduced model of WTs, the WF and Grid side converters controllers.

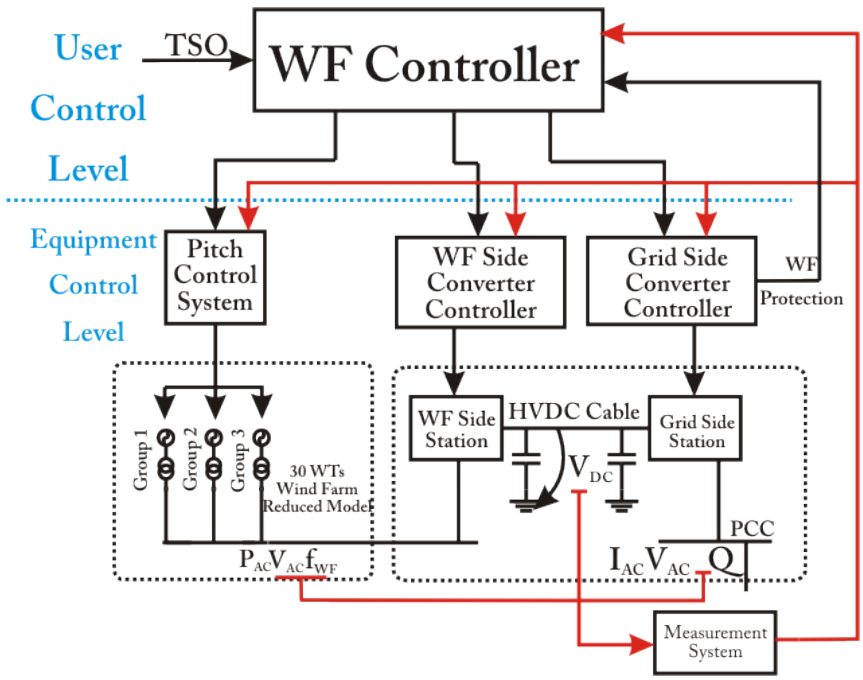

Figure 3.1.: Control architecture of the WF and transmission system

3.1. Wind Farm Controller

The WF Controller implements a number of functions that coordinate and protect the reliable operation of the WF. One function is the fulfillment of the grid code requirements regarding the active and reactive power control. Thus, for active power control, all the constraints schemes have been implemented. Also, the TSO must be allowed to set references of the reactive power balance in the PCC. Protection measures of the WF are included in this control block also. Low voltage ride through capability is implemented at this stage by

controlling the Grid and WF side converters appropriately. Therefore, the WF controller represents the interface between the WF and the TSO's requirements. The WF controller has the block diagram as in Figure 3.2 and has been implemented in Power Factory DIgSILENT using DSL.

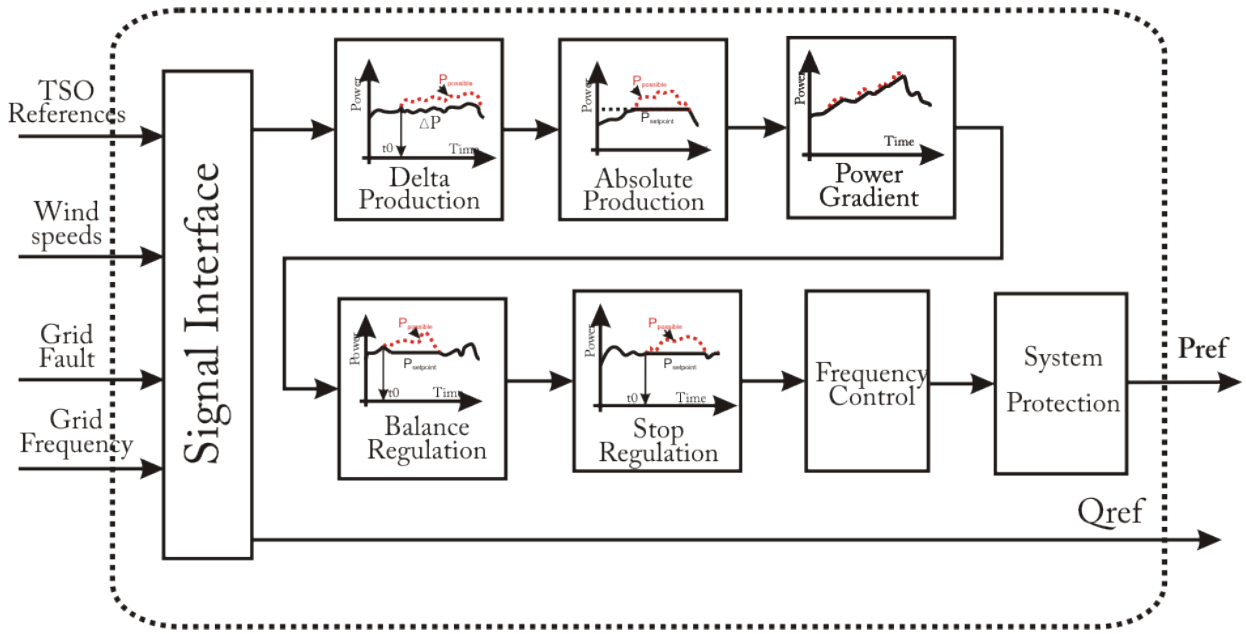

Figure 3.2.: WF Controller block diagram

The WF controller's inputs are measurement parameters (wind speeds, AC grid frequency etc) and references provided by the TSO (delta, absolute, stop, balance regulation constraints, reactive power setpoints in the PCC) and implemented in this simulation platform using user defined text files. Also, for power system protection reasons, error signals are received from the grid side converter control block. The output signals are active power reference to the pitch controllers of the WT systems and reactive power reference to the grid side converter. A brief description of each of the active power control blocks of the WF controller follows, the order being similar with the function priority defined in the grid code, from low to high.

The Delta Production Constraint is intended to provide the WF with active power reserve capability that may be available at any time there is still wind power high enough to cover the required reserve. In case of emergency situations (outage of one generating unit) the reserve power can be generated into the main power grid and regulate the power imbalance. Assuming small power coefficient variations for wind speeds smaller than the rated wind speed a simple algorithm that evaluates the available wind power using the cubic relationship of $P_{WT}(v_\infty^3)$ from Section 2.2.2, Equation 2.2 has been implemented in this block. The active power reserve margin is modelled in the simulation as a time varying input parameter P_{delta} in the range of 0 to 1 per unit. The reference power is thus calculated using Equation :

$$P_{ref_{delta}} = P_{available} - P_{delta} \tag{3.1}$$

where $P_{available}$ is estimated as Equation 3.2 if $v_\infty < v_{\infty rated}$ or as Equation 3.3 if $v_\infty > v_{\infty rated}$:

$$P_{available} = \frac{v_\infty^3}{v_{\infty rated}^3} \tag{3.2}$$

$$P_{available} = 1 \tag{3.3}$$

The grid code also describes a stop and absolute power regulation constraint that must be available in the WF controller. These active power constraints can be integrated into a single algorithm from the point of view of simulating power system stability over relatively long time frames. These regulation functions are used at TSO's specific requirement and should result in a constant power output equal with the initiating moment of the algorithm. A simple limiter with memory of the initial power reference has been set in the WF power controller block.

A smooth power reference output is required at the output of WF power controller in normal operating conditions. It is therefore necessary to implement a power gradient constraint designed to limit the change in reference power $P_{ref_{in}}$ with a specific slope determined by T_{grad}, the time gradient constraint related to the per unit rated power. Usually the WF is not allowed to change it's power output with more than 0.1 pu per second of the rated power[5]. The implemented gradient block is a linear function with one variable stat, x_{grad}, as in Equation 3.4:

$$\begin{cases} \frac{dx}{dt} = \frac{P_{ref_{in}} - x_{grad}}{T_{grad}} \\ P_{ref_{grad}} = x_{grad} \end{cases} \tag{3.4}$$

where $P_{ref_{grad}}$ is the power reference output for each iteration step of the simulation.

In [4, 5] it is required that the WF must be able to vary its active power output according to the grid frequency as exemplified in Figure1.3 from Section 1.3.1. This requirement has been implemented in the Frequency Control block. The power setpoint for nominal grid frequency and the associated deadband can be modified according to the TSO's specifications. The default parameters from the grid code are mentioned in Appendix D.1, Table D.1 and have been also used in the active power / frequency control.

The following relations (Equation 3.5), implemented in the control algorithm of the frequency control block, describe the reference power $P_f(f_{meas})$ dependency from Figure 1.3, Section 1.3.1:

$$P_f = \begin{cases} -\frac{P_{ref} \cdot P_{stp}}{f_\phi - f_{d+}} \cdot f_{meas} + \frac{P_{ref} \cdot P_{stp}}{f_\phi - f_{d+}} \cdot f_\phi, \quad if : f_{meas} > f_{d+} \\ P_{ref} \cdot P_{stp}, \quad if : f_{meas} \div [f_{d-}, f_{d+}] \\ -\frac{P_{ref} \cdot P_{stp}}{f_{d-} - f_n} \cdot f_{meas} + \frac{P_{ref} \cdot P_{stp}}{f_{d-} - f_n} \cdot f_{d-}, \quad if : f_{meas} < f_{d-} \end{cases} \tag{3.5}$$

where P_{ref} is the per unit power provided by the previous active power control block, P_{stp} is the per unit power reference setpoint for stable operation within the frequency deadband, P_f is the per unit power reference calculated by the frequency control block, f_{meas} is the actual per unit measured frequency at each iteration step, f_n is the per unit lower frequency limit for the control range during under-frequency, f_ϕ is the per unit upper frequency range for the control range during over-frequency, f_{d-} is the per unit lower frequency limit for the deadband during under-frequency, f_{d+} is the per unit upper frequency limit for the deadband during over-frequency. The per unit values are calculated using the reference grid frequency F_{ref}. The frequency measuring point for f_{meas} is chosen to be the PCC.

The power system protection feature is used whenever faults arise in the power system and its stability depends on the rapid shutdown of all active power generation machines. Only

voltage dips below the rated minimum line voltage in the PCC are taken into consideration in this project. The system protection must therefore rapidly support the avoidance of power system collapse. For example, in the power gradient block a very small regulating time constant T_p is selected in order to decrease faster the WF active power generation e.g. shutdown from rated to zero power in the interval of a couple of seconds. In the moment of activation of the protection system, a zero power input reference is fed to this block, and therefore, rapid WF shutdown of active power generation is achieved.

3.2. Equipment Level Controllers

This section is covering the design of the control system for the WT pitch angle, the WF and Grid side converters. These are the main components that play an active role in regulating the power output of the WTs and the behaviour of the entire WF when subjected to disturbances from the grid.

3.2.1. Pitch Control System

The purpose of the Pitch Controller has been initially to limit the power output of the WTs when the wind speeds are higher than the rated as it can be seen in Figure 3.3. Nowadays, due to newer grid codes, the pitch control system is required to control the pitch angle even at lower wind speeds than the rated. The active power constraint schemes, mentioned in Section 1.3.1 and implemented in the WF controller of Section 3.1, are responsible for setting power references to the reduced model WF pitch controller in the entire possible interval:

$$P_{ref} = 0 \div 1[pu] \tag{3.6}$$

Therefore, in the specific case of this project for the three reduced models implemented, there will be three corresponding pitch controllers with their own power references, although only small differences between these setpoints will occur due to the variation of wind speeds from the average value.

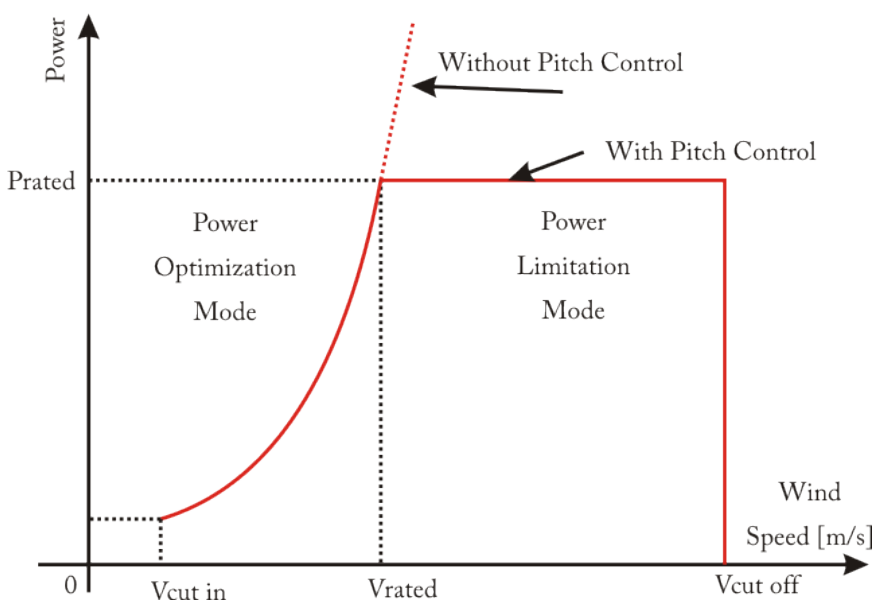

Figure 3.3.: Operation of the Pitch Control System for high wind speeds

The block diagram of the Pitch Controller has been presented in Section 2.2.4, Figure 2.20. The system is basically a PI controller and a first-order system representing the pitch servo mechanism. The actuator system accounts for the time delay that is introduced in the control algorithm and its transfer function is expressed in Equation 3.7:

$$H_\theta = \frac{1}{sT+1} \tag{3.7}$$

The PI controller has the following governing transfer function as in Equation 3.8:

$$H(s) = K_\theta(1 + \frac{1}{sT_\theta}) \tag{3.8}$$

The defining parameters are the system gain K_θ, and the PI's time constant T_θ. In [11], gain scheduling techniques have been applied to the controller's gain in order to perform better for high wind speeds by decreasing the proportional gain as the wind speed increases. In this project, a simplifying approach has been taken: a simple PI controller is implemented with satisfying results, therefore no gain scheduling of the proportional PI parameter, K_θ, has been further developed. The base values defined in [11] have been adopted for the PI controller's proportional gain and integral gain as defined below:

$$\begin{cases} K_\theta = 34.5 \\ T_\theta = 0.1 \end{cases} \tag{3.9}$$

Assessment of the performance of the pitch controller has been done by analyzing the pitch angle variation for wind speeds mostly in the limitation mode range and with a high average wind speed variation as described in Figure 3.4. High input power variations are expected due to such high variations in the wind speed. As it can be seen in Figure 3.5, the power output of the wind turbine stays within the control band with relatively small overshoots of 0.04 to 0.05 pu when the wind speed just increases above the rated. In the simulations a small value for the T_{servo} has been used (see Figure 3.6), ensuring thus a good responsiveness from the pitch controller.

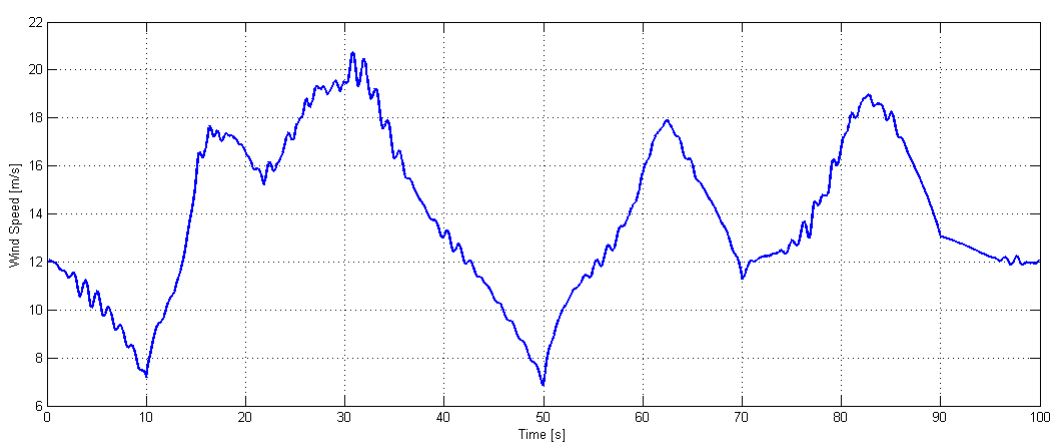

Figure 3.4.: Wind Speed variation applied to the pitch control system

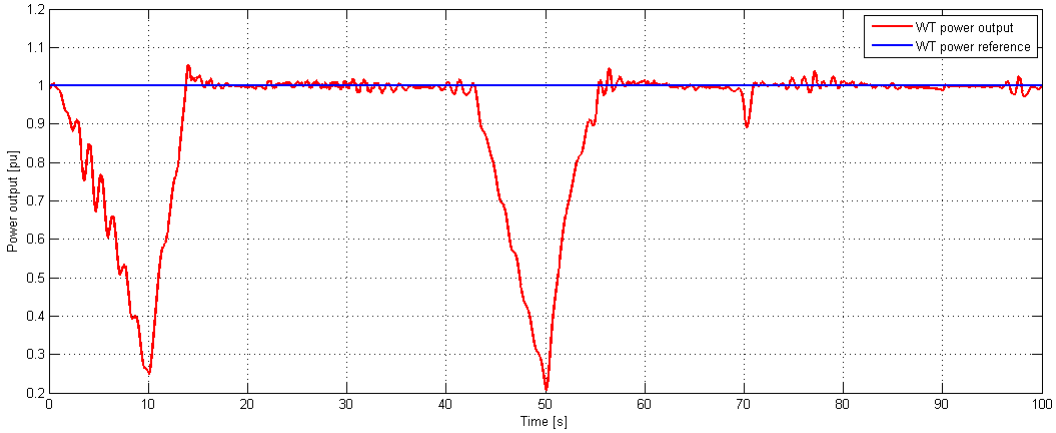

Figure 3.5.: Power output of the WT system

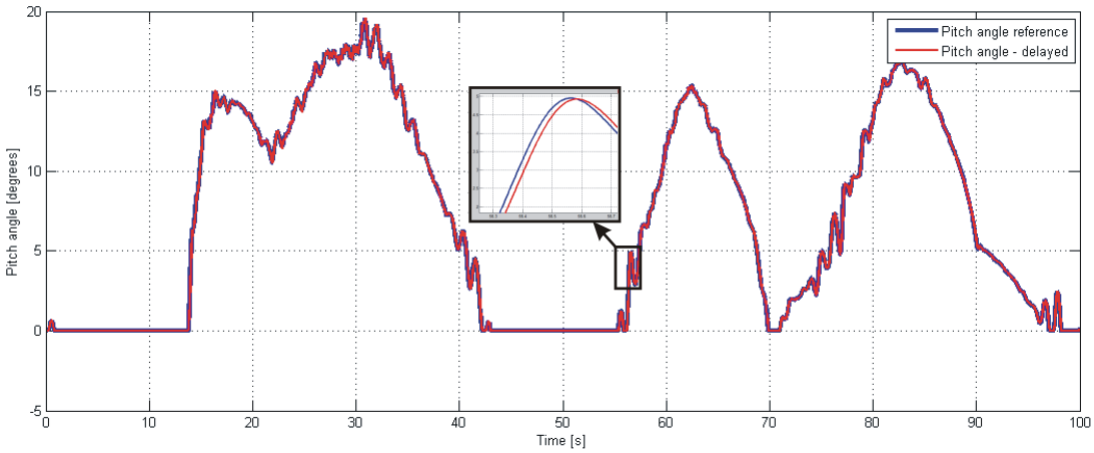

Figure 3.6.: Pitch angle variation of reference and actual

3.3. Control Design for Transmission System

Dynamic simulation of the Wind Farm is preceded in Power Factory DIgSILENT by the evaluation of the system states and the successful steady state initialization process. A requirement for making possible the calculus of the grid's steady state is an initial load flow iteration. Figure 3.7 presents the node assignment for each system component that has an active role in the load flow process. The external grid is assigned the grid balancing role - slack bus - controlling the AC voltage amplitude and angle at the reference setpoints. The grid side converter station is responsible with the DC voltage control and the reactive power balance in the PCC. The WF side converter station is slack bus in the WF internal grid, while the asynchronous machines are P-Q nodes[44].

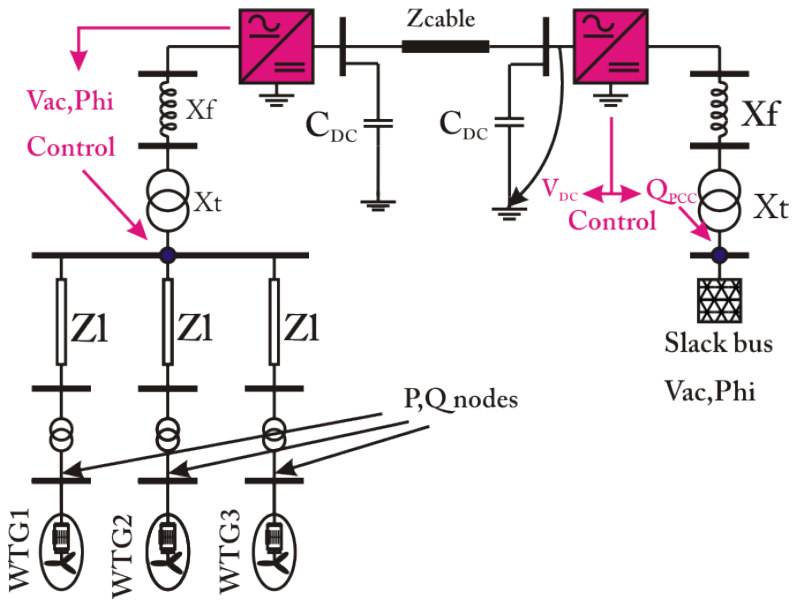

Figure 3.7.: Load flow control nodes in Wind Farm

3.3.1. WF Side Converter Control

As described in Section 2.4.2, the WF side converter is responsible with controlling the AC voltage and frequency in the internal AC grid of the WF. A method to control the fore mentioned parameters is needed. The control structure adopted for the WF controller is based on [11] and presented in Figure 3.8.

The constant voltage / frequency ratio control block is used for varying the frequency in the internal grid of the WF with the purpose of varying the generator synchronous frequency in a simple and reliable method, thus maximizing power output from the WF in the optimization range of wind speeds. The internal grid can be viewed as a microgrid and therefore voltage and frequency stability can be achieved using voltage and frequency droop control[46]. Using the voltage reference two PI controllers are employed for voltage and current regulation respectively. The PWM modulation index and the frequency setpoints are the parameters fed to the WF converter. Variables $\mid M \mid$ and f_0 can be adjusted independently by the VSC converter to give any combination of voltage magnitude and phase as desired to maintain the grid balance.

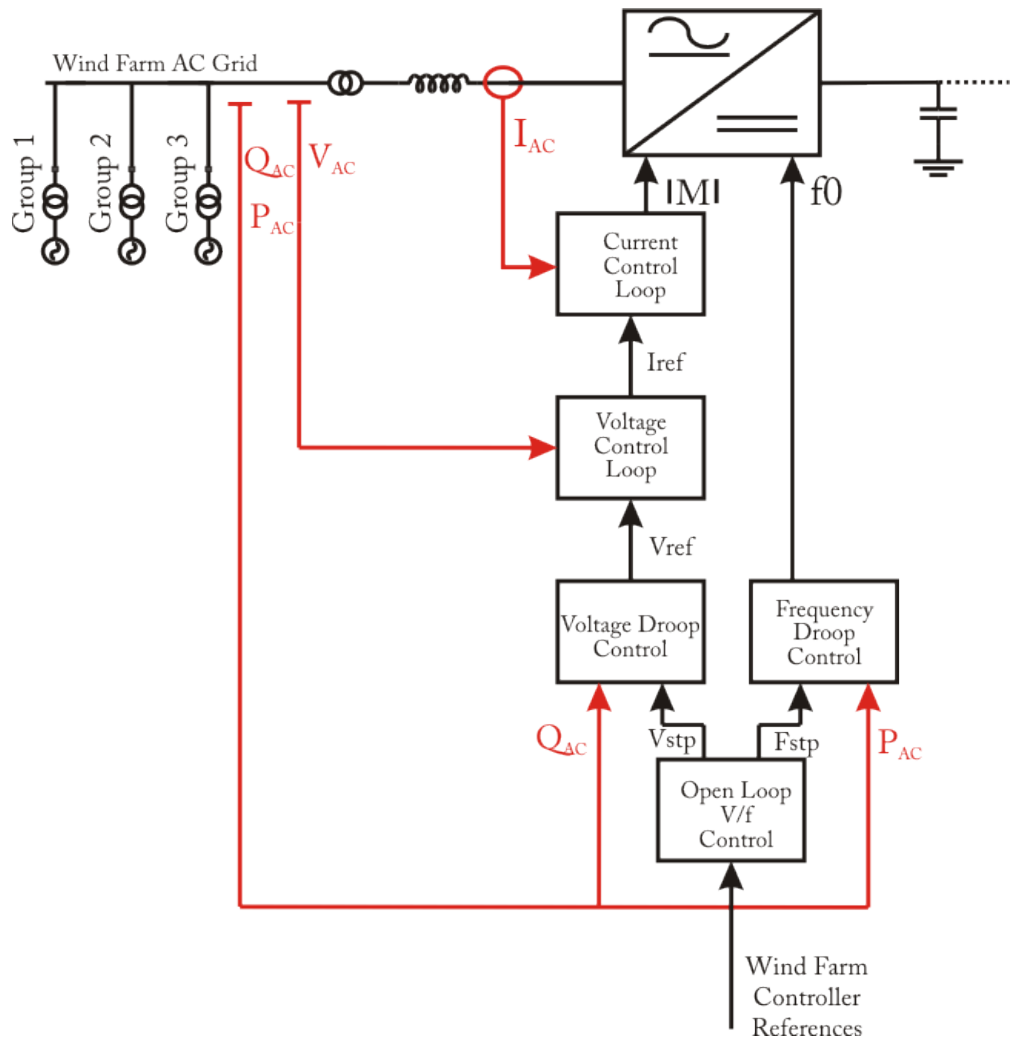

Figure 3.8.: WF Side Converter Control block diagram

Scalar Control of Induction Generator - Constant Voltage / Frequency ratio

The WT system is generating power depending on the wind speed and the power coefficient $C_p(\lambda, \theta)$ as in Equation 2.2. When strictly considering wind speeds lower than the rated value, the pitch controller is keeping the pitch angle to zero in order to maximize power output due to the position of the WT blades. The WT rotor speed Ω_r is expressed in steady state operation in relation with the generator's high speed ω_g as in Equation 3.10:

$$\Omega_r = \frac{\Omega_g}{K_g} \tag{3.10}$$

where K_g is the drive train speed ratio.

The electromechanical torque available at the generator shaft and its dependency with voltage and frequency is expressed in Equations 3.11 and 3.12 respectively[54].

$$T_{base} = \frac{P_{base}}{\Omega_g} = \frac{P_{base} \cdot 60}{2\pi \cdot n} \tag{3.11}$$

$$T_{base} = \frac{\eta \cdot \sqrt{3} \cdot V \cdot I \cdot cos\varphi \cdot 60}{2\pi \cdot f \cdot \frac{60}{p} \cdot (1-s)} = k \cdot \frac{V}{f} \tag{3.12}$$

Therefore, steady state operation can be achieved by varying the voltage and frequency at the generators mains with a constant ratio between them. When fixed speed operation of the WT induction generator is chosen with a grid tied synchronous frequency, a non optimum power extraction point is achieved. This phenomena can be observed in Figure 3.9 as the intersection points of the power curves with the vertical red line, where only several wind speeds have been plotted for exemplification. The actual maximum power extraction is achieved for variable frequency operation in the intersection points of the black line with the power curves.

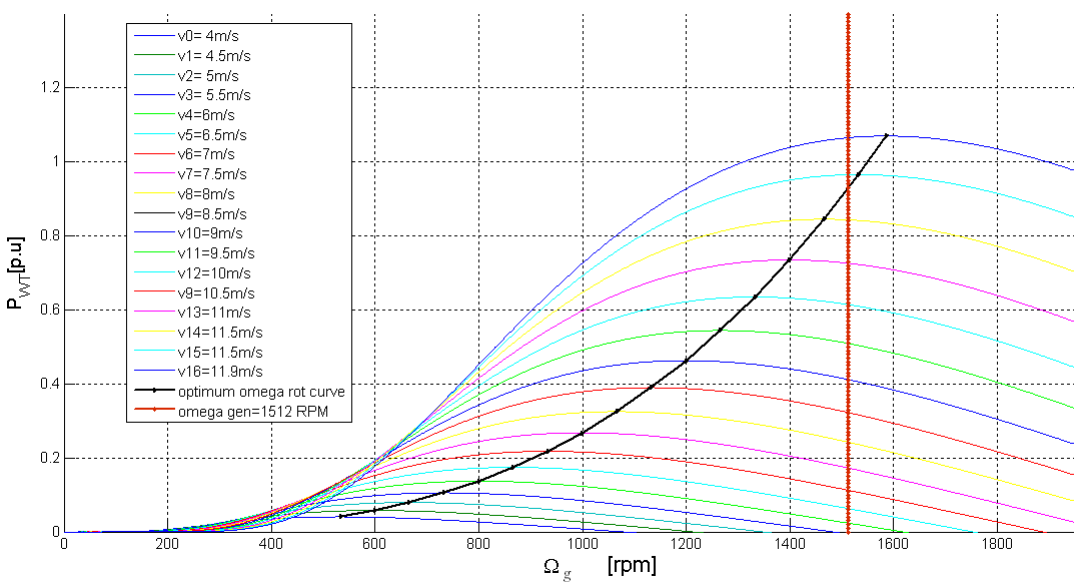

Figure 3.9.: Generator power output in relation with Ω_g for various wind speeds[11]

Constant voltage versus frequency ratio control is the simplest method of controlling the induction generator's speed. This speed can be controlled using a reference setpoint provided by the wind speed instantaneous value and calculated so as to provide better wind power extraction. Basically, the scalar V/f control represents feeding the generator with a 3-phase voltage that has an amplitude proportional to the applied frequency. Two exceptions apply to this linear performance as can be seen in Figure 3.10. In practical applications, the V/f slope is calculated based on the rated terminal supply voltage and frequency from the generator's datasheet.

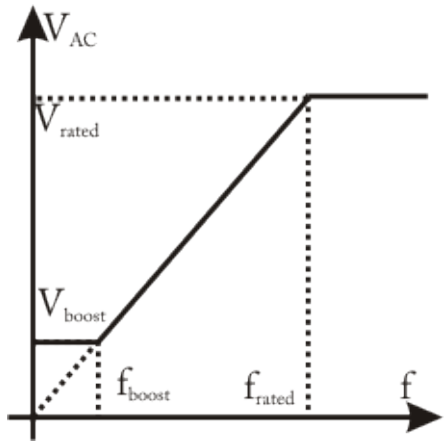

Figure 3.10.: Scalar V/Hz control

The boost frequency f_{boost} is usually chosen as a percentage of this value, depending on the actual requirements of the WT, thus obtaining optimum power. The values for the V_{boost} and f_{boost} have been previously calculated in [11] and a generator frequency versus wind speed dependency as in Figure 3.11 has been determined for maximum power point tracking.

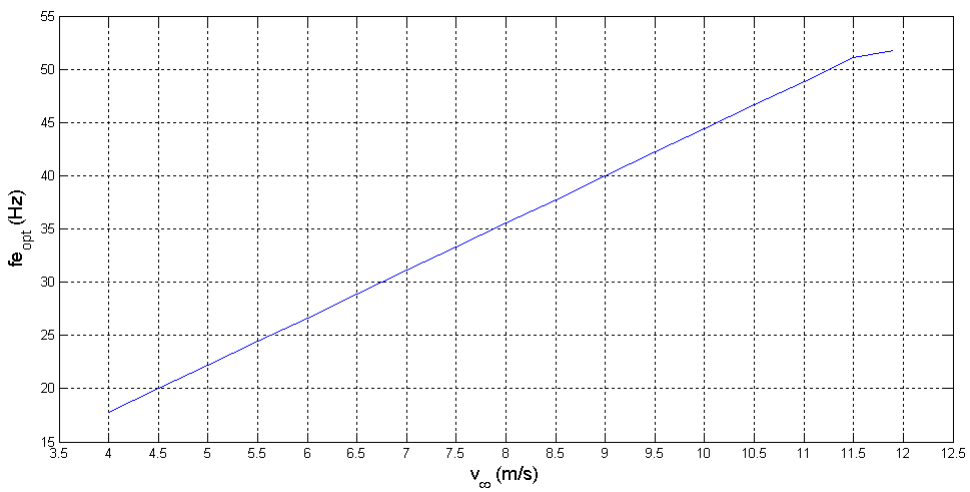

Figure 3.11.: Optimum frequency for the optimization wind speed range

By continuously calculating a weighted average of the wind speed $\tilde{v}_\infty$ for the WF as in Equation 3.13, an optimum frequency set-point can be calculated.

$$\tilde{v}_\infty = \frac{v1_\infty \cdot P_{3\infty} + v2_\infty \cdot P_{2\infty} + v3_\infty \cdot P_{3\infty}}{(P_{1\infty} + P_{2\infty} + P_{3\infty})} \tag{3.13}$$

where $P_{i\infty}$ is the available wind power for the WT group $i = 1 \div 3$.

The frequency setpoint is used both for setting the reference frequency and voltage, thus keeping their ratio constant. By including in the calculus the available wind power, a much better average wind reference value is obtained for power optimization. The optimum frequencies range between minimum 17 and maximum 53.3 Hz for the optimization speed interval. A gradient limiter is also implemented with a time constant in the range of a couple of seconds in order to filter out any sharp variations in frequency and voltage reference. Limits apply for the reference voltage in order not to exceed 1 per unit or drop below the boost value.

Internal Grid Voltage Droop Voltage stability in the internal AC grid is dependent on the demand of reactive power required by the asynchronous generators[46]. The demand of reactive power is different depending on the wind speed at that moment therefore, by applying a voltage droop characteristic, the PWM converter will insure the stability of the voltage in the grid. In other words, voltage control has the essential purpose of limitting the reactive currents in the internal grid. Small errors in the voltage references lead to large errors in the currents.The voltage reference applied to the outer voltage loop is defined by the variation of the AC voltage with the measured reactive power as in Equation 3.14 and shown in Figure 3.12:

$$V_{ref} = V_{stp} + k_v \cdot Q_{meas} \tag{3.14}$$

where:

k_v is the voltage droop coefficient

V_{stp} represents the voltage set-point fed by the V/f control system.

The voltage droop coefficient is in the range of 0.03 to 0.05[34]. For voltage references above the setpoint value, the PWM converter system consumes reactive power while for smaller values there is reactive power generation in the WF internal grid.

The voltage reactive power droop :

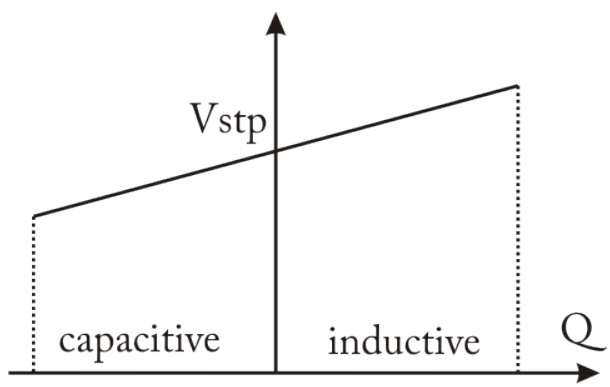

Figure 3.12.: Voltage - Reactive power droop characteristic

Internal Grid Frequency Droop

The frequency active power droop developed in [34] is ensuring stable active power operation within the internal WF grid, as in Figure 3.13:

$$f_{ref} = 1 - K_f(1 - P_{meas}) \tag{3.15}$$

where: K_f is the droop coefficient for frequency, $K_f = \frac{\Delta f}{\Delta P}$.

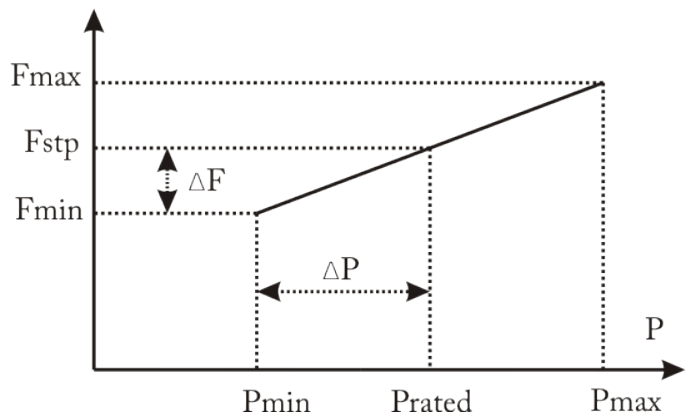

Figure 3.13.: Frequency - Active Power droop characteristic

Voltage and Current Control Loops

The voltage and current control loops are implemented using standard PI controllers as it can be observed in Figure 3.14.

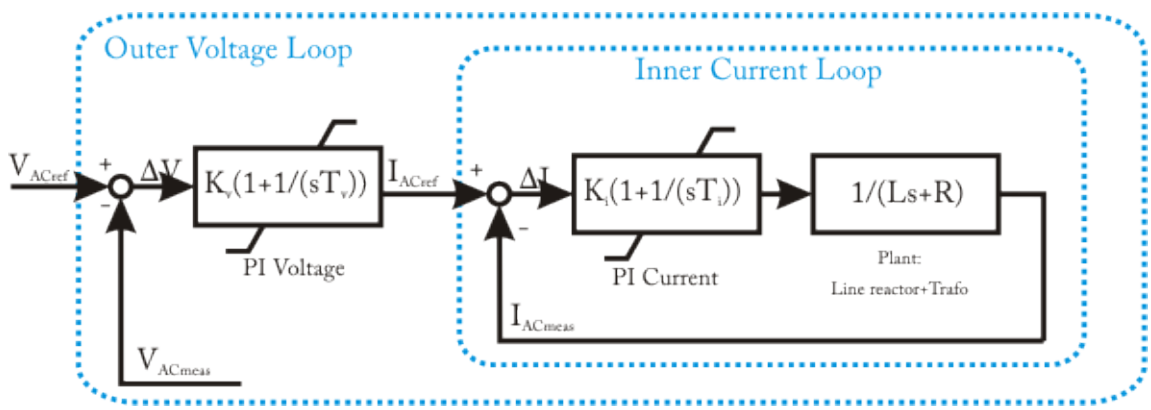

Figure 3.14.: Inner current and outer voltage loops

The inner current controller ensures fast tracking of the measured AC current amplitude.

3.3.2. Grid Side Converter Control

The grid side converter control system is based on a power systems modelling approach of simulating a steady-state (RMS) network model for mid term and long term transients under balanced network conditions developed in Power Factory DIgSILENT. This model is only valid for symmetrical faults in the electrical grid[55]. Furthermore, for simulating stability phenomena, the electrical grid is calculated using phasors. The passive electrical network is modelled as a symmetrical, steady state representation in DIgSILENT and therefore, the fundamental components of the variables in this system (currents, voltages etc) are calculated[55]. This simplification yields conservative results, but is necessary in order to deal with the analysis of large-scale power systems. For the purpose of studying the interaction between the WF and the external grid in a balanced RMS simulation the following events may be studied:

- mid term stability of the power flow in the AC grid;

- voltage stability in the PCC and the DC bus transmission system;
- active and reactive power compliance of the WF with the TSO's dynamic requirements;
- symmetrical short circuit events;
- power plant shutdown or loss of generation capacity.

For the purpose of controlling the fundamental components of the currents and voltages (real, imaginary) the control system in Figure 3.15 has been developed.

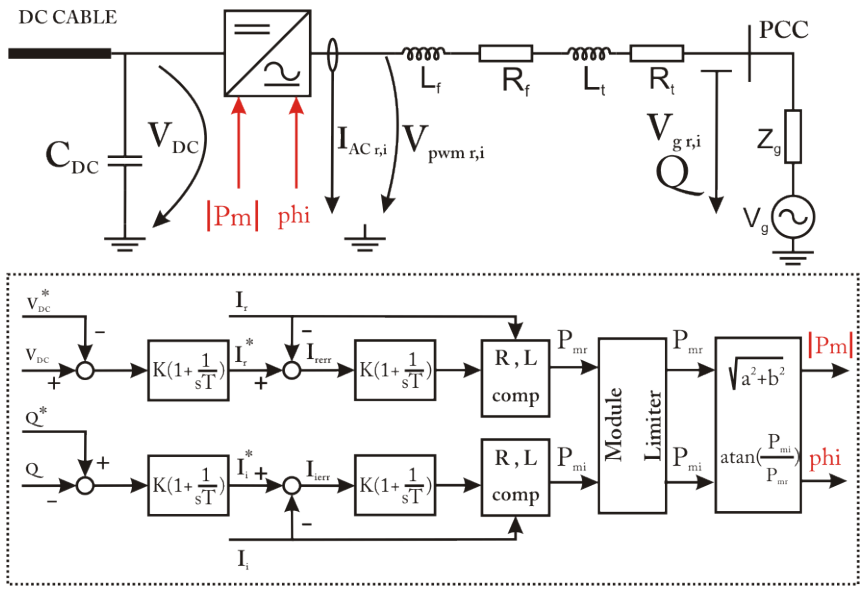

Figure 3.15.: Grid Converter control structure

In Figure 3.15 the control point for the AC side is normally the PCC, where the controlled parameter is the reactive power balance. The DC voltage must be also controlled by the grid side converter.

The following assumptions have been taken in the control model:

- only positive sequence components are considered, therefore the system is assumed to be operating in balanced conditions;
- the voltage phase angle θ_{PCC} in the PCC to which all the calculations are referenced is zero.

Several control schemes have been developed in stationary reference frame [47, 48, 50, 51, 52] containing decoupling methods for the imaginary and real current components. By using the power system representation approach of the electrical quantities (phasors) and defining the controlled node of the grid side converter to be the reference point of the voltage phase angle, a decoupled control scheme is available. Power Factory DIgSILENT provides the facility of developing such a system. In what follows, the control algorithm is deduced from the voltage drop of the line reactor in Figure 3.15. The individual inductances and resistances of the line L_f, R_f and transformer L_t and R_t have been combined in the lumped parameters L_r and R_r. Using these simplifying notations, the per phase voltage drop between the PWM converter and the PCC can be calculated as in Equation **??**:

$$v_{pwm} - v_g = L_r \cdot \frac{di_{AC}}{dt} + R_r \cdot i_{AC} \tag{3.16}$$

where lowercase letters denote the instantaneous parameters of the AC current I_{AC} , the PWM converter voltage V_{pwm} and the grid voltage V_g.

Consequently, Equation 3.17 represents the matrix form of the previous equation expanded for all three phases:

$$\frac{d[i_{AC}]}{dt} = [A][i_{AC}] + [B][v_{pwm}] + [C][v_g] \tag{3.17}$$

where:

$$[i_v] = \begin{bmatrix} i_{ACa} \\ i_{ACb} \\ i_{ACc} \end{bmatrix}; [v_{pwm}] = \begin{bmatrix} v_{pwm_a} \\ v_{pwm_b} \\ v_{pwm_c} \end{bmatrix}; [v_g] = \begin{bmatrix} v_{g_a} \\ v_{g_b} \\ v_{g_c} \end{bmatrix}$$

$$[A] = \begin{bmatrix} -\frac{R_r}{L_r} & 0 & 0 \\ 0 & -\frac{R_r}{L_r} & 0 \\ 0 & 0 & -\frac{R_r}{L_r} \end{bmatrix}; [B] = \begin{bmatrix} \frac{1}{L_r} & 0 & 0 \\ 0 & \frac{1}{L_r} & 0 \\ 0 & 0 & \frac{1}{L_r} \end{bmatrix}; [C] = \begin{bmatrix} -\frac{1}{L_r} & 0 & 0 \\ 0 & -\frac{1}{L_r} & 0 \\ 0 & 0 & -\frac{1}{L_r} \end{bmatrix}$$

Transforming equation 3.17 to α, β stationary reference frame using Clark transformation from Appendix D.3,

$$\frac{d}{dt}\begin{bmatrix} i_{ACr} \\ i_{ACi} \end{bmatrix} = \begin{bmatrix} -\frac{R_r}{L_r} & 0 \\ 0 & -\frac{R_r}{L_r} \end{bmatrix}\begin{bmatrix} i_{ACr} \\ i_{ACi} \end{bmatrix} + \begin{bmatrix} \frac{1}{L_r} & 0 \\ 0 & \frac{1}{L_r} \end{bmatrix}\begin{bmatrix} v_{pwm_r} \\ v_{pwm_i} \end{bmatrix} + \begin{bmatrix} -\frac{1}{L_r} & 0 \\ 0 & -\frac{1}{L_r} \end{bmatrix}\begin{bmatrix} v_{g_r} \\ v_{g_i} \end{bmatrix} \tag{3.18}$$

Normally, in the control scheme a stationary to rotating reference frame transformation is used for grid voltage synchronization as in Equation 3.19, thus taking into account the voltage angle in the PCC and synchronizing with the sinusoidal alternating signal.

$$\begin{bmatrix} i_{vd} \\ i_{vq} \end{bmatrix} = \begin{bmatrix} cos\theta & sin\theta \\ -sin\theta & cos\theta \end{bmatrix}\begin{bmatrix} i_{vr} \\ i_{vi} \end{bmatrix} \tag{3.19}$$

Since in this project the voltages and currents are fundamental components and the reference voltage angle is considered to be always null, the d, q quantities will be identical with the real and imaginary values as in Equation

$$\begin{cases} i_{vd} = cos(\theta = 0)i_{vr} + sin(\theta = 0)i_{vi} = i_{vr} \\ i_{vq} = -sin(\theta = 0)i_{vr} + cos(\theta = 0)i_{vi} = i_{vi} \end{cases} \tag{3.20}$$

A control algorithm can be applied in Power Factory DIgSILENT as in Figure 3.15, where the signals controlled are the real and imaginary parts of the pwm converter's AC currents I_{ACr} and I_{ACi}. Namely, transferring to effective values from Equation 3.18, Equation 3.21 results:

$$\begin{cases} \frac{dI_{ACr}}{dt} = -\frac{R_r}{L_r}I_{ACr} + \frac{V_{pwm_r}}{L_r} - \frac{V_{g_r}}{L_r} \\ \frac{dI_{ACi}}{dt} = -\frac{R_r}{L_r}I_{ACi} + \frac{V_{pwm_i}}{L_r} - \frac{V_{g_i}}{L_r} \end{cases} \tag{3.21}$$

The voltage on the converter side is expressed as:

$$\begin{cases} V_{pwm_r} = L_r \cdot \frac{dI_{AC_r}}{dt} + R_r I_{ACr} + V_g \\ V_{pwm_i} = L_r \cdot \frac{dI_{AC_i}}{dt} + R_r I_{ACi} + V_g \end{cases} \tag{3.22}$$

Since I_{ACr} and I_{ACi} are the effective components of the sinusoidally alternating currents i_{ACr} and i_{ACi}, the control can contain PI controllers without any steady state error. The advantage of using this converter control structure is the elimination of the phase locked loop block which is known not to perform well in the event of rapid voltage fluctuations e.g. three phase short circuits. In the control block the outputs of the controller are $\mid P_m \mid$ and ϕ which represent the magnitude and angle of the PWM generated voltage with reference to the grid voltage.

The control system is completed by the outer loop controllers thus creating a cascade control structure. In the control design it is important to consider that the inner and outer control loops are decoupled and have no interactions on one another. Practically, this consideration is possible by setting the regulating speeds of each of the control loops to be different with the outer loop time constant 5 to 20 times slower[56].

3.3.3. Inner Current Control Loop Design

The design of the PI current controllers follows standard procedures known as "technical optimum"[56] in which the controlled plant is represented by the cumulative impedance of the line reactor and transformer. Matlab sisotool has been used in accordance with guidance in [60]. Since the converters have the same power ratings, voltage levels and design specifications, the equivalent parameters will be equal and thus the same proportional and integral gains of the PI can be used for both converters. The design is performed in s domain. For this plant representation the assumption of zero control delay between the reference current setpoint and the command value is taken. For both converters, the grid and WF side, the controlled plant for the current controllers is represented as in Figure 3.16. In this figure the input is the reference current provided by the outer loops I^*, the current output I_{meas} and a perturbance signal w. In this design the simplifying considerations are related to the assumption of no delays in the system.

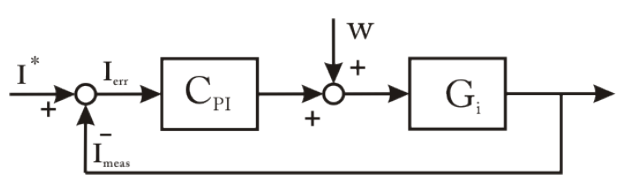

Figure 3.16.: Current control loop

The PI controller's transfer function C_{PI} is expressed as:

$$C_{PI} = K_i \cdot (1 + \frac{1}{sT_i}) \tag{3.23}$$

The controlled plant's transfer function, G_i is expressed as:

$$G_i = \frac{1}{Ls + R} \tag{3.24}$$

where L and R are the equivalent inductance and impedance of the equipment connected between the converter and the point in which the control takes action.

The closed loop transfer function can be calculated as in Equation 3.25:

$$Y(s) = \frac{G_i \cdot C_{PI}}{1 + G_i \cdot C_{PI}} = \frac{\frac{K_i}{L}s + \frac{K_i}{LT_i}}{s^2 + s\frac{R+K_i}{L} + \frac{K_i}{LT_i}} \tag{3.25}$$

The requirements for the design of the current controller have been selected to be as below based on the guiding information in [60]:

- current controller closed loop with phase margin larger than 45 degrees;

- typical damping ratio has been assumed, $\xi = \frac{\sqrt{2}}{2} = 0.707$

For the dimensioning of the PI parameters Matlab sisotool has been used. The design of the PI controller has been performed using the pole placement method. Since the controlled plant contains only one pole and no zeros the system will always be stable in relation with the gain margin. Therefore, the gain K_i is selected in order for the dominant poles to have the damping ratio equal to ξ. Following the rules of the "technical optimum" design specifications, the PI controller's integration gain should be chosen equal to the plant time constant T[56]:

$$T = \frac{L}{R} \tag{3.26}$$

The integration time constant has been chosen so as to cancel the dynamics of the plant, meaning that the zero of the PI is placed as close to the pole of the plant. The root locus and the Bode diagram of the open loop system is shown in Figure 3.17. From the root locus, the position of the poles of the PI output a damping ratio of 0.7. In the bode diagram the phase margin of the open loop system is 70.7 degrees.

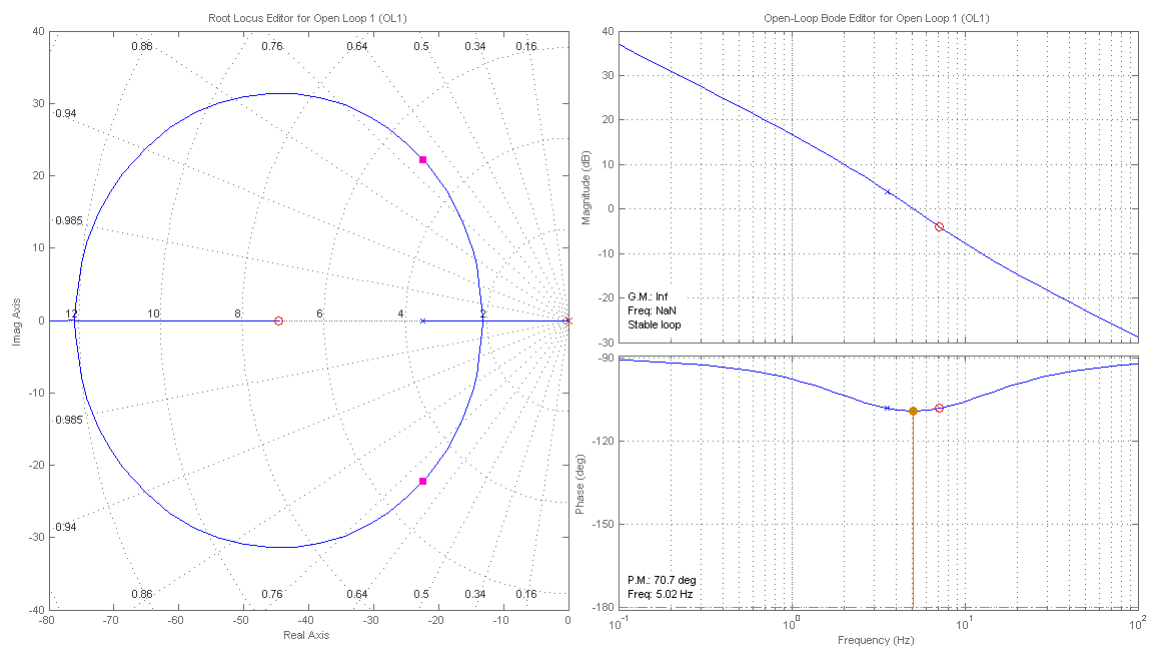

Figure 3.17.: Open loop root locus and Bode diagram

The Bode diagram for the closed loop system is shown in Figure 3.18 and a small frequency bandwidth is obtained of 40 rad/s. It is assumed that for the purpose of simulation of the ideal plant this value is sufficient. Also, the control is intended for RMS stability, therefore, due to the large step size in simulation, fast transients will not appear.

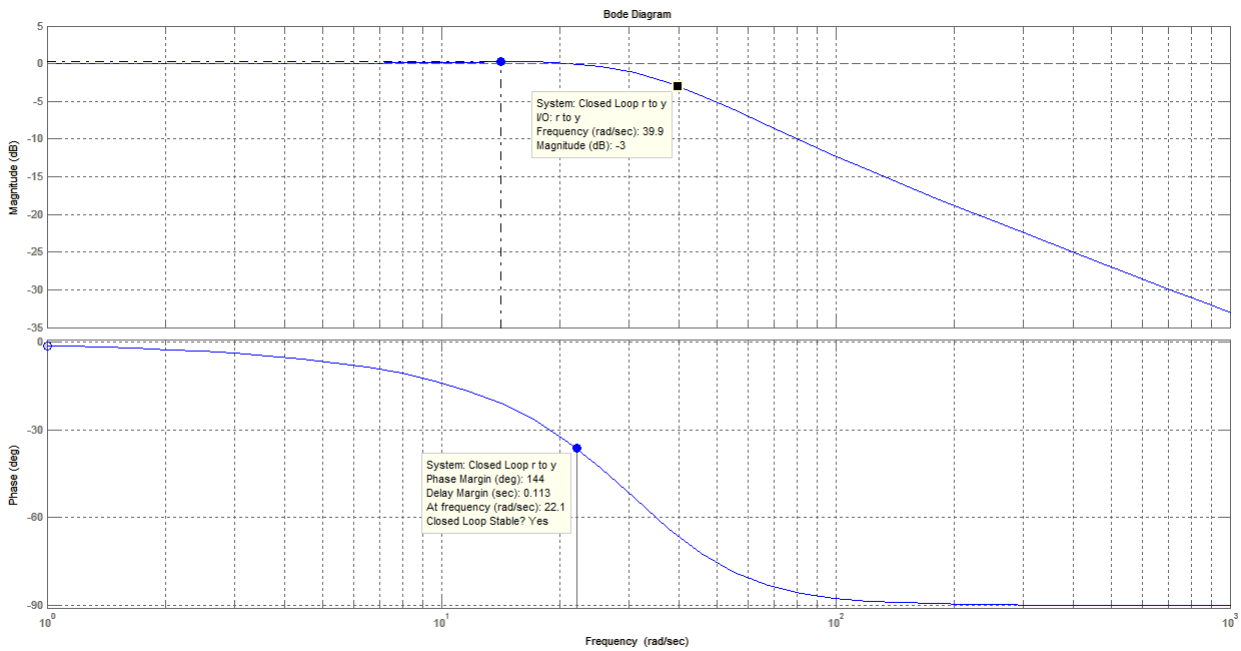

Figure 3.18.: Closed loop Bode diagram

The step response of the closed loop transfer function of the controlled plant and PI controller are shown in Figure 3.19. The steady state value is unity, an overshoot of 6.58% is obtained and a rise time of 0.05 seconds. The PI controller that is introduced in the closed loop transfer function will provide certainty for unity final value of the step input with zero steady state error. The parameters of the PI controller are listed in Appendix D.2

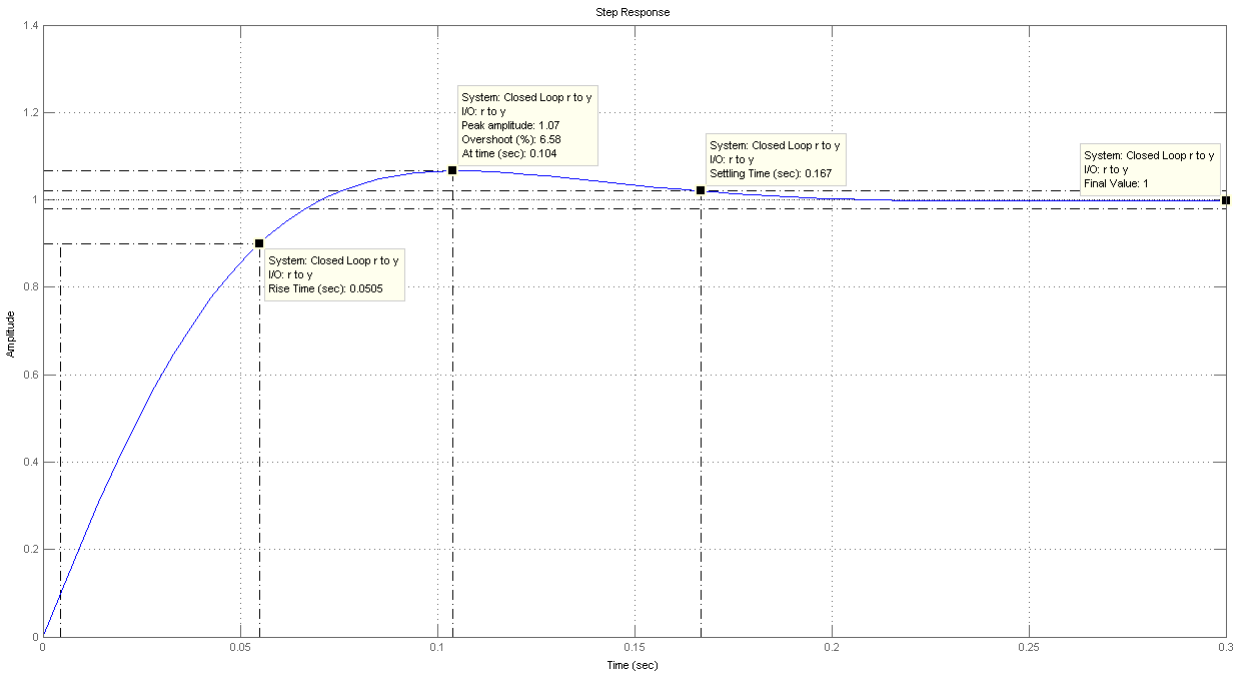

Figure 3.19.: Step response of the closed loop system

3.3.4. DC Voltage and Reactive Power Control Loops Design for Grid Side Converter

The converter in the grid side station is responsible with maintaining the DC link voltage on the HVDC transmission within its limits. In the case of controlling the DC voltage, in [42] it is explained the derivation of the control equation for the d,q control system which can be successfully applied also in the specific case of the assumptions taken in this project. Briefly, the control equation will be deduced in what follows by applying the power conservation law between the two sides (AC and DC) of the converter. The three phase active and reactive power on the AC side, as well as the DC power are expressed in equations 3.27, 3.28, 3.29.

$$P_{AC3ph} = v_{ga} i_{pwma} + v_{gb} i_{pwmb} + v_{gc} i_{pwmc} \tag{3.27}$$

$$Q_{AC3ph} = (v_{ga} - v_{gb}) i_{pwmc} + (v_{gb} - v_{gc}) i_{pwma} + (v_{gc} - v_{ga}) i_{pwmb} \tag{3.28}$$

$$P_{DC} = V_{dc} I_{dc} \tag{3.29}$$

The active and reactive power can be also expressed in complex form to be as :

$$\begin{cases} P = Real[V_g \cdot I^*_{AC}] \\ Q = Imag[V_g \cdot I^*_{AC}] \end{cases} \tag{3.30}$$

where V_g and I_{AC} are the phasors of grid voltage and current, and I^*_{AC} is the conjugate of the grid current.

Following the considerations in [42] where d,q control has been used and setting the reference voltage angle θ to zero, the following Equations results, where instead of d,q quantities the stationary reference frame values are used.

$$P_{AC} = V_{gr} I_{pwmr} \tag{3.31}$$

$$Q_{AC} = V_{gi} I_{pwmi} \tag{3.32}$$

Assuming that the PWM converter has negligible power losses the AC and DC power must be equal in order to obtain stability of the system:

$$P_{AC} = V_{gr} I_{pwmr} = P_{DC} = I_{dc} V_{dc} \tag{3.33}$$

Rearranging equation 3.33 results in the control equation 3.34,

$$I_{dc} = \frac{V_{gr} I_{vr}}{V_{dc}} \tag{3.34}$$

Keeping the power flow stable means that the above equation must be satisfied continuously. Any unbalance in the active power transferred through the converter will be the cause of DC voltage fluctuations. A PI controller can be developed that controls the DC voltage link by setting current references for the real part of the AC current I_r.

Typically, the DC link voltage is allowed to have a 5% variation from the rated value[43]. It is therefore one requirement for the DC voltage controller to have an overshoot of less than 5% for a unity step input. Zero steady state error is also necessary for stable operation of the system. Therefore, the common method of controlling the DC link voltage is by including a PI controller with a negative feedback loop. The design of the outer loop PI controller has been performed also in the Matlab design application, Sisotool, considering the controlled plant from Figure 3.20 to be G_{Vdc} as in Equation 3.35, where the term $\frac{3P_m}{2\sqrt{2}}$ appeared due to the consideration of sinusoidal modulation of the PWM converter.

$$G_{Vdc} = \frac{3P_m}{2\sqrt{2}C_{dctotal} \cdot s} \tag{3.35}$$

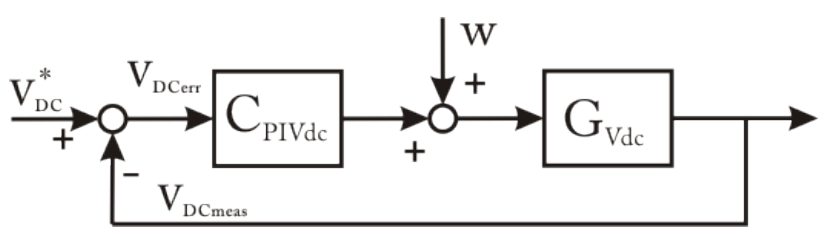

Figure 3.20.: Outer control loop for DC voltage controller

The PI controller is defined by C_{PIVdc}:

$$C_{PIVdc} = K_{vdc} \cdot (1 + \frac{1}{s \cdot T_{vdc}}) \tag{3.36}$$

The closed loop transfer function Y_{Vdc} is defined by:

$$Y_{Vdc} = \frac{C_{PIVdc} \cdot G_{Vdc}}{1 + C_{PIVdc} \cdot G_{Vdc}} = \frac{K_{Vdc}}{T_{Vdc}} \cdot \frac{s + \frac{1}{T_{Vdc}}}{T \cdot \frac{2\sqrt{2}}{3P_m} C_{DC} \cdot s^2 + K_{Vdc} T_{Vdc} \cdot s + 1} \tag{3.37}$$

The time constant of the outer loop PI controller has been selected to be slower than that of the current controller as in Equation 3.38, this having a direct influence on the selection of the zero in Figure 3.21.

$$T_{Vdc} = 10 \cdot T_i \tag{3.38}$$

The open loop root locus and bode plot are displayed in Figure 3.21. The controlled plant has only one pole in the origin, therefore the system is stable and the gain margin is practically infinite. The PI is used to insure that the steady state error is zero. The phase margin results in 86.2 degrees. Figure 3.22 displays the closed loop bode plot and the step response of the closed loop system. The PI is as expected much slower in terms of the step response compared to the current loop with a settling time of 3 seconds and a small overshoot of 5%. Zero steady state error is achieved.

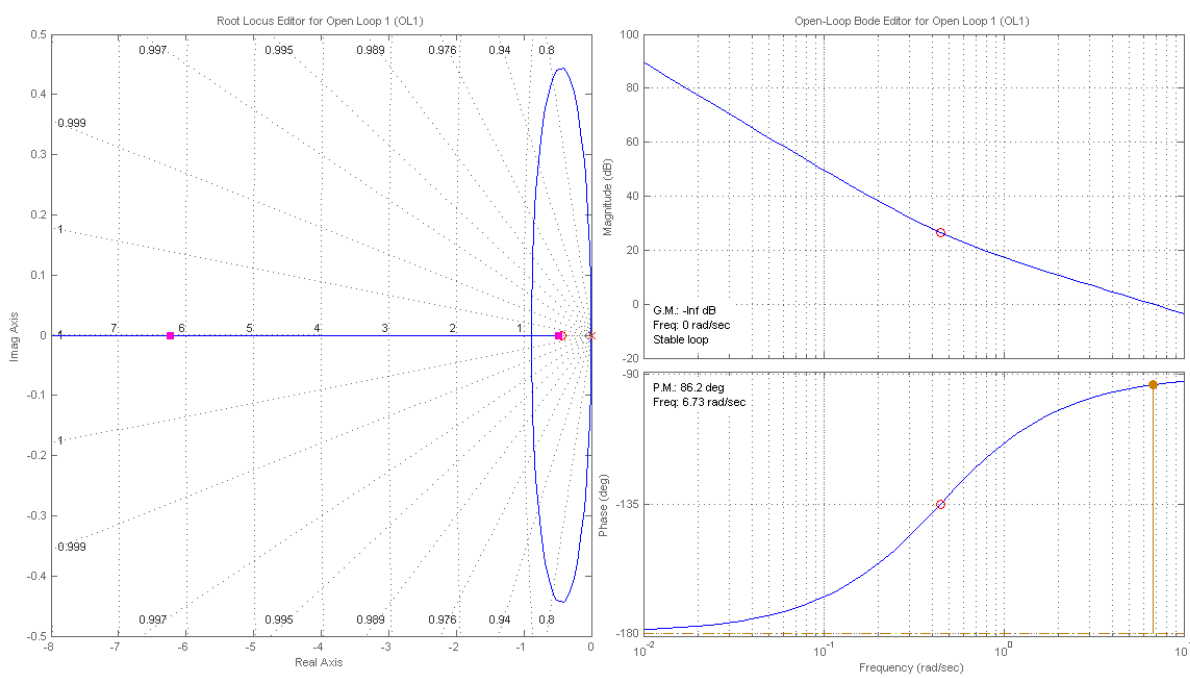

Figure 3.21.: Root locus and bode plot for the open loop system

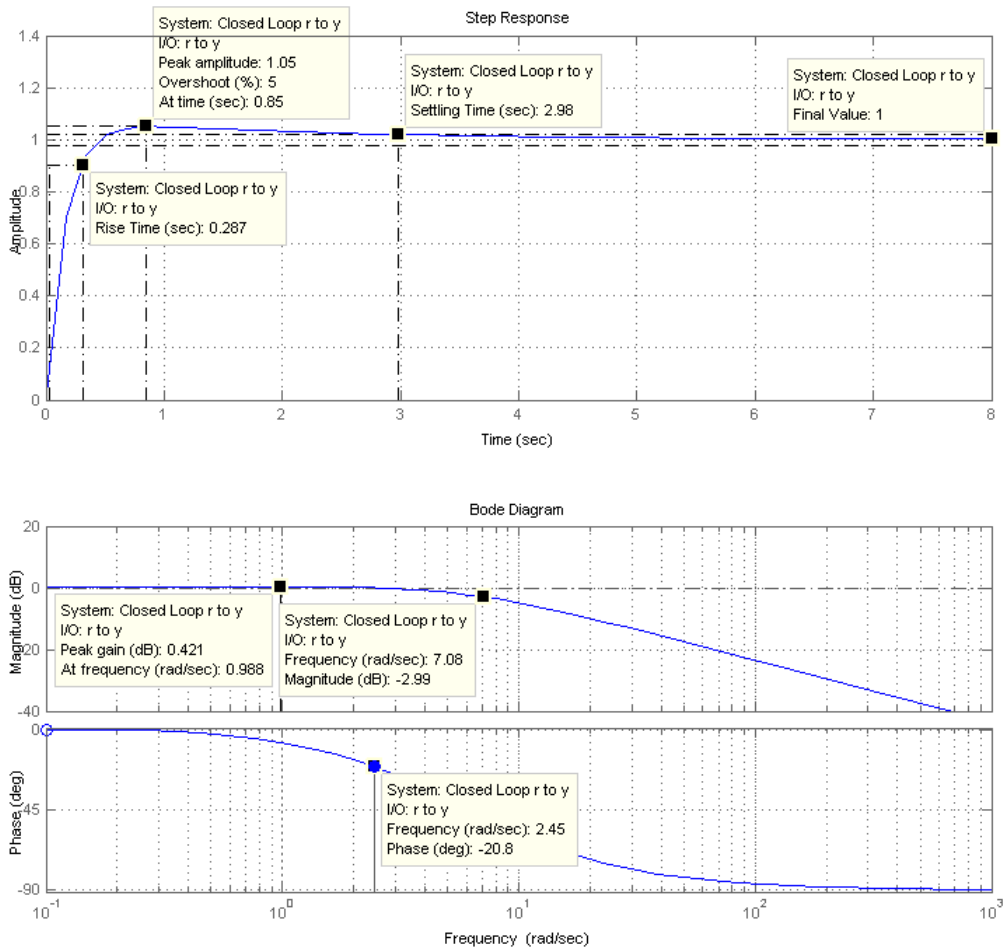

Figure 3.22.: Step response and bode plot of the closed loop system

On the other hand, the TSO usually requires that on the PCC the reactive power absorbed or injected in the system must have a determined and controllable value. The receiving end station control system must be able to regulate the DC voltage on the DC transmission link and also the reactive power balance in the plant's PCC. Therefore the imaginary current reference I_i^* must be also controlled in order for the reactive power to have the desired value. For the reactive power controller the same PI controller is adopted in order for the reactive outer loop to have the same dynamics as the DC voltage controller and thus not to interfere with the inner loops. The parameters of the PI controller are listed in Appendix D.2.

3.3.5. AC Voltage control loop design for WF converter

The AC voltage control loop represents the outer loop in the control algorithm adopted for the WF controller, with an inner current loop designed as in Section 3.3.3. Therefore, the basic idea is to create an AC voltage controller that will not interfere with the inner loop. As in Section 3.3.4, a PI controller with a time constant 10 times slower has been adopted:

$$T_{AC} = 10 \cdot T_i \tag{3.39}$$

The control system is as previously a standard PI controller with a negative feedback loop, as depicted in Figure 3.23:

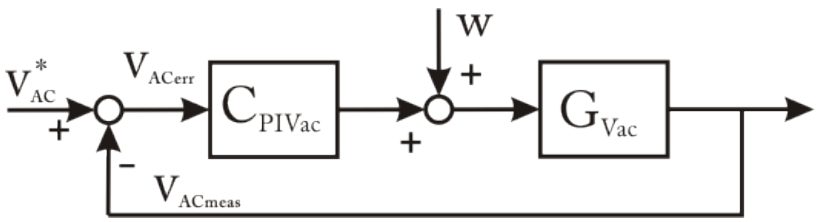

Figure 3.23.: AC Voltage control system

The PI controller transfer function C_{PI} is defined by:

$$C_{PIVac} = K_{Vac} \cdot (1 + \frac{1}{s \cdot T_{Vac}} \tag{3.40}$$

The controlled plant transfer function G_{Vac} is considered to be the current transfer function in series with the equivalent impedance of the 30 WT generators Z_{eq}. The line impedance has been neglected. The controlled plant transfer function is:

$$G_{Vac} = \frac{Z_{eq}}{Ls + R} \tag{3.41}$$

where $Z_{eq} = Z_{gen}/N_{WT}$, with N_{WT} is the number of wind turbines.

The root locus plot and the step response of the closed loop system is displayed in Figure 3.24. The system response is in the order of seconds, much slower than the one of the current loop thus keeping the two loops decoupled. The parameters of the PI controller are listed in Appendix D.2.

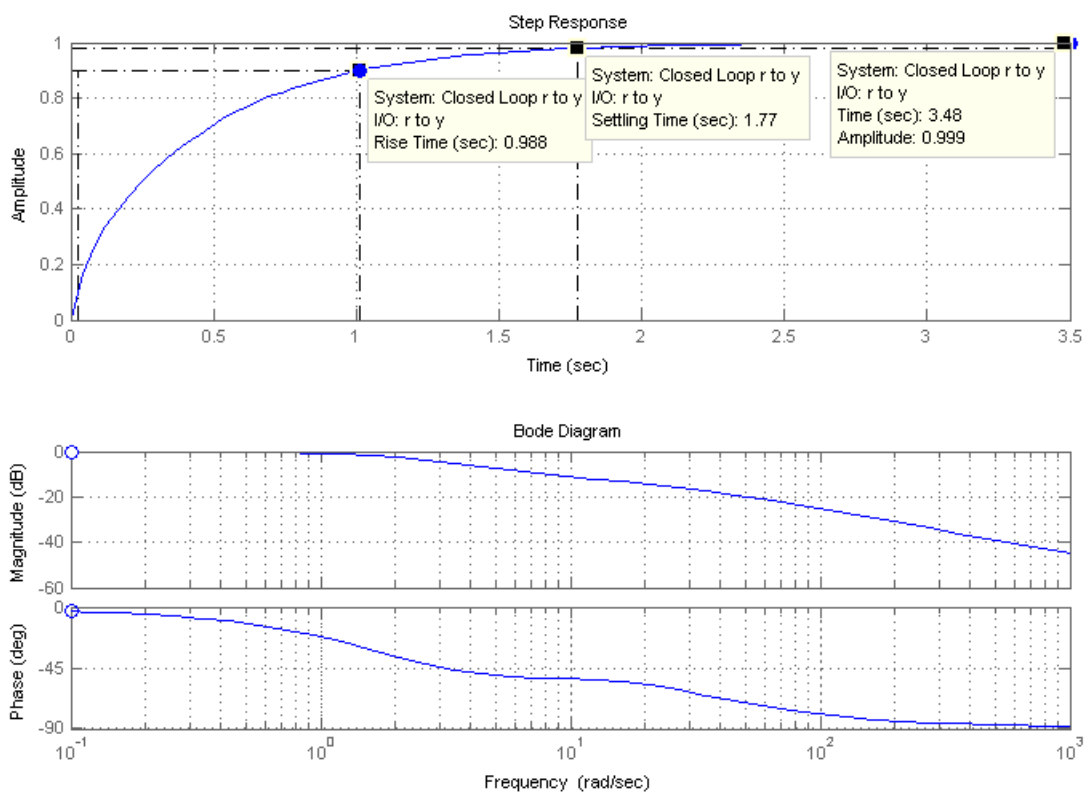

Figure 3.24.: Step response and bode diagram for the closed loop V_{ac} control system

3.4. Summary

This chapter presented the control of the main components of the WF simulation platform.

- the Wind Farm controller with mainly the active power regulation functions has been described. It contains the frequency control, delta production, absolute production, power gradient constraint and stop regulation functions.
- the Pitch Controller is developed based on [11] and additionally, a simple actuator model for the pitch control servo mechanism is detailed.
- the WF side converter's control system is described: it contains voltage and current control loops implemented with PIs, a frequency and voltage droop characteristic for the reference setpoints, and V/f controller.
- the Grid Side converter control system is described: it is developed with two inner current control loops for the real and imaginary currents (represented as phasors), one DC voltage control loop, and one reactive power control loop.
- Design considerations for the PIs of the fore mentioned controllers has been performed.

4. Wind Farm Operation - Stability Study

Assessment of the WF model is made in this chapter by analysis of the simulation results in stability studies. Throughout this chapter the general notation for per unit values was related, as in the previous chapters, to the rated apparent power (85 MVA) of the system. Therefore, as an example, when in graphics the per unit value of 0.8 for the active power appears it represents full power operation of the WF (69 MW). The same applies for the reactive power values. One exception applies in the case of Section 4.3, where the active power reference received from the TSO are calculated on the basis of 69 MW corresponding to 1 per unit. In Subsection 4.3.3, the absolute values for active power are used due to the fact that the components studied (WF and grid connected synchronous generator) have different rated apparent powers.

This part of power system analysis is focused on the power system stability requirements. Mainly, frequency and voltage support in the PCC are studied and assessed. The method of maintaining the balance in the PCC is by regulating the active and reactive power depending on the performance of the power grid. Several study cases are assembled and simulated. In Section 4.1, normal operation of the WF with a very strong connection in the PCC is verified. In this study case, focus is directed to the assessment of the WF and transmission system models. Stable WF and power system operation is the main goal, namely, all the controlled variables must be within the control band (currents and voltages). The WF must generate the reference power if the wind permits and in any case go beyond the rated values. Active and reactive power balance in the PCC must be obtained. Voltage must remain within the control band on the DC link as well as in the AC internal and external grids. In Section 4.3, active power control functions are verified, therefore, frequency stability is the main goal of this study case. Section 4.4 analyzes the reactive power compliance in the PCC and also the support that a WF equipped with an HVDC transmission system has to offer in order to generate or, rather rarely, consume reactive power. Voltage stability is thus verified in what follows.

4.1. Operation of WF - Normal Operating Conditions - Fixed Speed Study Case

In this section the WF operation will be evaluated in its entire structure, mainly the WF side converter voltage and frequency droop functions being studied. Also, it is of interest to study the power flow from the generation site to the receiving point, the PCC. For this purpose a study case has been set up with the following assumption:

- variation of the wind speeds in the entire possible range, for testing the functionality of the Pitch controller in power limitation mode
- power grid with no frequency deviation higher than the allowed standard values;
- no reactive power reference demand from the TSO;
- the TSO demands maximum active power generation from the WF;

The simulated wind speeds are shown in Figure 4.1. The main purpose of increasing the wind speed above the rated value was the verification of the Pitch controller. The wind speeds adopted in this study case were programmed to have the same time dependency with small deviations from the average wind speed. A maximum average wind speed of 17 m/s and a minimum of 5 m/s have been set. The turbine power for all the three WTs is shown in Figure 4.2. The power output from the WF in the remote point of generation and the actual active power generated in the PCC are shown in Figure 4.3. As it is expected the WF power output has a smoother characteristic than that of one row of WTs. The pitch controller enters in power limitation mode and varies positively the pitch angle. The pitch angle variation is shown in Figure 4.4, with a maximum pitch angle of 14.1 degrees. No visible ripple or fluctuation of the power output is present in the moment of switching between optimization and limitation mode.

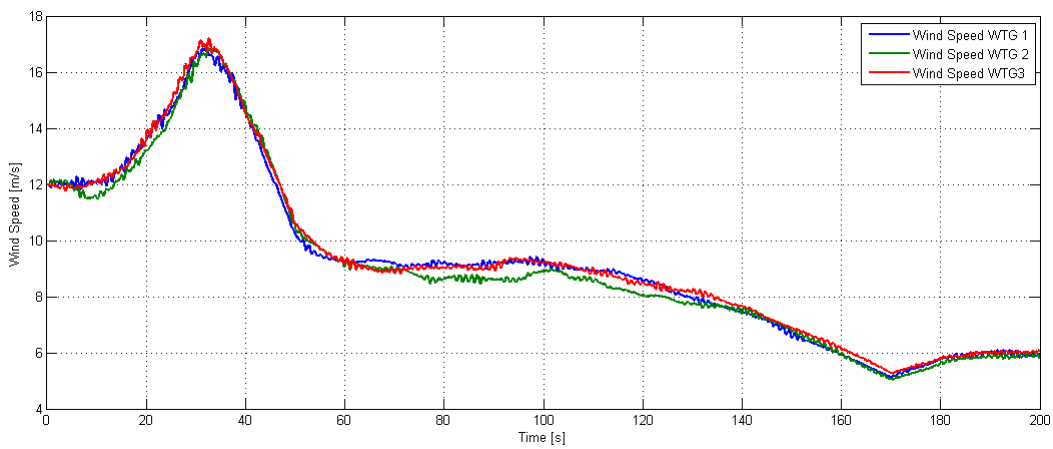

Figure 4.1.: Wind speed variation for each of the three WT groups

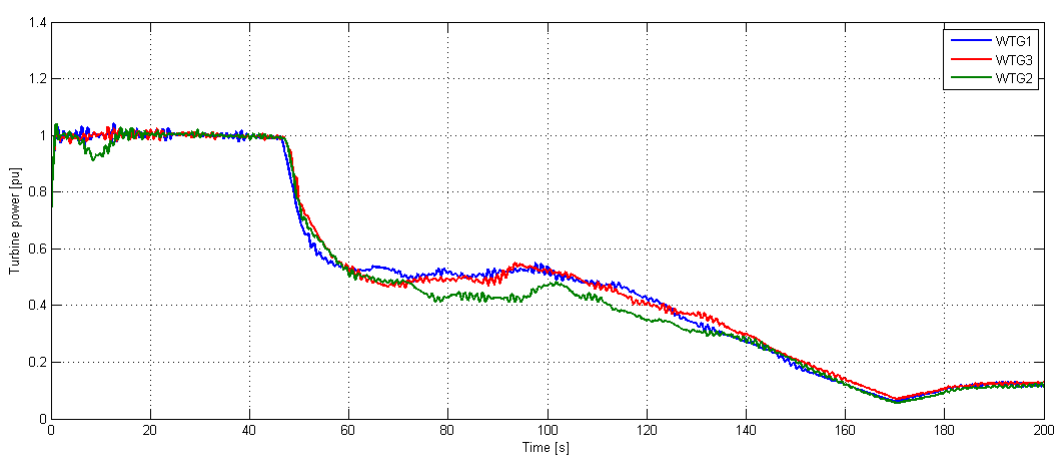

Figure 4.2.: Turbine power for each of the three WT groups

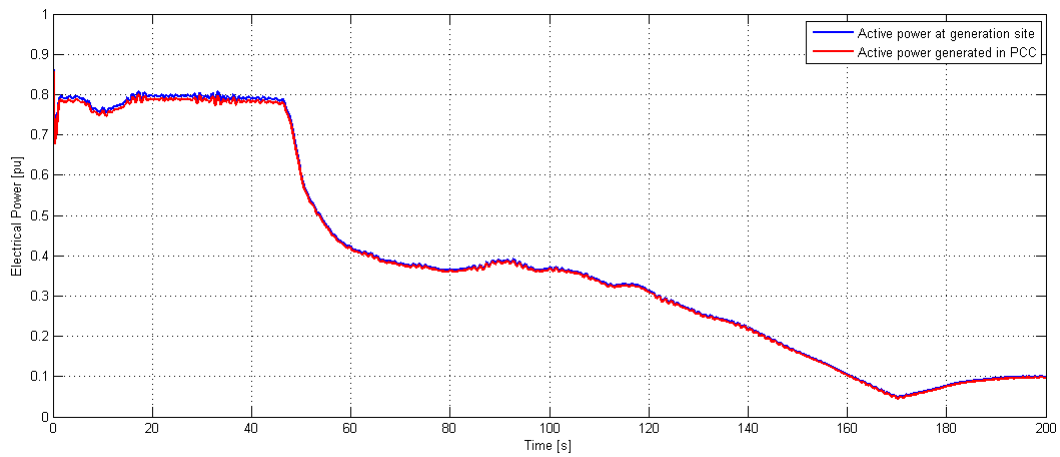

Figure 4.3.: Active power generation - WF and PCC points

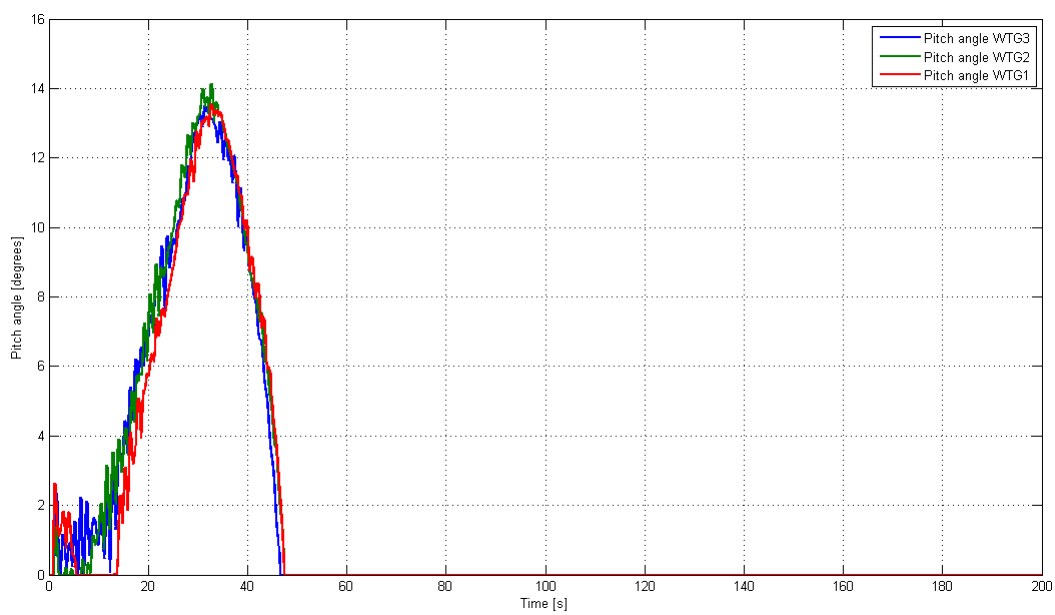

Figure 4.4.: Variation of the pitch angle in power limitation mode

The AC voltage on the internal WF grid is displayed in Figure 4.5. Small variation of the AC voltage can be seen, but overall, the values are well within typical allowed range of +/- 5% U_{rated}. A small decrease can be observed between 40 and 60 seconds, accounting for the droop voltage setpoint variation. This setpoint is modified directly by the demand of reactive power from the WT generators, which is decreasing for with the decrease in wind speed. The frequency of the WF's internal AC grid voltage is displayed in Figure 4.6. A small variation of the frequency can be also observed due to the frequency droop control action. The droop shape is correlated with the active power output of the WF. The AC current in the main collection AC bus of the WF is shown in Figure 4.7. The AC current and voltage are stable and well within the rated limits. Stable operation of the PI current and voltage controllers in the WF converter station is verified. The AC current is proportional with the active power generation of the WF.

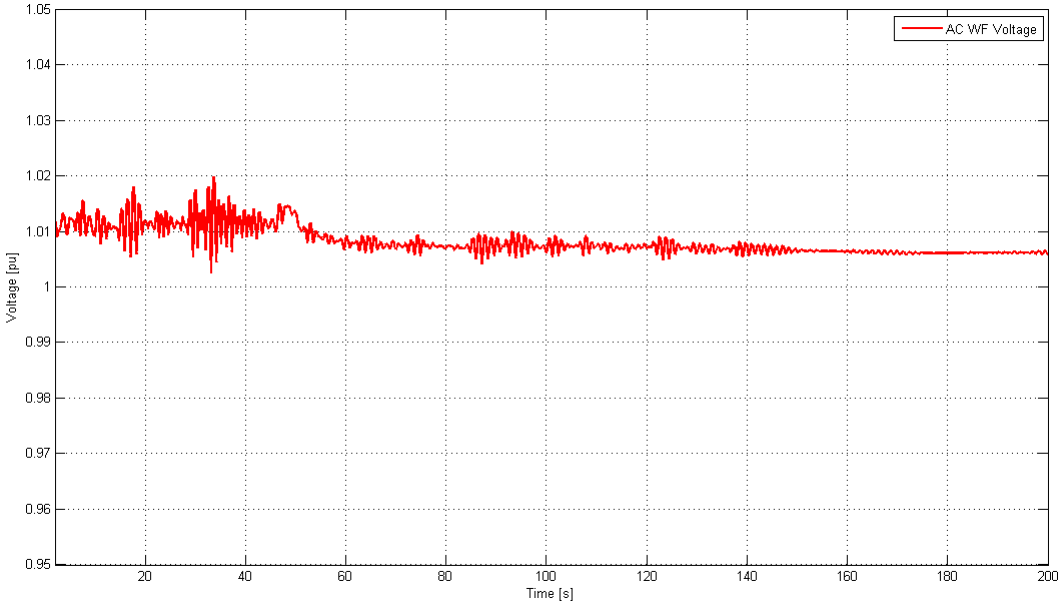

Figure 4.5.: AC voltage variation in the internal AC grid of WF

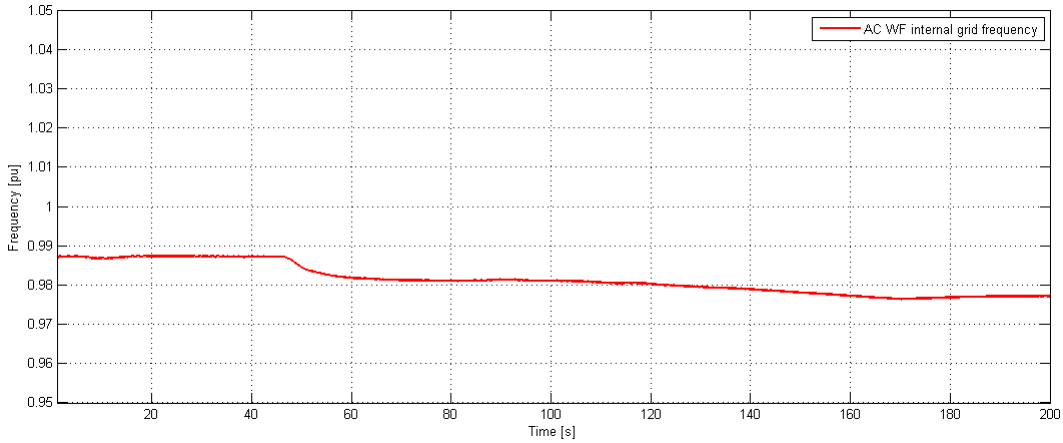

Figure 4.6.: Frequency in the WF AC grid

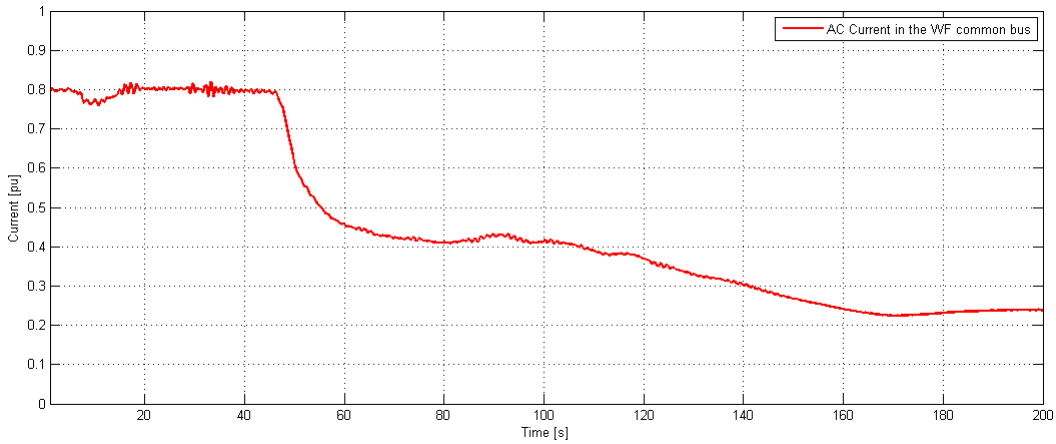

Figure 4.7.: AC current in the WF's common bus

The DC bus voltage is presented in Figure 4.8. Small ripple is observed with maximum values not exceeding 1 %. Stable operation of the DC voltage controller is thus verified. The DC link voltage is directly dependent on the ability of the main power grid to absorb the entire generated power of the WF. Since in this study case, the power grid is set to be stiff (large acceleration time constant and high short circuit power) it is also another reason that the DC voltage is not increasing. The AC main power grid frequency is almost constant, very close to 1. The real and imaginary parts of the AC converter current are shown in Figure 4.9. The grid side converter is controlling the real and imaginary components of the AC converter current by defining the AC voltage (phase and amplitude). In Figure 4.9 it can be seen, on one hand, the proportionality between the active power and the real part of the AC current, and on the other hand, the proportionality between the reactive power and the imaginary component of the grid current. It is also observed the current references are well controlled by the inner current loops.

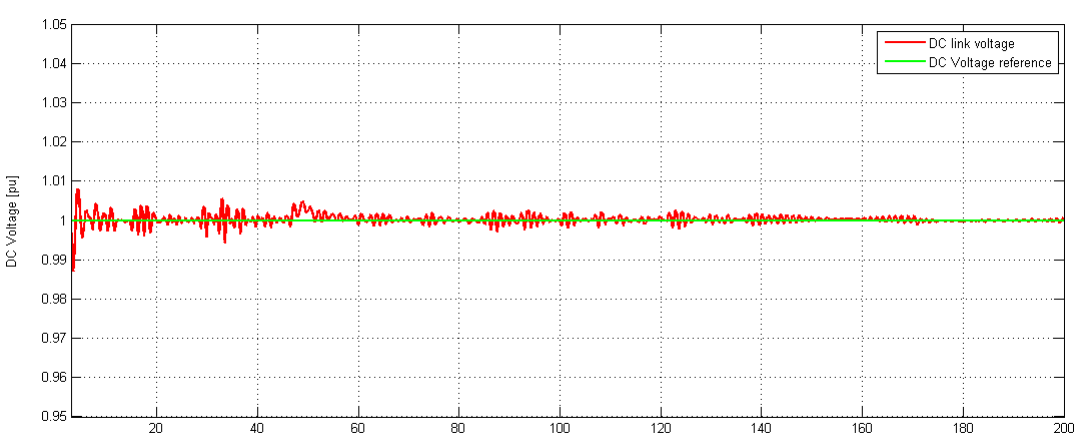

Figure 4.8.: DC Voltage on the HVDC transmission cable

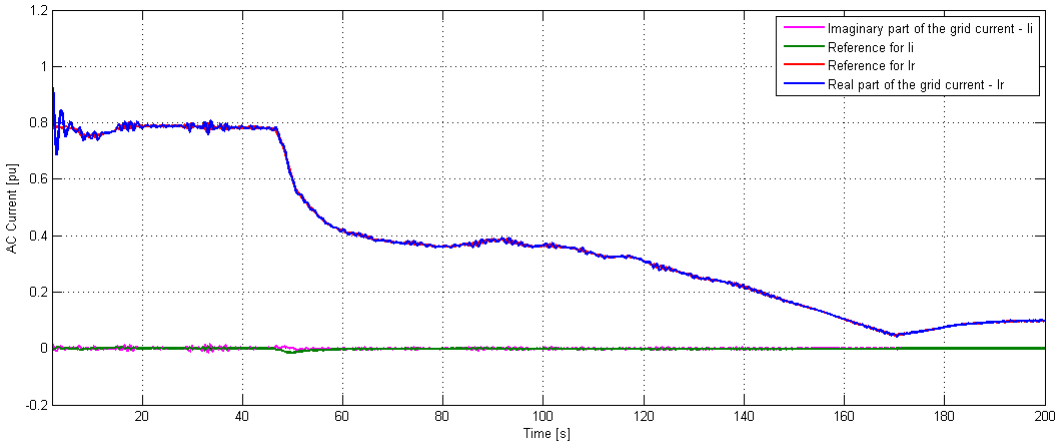

Figure 4.9.: AC grid current - real and imaginary

The AC voltage in the PCC and the grid side converter's connection point are shown in Figure 4.10. The direction of the power flow can be observed in this Figure, from the WF and towards the power grid. The small variations in the voltage amplitude are within the allowed voltage ranges. The reactive power in the PCC is displayed in Figure 4.11. The reactive power reference is zero. Small variations in the reactive power balance are occurring, with maximum values not exceeding 0.02 pu, five times smaller than the allowed reactive power band (see Figure 1.10 from Section 1.3.2).

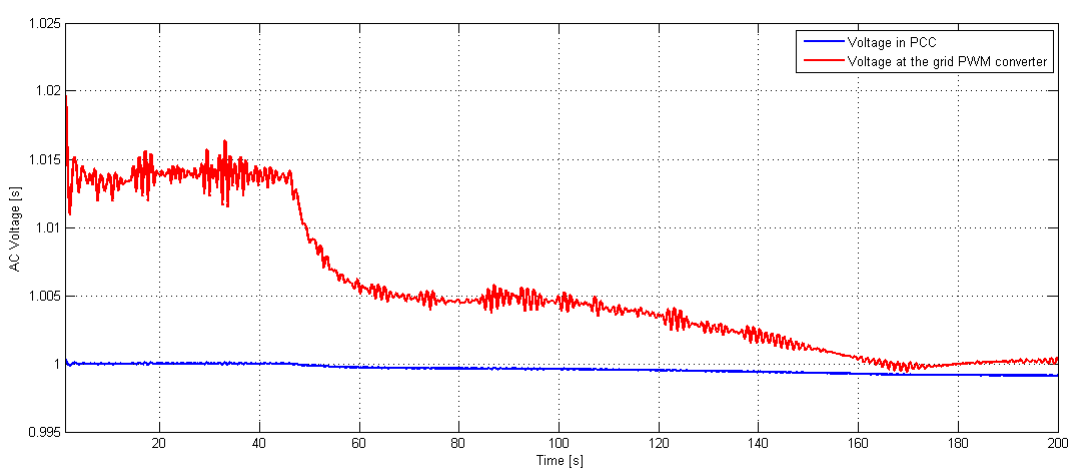

Figure 4.10.: AC Voltage in the PCC and the converter's connection point

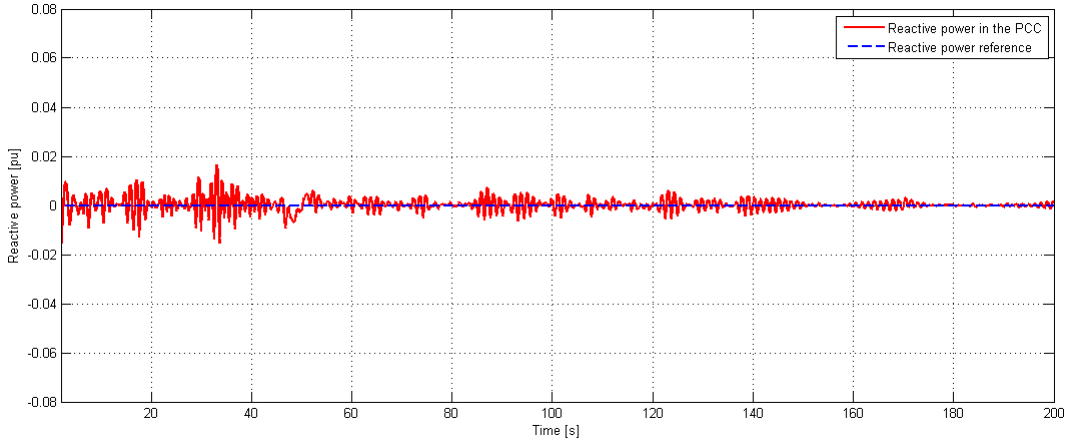

Figure 4.11.: Reactive power in the PCC

4.2. Variable Speed Operation of WTs in a Variable Frequency Internal Grid

In this Subsection the operation of the WF in a variable frequency internal network is assessed. The main purpose of the V/f control in the WF grid is the maximization of the WF power output by changing the voltage frequency and amplitude correlated with the average wind speed. Since the WF has thirty WTs on three rows (as in Section 1.5, Figure 1.15) and the PWM converter can generate only one voltage frequency in the internal AC grid, an average reference frequency must be calculated. Based on Figure 3.11 and Equation 3.13, the AC voltage frequency is calculated and sent to the WF side PWM converter. In this assessment to better view the power gain of the variable speed operation, the following assumptions have been taken:

- wind speeds do not vary, and are defined solely by ramps at different constant wind speeds;
- only one WF row is studied;
- simulation time interval of 200 seconds.

Figure 4.12 displays the wind speed characteristic applied to one WT group, and by not using the wind model, a clear view of the power gain can be viewed. Figure 4.13 shows the power output from one WT group row in a variable frequency grid and in a fixed frequency grid (f=50 Hz). It is observed that a small power increase is present due to the frequency variation (Figure 4.14), with maximum values below 5%.

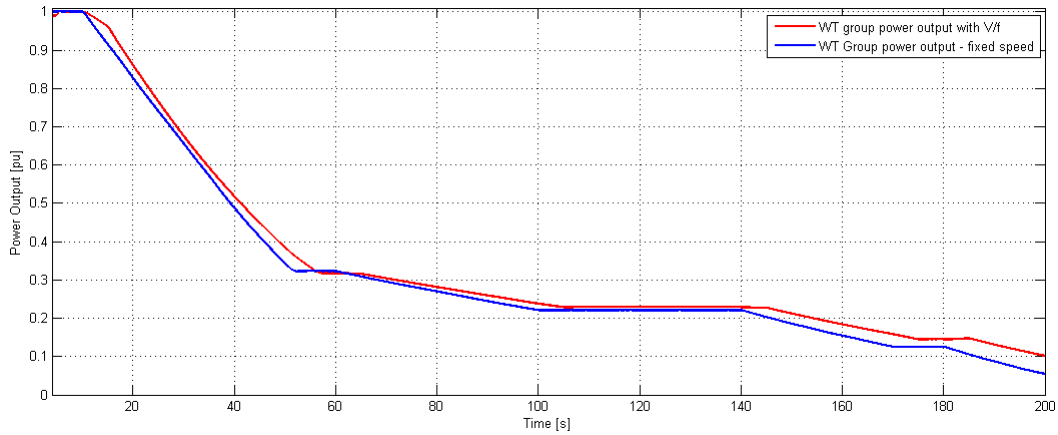

Figure 4.13.: WT group power output for variable and fixed frequency operation

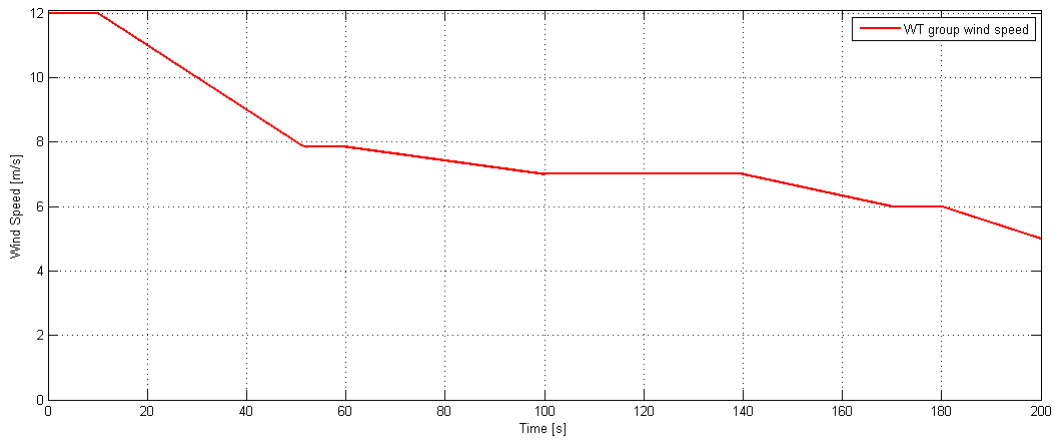

Figure 4.12.: Wind speed characteristic input

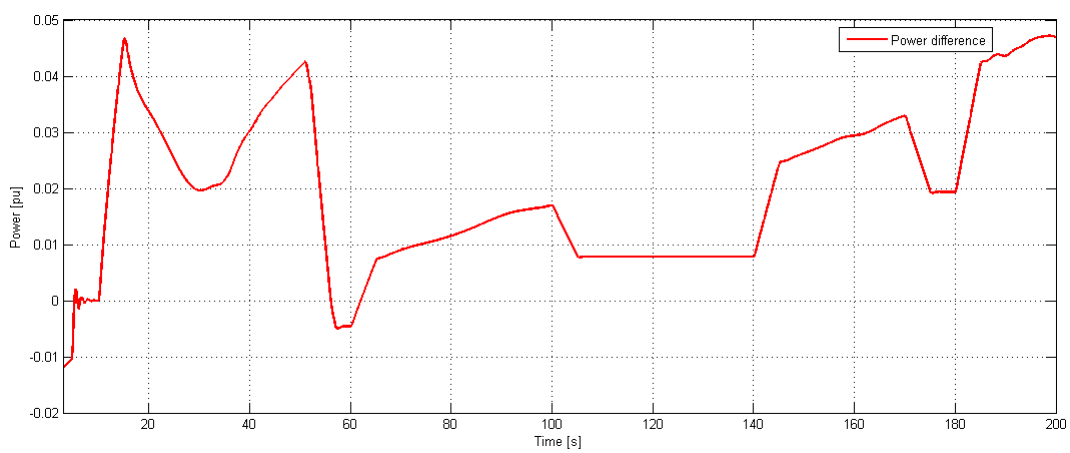

Figure 4.14.: Power gain in variable speed operation

The main electrical parameters of interest are the AC voltage and frequency at the mains of the WT group. Figure 4.15 shows the WT AC voltage applied as well as the AC voltage reference supplied to the PWM converter controller. The voltage is almost all the time superposed to the reference, therefore very small errors are present. Figure 4.16 displays the frequency variation in the simulated time interval. From both figures it is observed that a constant ratio between the voltage and frequency is maintained.

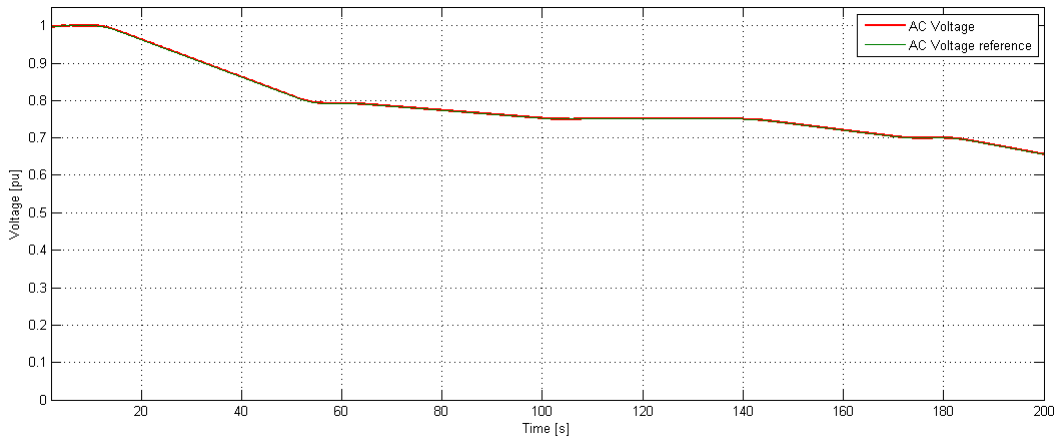

Figure 4.15.: AC voltage applied at the WT group's mains (variable speed)

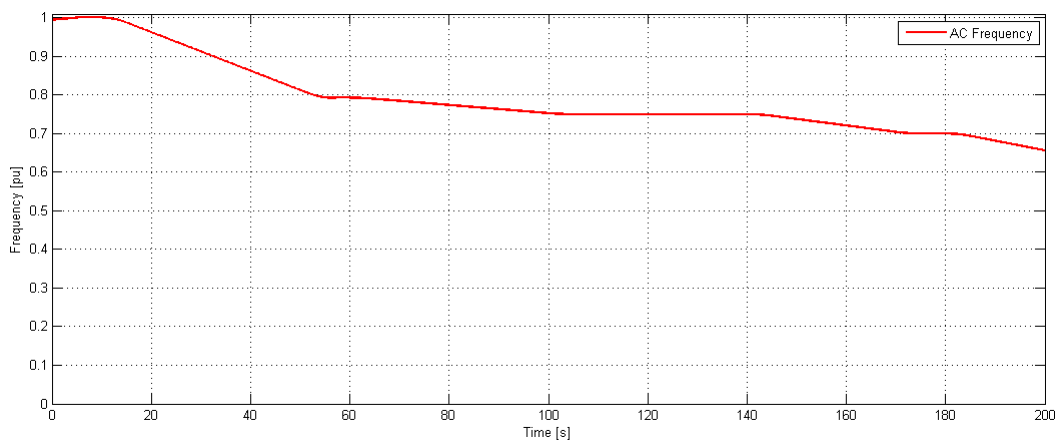

Figure 4.16.: Frequency in the variable speed case

4.3. Active Power Control under Different Operating Conditions

In this Section the power regulation functions required by the Danish TSO[4, 5] and implemented in the WF controller are verified. The following active power regulation functions have been studied:

- Frequency control (see Subsection 4.3.3) - when the frequency of the power system modifies, the WF must control actively the power production in order to participate in the frequency stability efforts;
- Stop regulation (see Subsection 4.3.2) - in case the wind speed increases, the WF must be able to maintain the current production due to certain production constraints ;

- Power gradient constraint (see Subsection 4.3.2) - limitting the maximum speed with which the power reference changes;
- Absolute production constraint (see Subsection 4.3.2) - this control algorithm will limit the power production to a set maximum reference point
- Delta production constraint (see Subsection 4.3.1) - this control technique ensures that regulating power reserves are allocated, the power production being less than what it could have been possible at present.

4.3.1. Delta Production Constraint

The TSO is requiring from the WFs to make available reserve power at any time provided the wind speed allows. The Delta Production control is setting a lower power reference point to each of the WTs in the WF than the power available currently in the wind. It may be realistic to assume that the TSO may require a 10 % primary reserve power from the WF operator. This power reserve can be made available at any time and in a very fast time frame.

A simulation study is set up in this Section in order to verify the performance of the Delta production control algorithm. The following actions and assumptions are taken:

- a reserve margin reference with the characteristic in Figure 4.17 is provided externally by the TSO;
- wind speeds vary in the optimization range, thus not allowing the required reserve margin to be maintained all the time;
- wind speeds are correlated only by a time delay;
- simulation time frame of 200 seconds.

Figure 4.17 presents the adopted delta production characteristic for this simulation study. A maximum power reserve demand of 0.15 pu is set. The wind speed variation is displayed in Figure 4.18 for all the three WT groups with a small time delay in the range of tens of seconds.

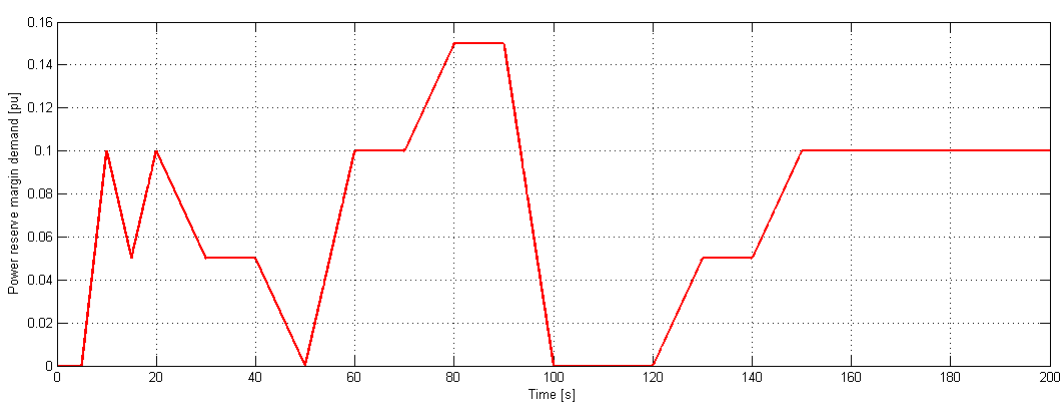

Figure 4.17.: Delta production demand from the TSO

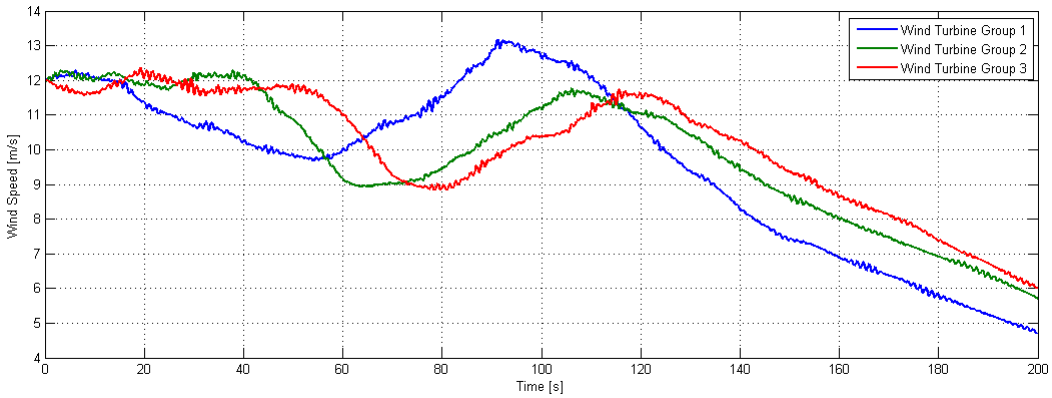

Figure 4.18.: Wind speed input for each WT group

In Figures 4.19, 4.20, 4.21 the results for the delta production control for each of the three WT groups are presented. In the plots the available wind power is calculated in a simple way, on the basis of the cubic value of the wind speed, therefore, small errors may appear in case of high variations in the wind speed. The margin is well maintained in the case of values greater than 0.1. Larger errors appear when the reserve margin is 0.05, therefore, differences in the setpoint and the reference power are present.

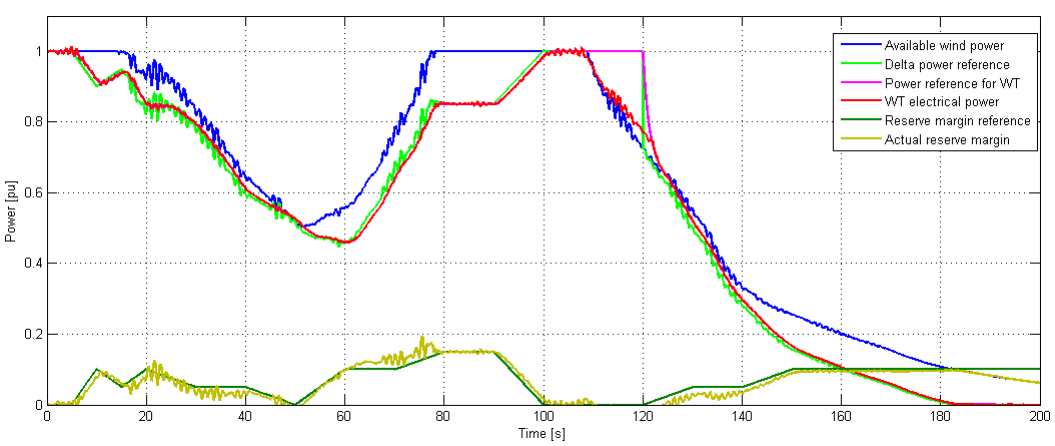

Figure 4.19.: Power reserve margin results for WT group 1

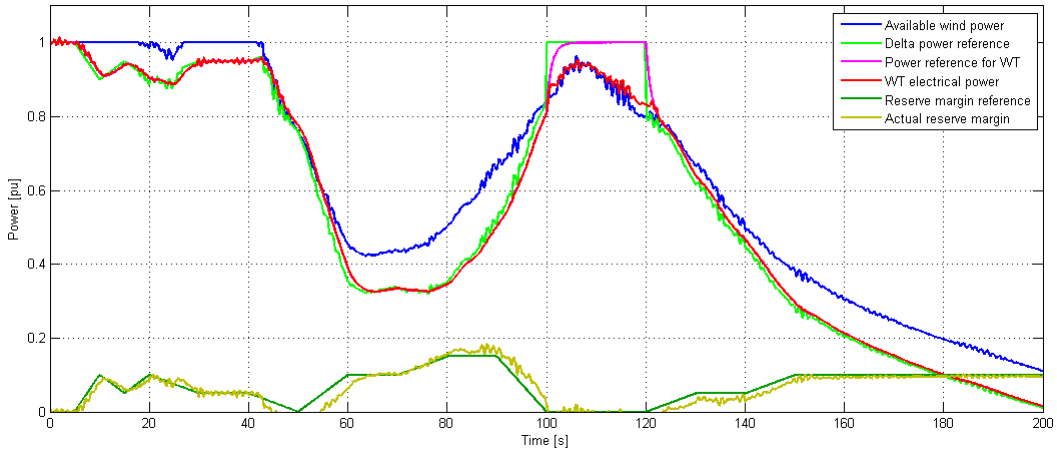

Figure 4.20.: Power reserve margin results for WT group 2

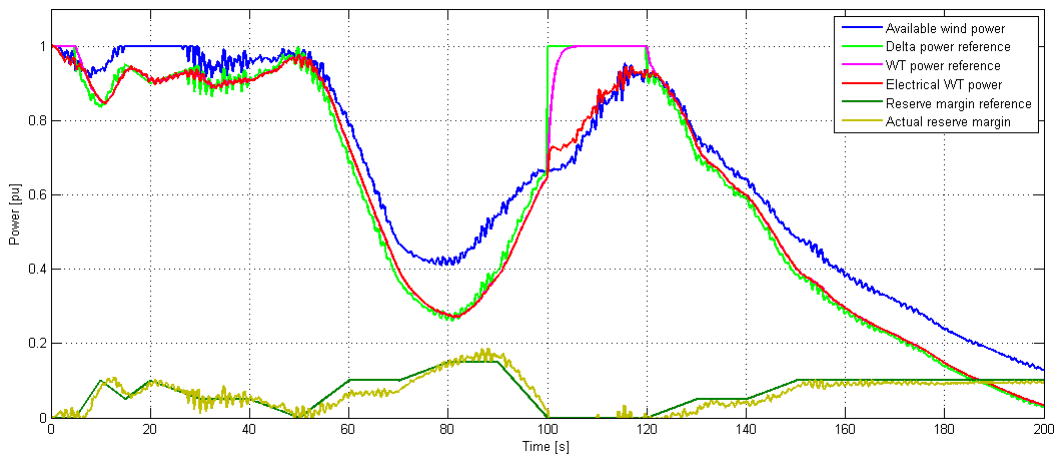

Figure 4.21.: Power reserve margin results for WT group 1

Figure 4.22 presents the overall WF reserve power margin, while in Figure 4.23 the electrical power output of the WF in the remote site is viewed. Relatively good results are obtained, though in a realistic scenario the change in the reserve margin demand will not be as often, therefore smaller errors will be obtained.

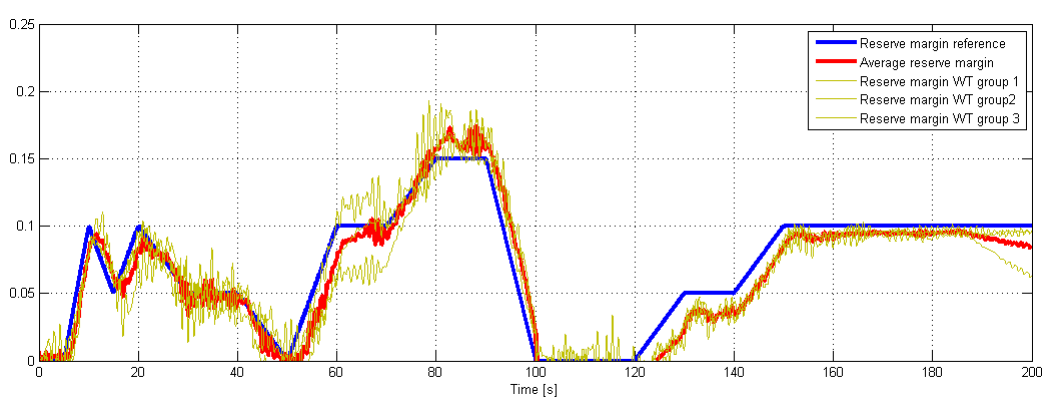

Figure 4.22.: Reserve power margin compliance of the WF

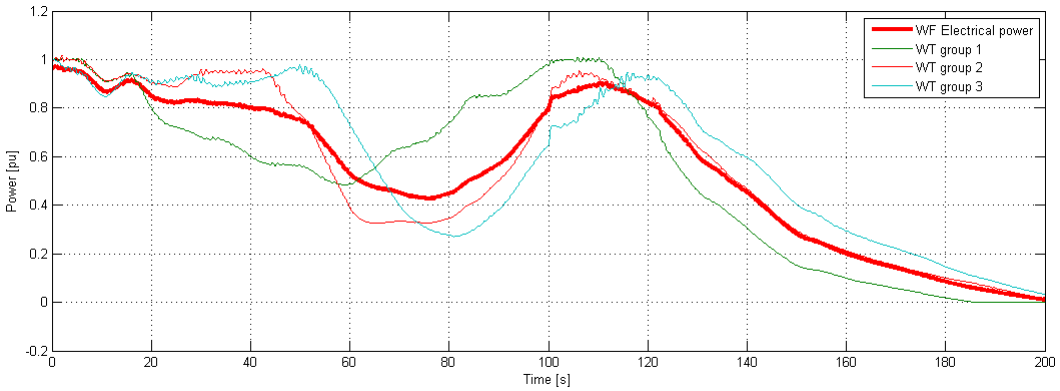

Figure 4.23.: WF electrical power output

4.3.2. Absolute Production, Stop Regulation and Gradient Constraints

The absolute production constraint algorithm is represented by a simple limiter of the WT overall power reference. For exemplification on this WF platform, the same wind speed conditions have been applied as in the previous study case, Figure 4.18. In Figure 4.24 the output of each of the WT groups is limited the three set values. The stop regulation has a similar approach, practically being implemented in the same way, the only difference being that the TSO provides only a triggering signal that will impose a certain maximum production, and the WF will try to keep the triggered value of the power. The gradient constraint is present throughout the results in this chapter, for exemplification, in Figure 4.24 a high value of the gradient time constant has been set, at 0.1 pu power reference variation in 4 seconds. Usually, the power gradient value is lower, at 0.1 pu power reference variation in 1 second. The power output in the PCC is presented in comparison with the power at the WF site in Figure 4.25.

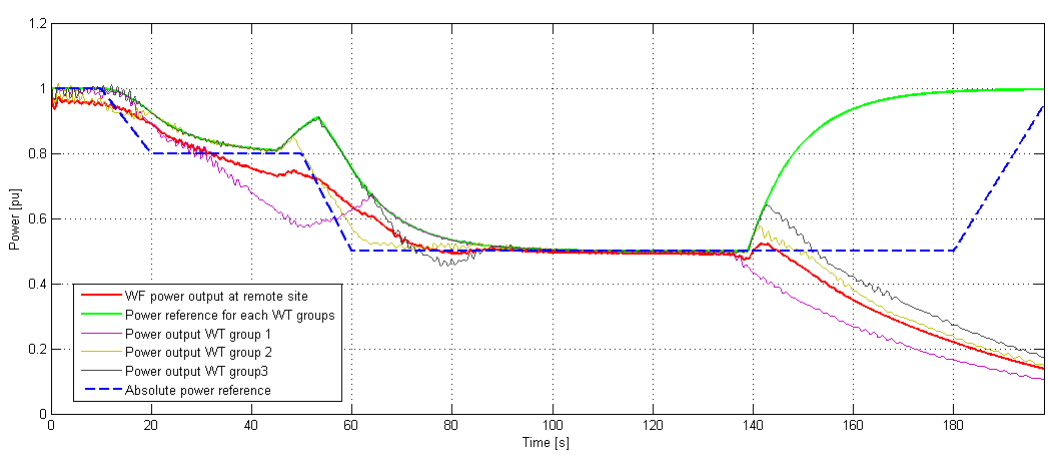

Figure 4.24.: Power Output of each of the three WT groups in absolute production control

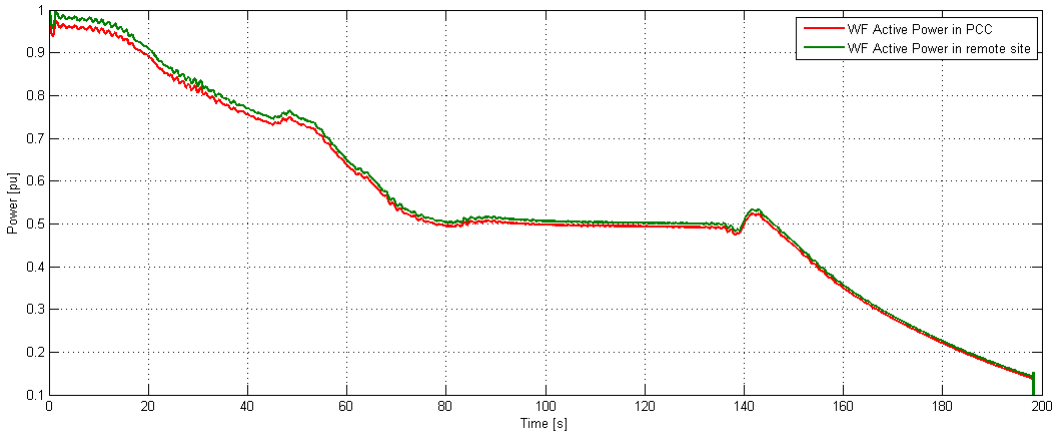

Figure 4.25.: WF active power output in WF and remote site

4.3.3. Frequency Control

In this study, the analysis is focused on the frequency control function of the WF's active power in the PCC as explained in Section 1.3.1, Figure 1.3. The main idea behind the frequency control algorithm defined by Equations 3.5 from Section 3.1 is that power system instability may arise if the active power generation in the PCC remains uncontrolled e.g. due to the lack available system inertia. Power imbalance is directly related to frequency fluctuations, therefore, keeping the frequency in a desired margin ensures power system stability for active power. Usually the frequency stability is mainly the responsibility of the large power stations. For this purpose the grid model in DIgSILENT has been used in parallel with a synchronous machine available in the software's library with the rated parameters as in Appendix D.4.1. Its purpose is strictly related to the increase or decrease of power injection in the electrical grid model, which will have the inherent result of increasing or decreasing the electrical frequency. This addition at the initial system configuration has been done due to the fact that frequency increase cannot take place in the simulation without the increase of generated power in the PCC above the value of the initial steady state conditions from which the simulation starts. Since the WF's initial conditions are requiring WF start up with rated output power generation value, the synchronous generator represents an easy to implement method for grid frequency increase or decrease. Practically, this situation can be considered realistic if considering the synchronous generator part of a CHIP unit. The rate of increase in frequency is related to the grid parameter - acceleration time constant T_a - which is calculated on the basis of the combined mechanical inertia of all synchronous machines H in the power grid[55]:

$$T_a = 2 \cdot H \tag{4.1}$$

A stiff grid has its acceleration time constant above 100 seconds, while the systems more prone to frequency fluctuations due to active power fluctuations have a time constant in the range of tens of seconds. The augmented system for this simulation study has the structure as in Figure 4.26.

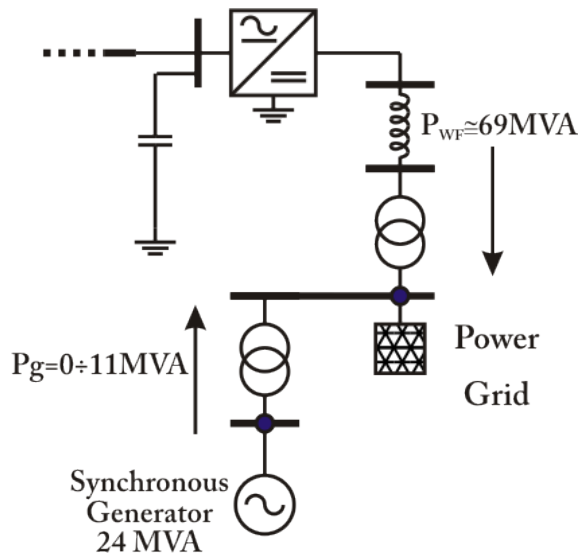

Figure 4.26.: Synchronous generator in the PCC for frequency variation

A study case in which the performance of the frequency control algorithm is assessed. The following actions and assumptions are taken:

- standard frequency control setpoints are adopted (see Appendix D.1);
- long start up at 0.5 pu and relatively fast shutdown of the synchronous generator as in Figure 4.27;
- the average wind speed is at rated value;
- the electrical grid has a typical acceleration time constant $T_a = 100s$ and a high short circuit power $S_{sc} = 1200MVA$;
- no frequency control action is taken from the grid, in DIgSILENT the secondary frequency bias parameter is set to 0.
- simulation time frame of 150 seconds.

Figure 4.27 shows the power output from the WF and the synchronous generator. Constant power output from the WF can be seen, close to the rated value.

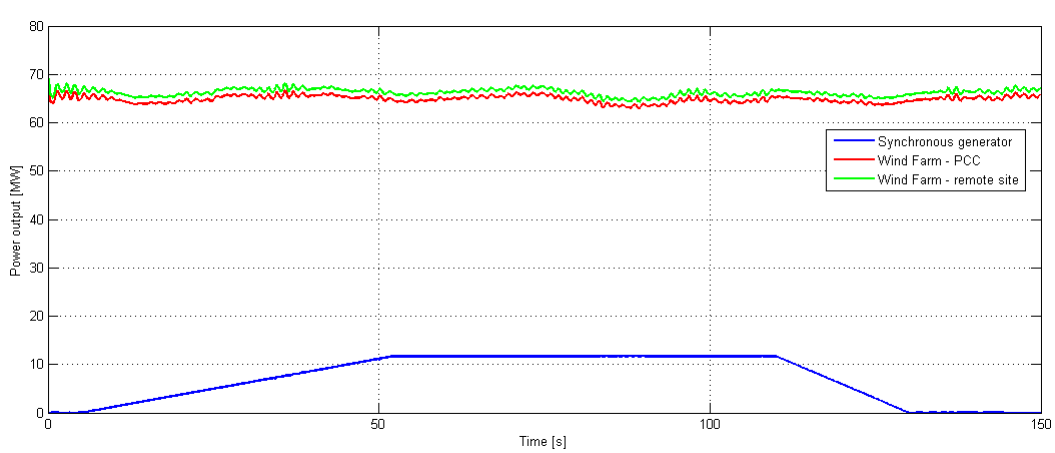

Figure 4.27.: Active power output for the WF and synchronous generator

Figure 4.28 displays the frequency variation in case there is no frequency control action from the WF nor the power grid. The maximum frequency reached is 52.75 Hz, therefore above the maximum accepted range. It is evident that the system loses its frequency stability and the circuit breakers will inherently trip in a real case situation.

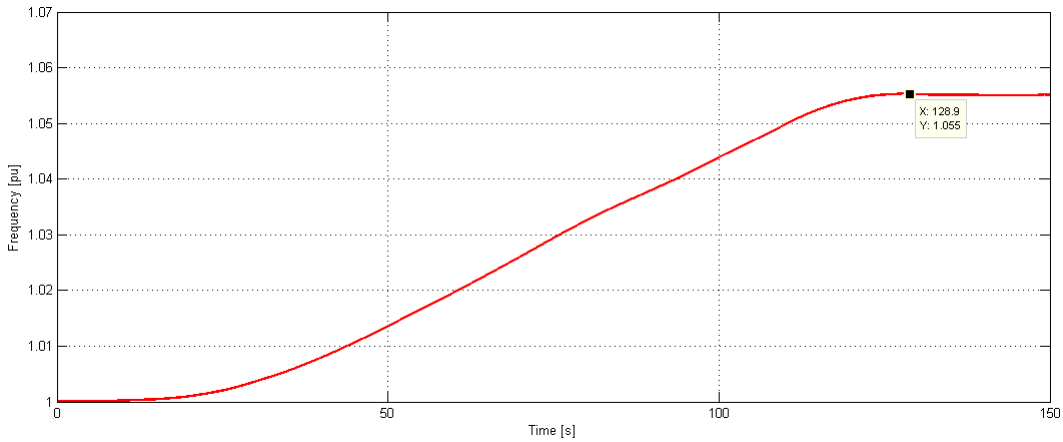

Figure 4.28.: Grid frequency in case of no frequency control

The results for the Frequency control algorithm are displayed in Figures 4.29, 4.30 and 4.31. In Figure 4.29, the maximum frequency deviation that resulted in this simulation test was of 0.8 %, respectively 0.4 Hz deviation from the nominal 50 Hz, which is as expected in the control band. Also, it is important to observe that the power grid will remain in an accelerated state even though the synchronous generator is stopped, namely at the limit of normal operation, with an operating frequency of 50.15 Hz (1.003 pu). Further control action from the WF is not required by the grid code. In Figure 4.30, the power output of the WF is being reduced, thus keeping the voltage frequency in the control band. The Frequency control can be interpreted graphically as an active power regulation function by observing the fact that the area (energy) by which the WF power reduces is equal with the area (energy) of the power increase of the synchronous machine. Figure 4.31 displays the reactive power balance in the PCC and shows that the reactive power is also being kept within the control band of $+/-0.1$.

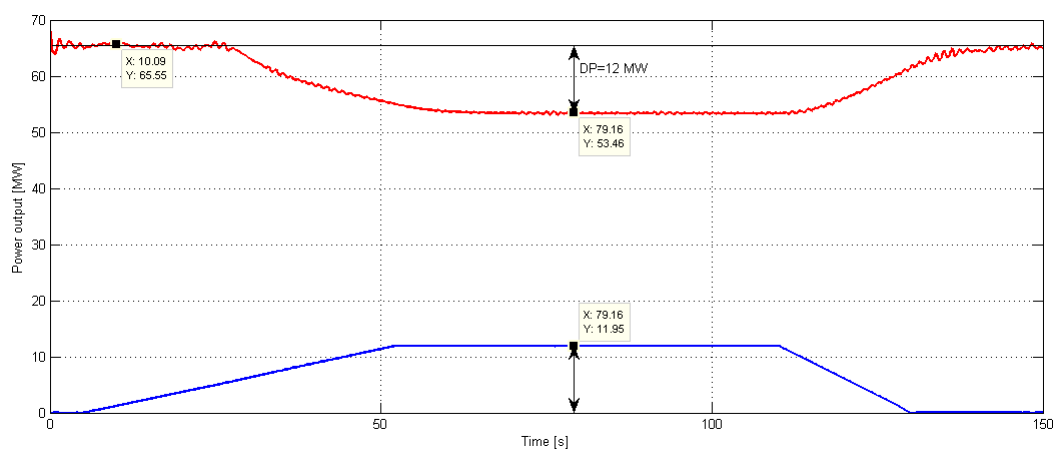

Figure 4.30.: Active power of the WF and synchronous generator

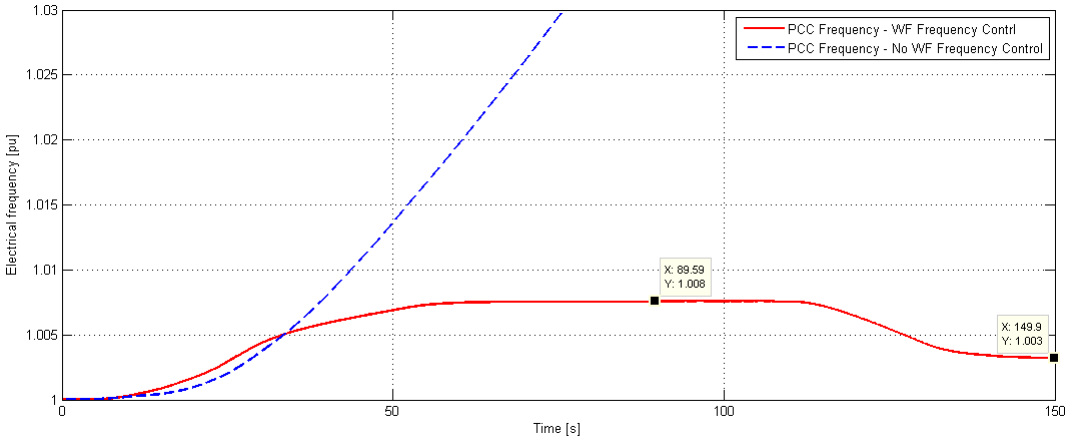

Figure 4.29.: Frequency stability in the PCC

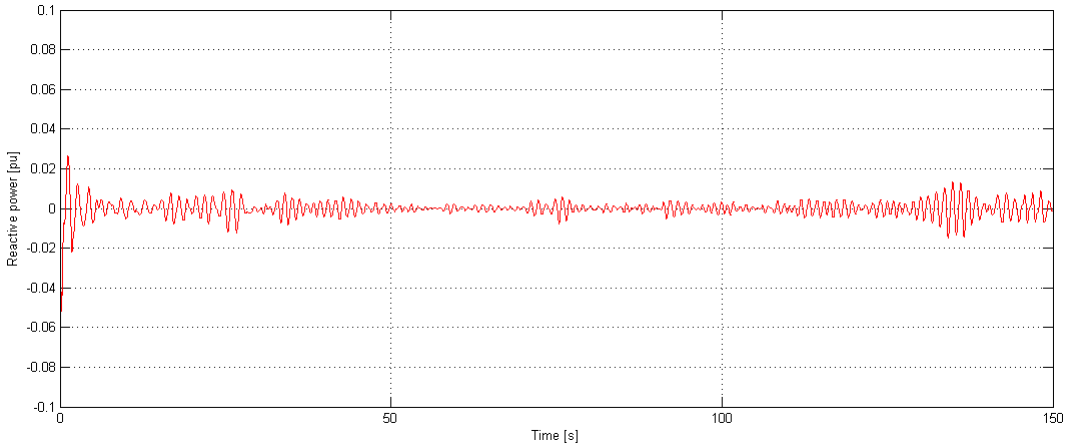

Figure 4.31.: Reactive power in the PCC

4.4. Reactive Power Support in the PCC

One of the main issues when connecting large WF plants in the power grid is the reactive power compliance presented in Section 1.3.2. This simulation platform is able to control the reactive power output of the WF due to the use of the HVDC transmission stations. The TSO sends reactive power demand reference to the WF controller, which will transmit the reference to the reactive power controller in the grid side converter. The grid side station converter is setting references to the current controller and changes therefore the reactive power in the PCC.

The analysis of the reactive power output of the grid connected converter for the wind speed characteristic in Section 4.3, Figure 4.18 is detailed below. A reactive power reference as in Figure 4.32 is set.

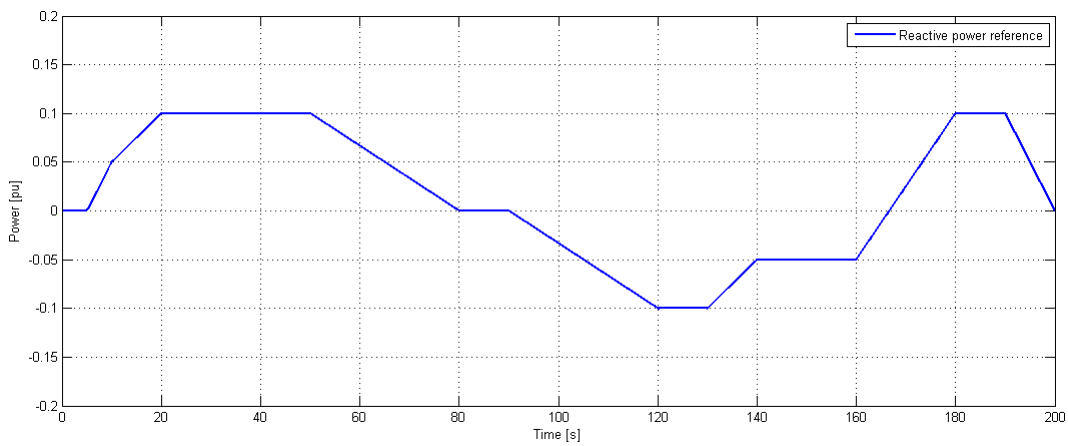

Figure 4.32.: Reactive power reference from the TSO

The active and reactive power generated in the PCC are displayed in Figure 4.33. The actual reactive power output is following steadily the reactive power reference from the TSO while the power output of the WT is unaffected by the reactive power demand. A different situation appears when the reactive power demand increases above the possible total instantaneous power output of the PWM converter. Priority in this case has the active power output over the reactive power demand in order to maintain the DC link voltage stable and thus WF system stability. One exception may apply to the active power priority rule: the case in which a fault appears on the network determining voltage dips below the allowed limits. For low voltage sags the power capability of the network is greatly decreased therefore no full rated active power transmission is possible anyway. In this case the WF may be required to provide full reactive power support in the PCC (generating maximum reactive current and no active current) in order to try to maintain the AC voltage level as high as possible. A direct relation between the active and reactive power is seen with the real and imaginary PWM converter currents (and references) as it is shown in Figure 4.34. The DC voltage on the DC bus is displayed in Figure 4.35. The DC voltage is maintained well within the stability limits and the required 5% variation from the rated value, with a maximum DC voltage of 0.5 %. The power losses on the DC link bus, the PWM converters, line reactors and transformers are displayed in Figure 4.37. The maximum simulated value is 0.017 pu (1.7%) and is reached when the WF is transmitting full power to the grid. The AC voltage in the PCC and in the PWM converter's connection point are detailed in Figure 4.36. The proportional relationship between the reactive power output and the difference in these two

voltages can be observed.

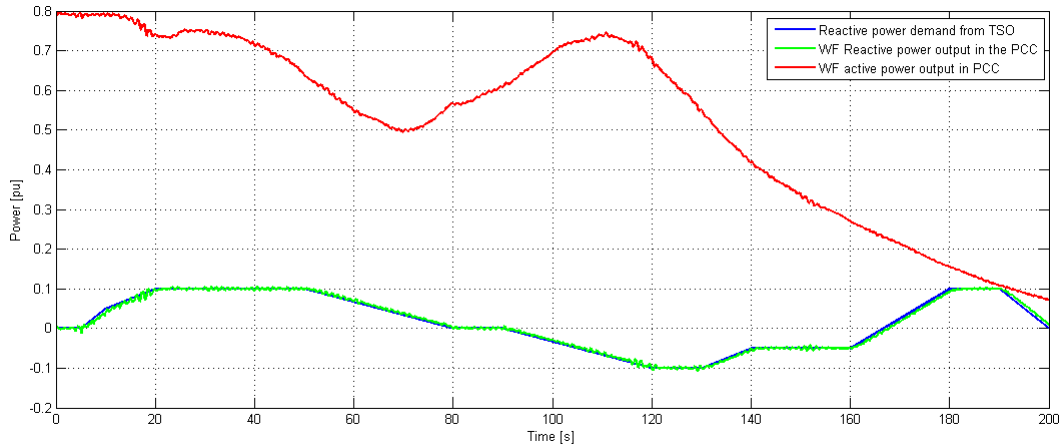

Figure 4.33.: Active and reactive power generated in the PCC by the WF

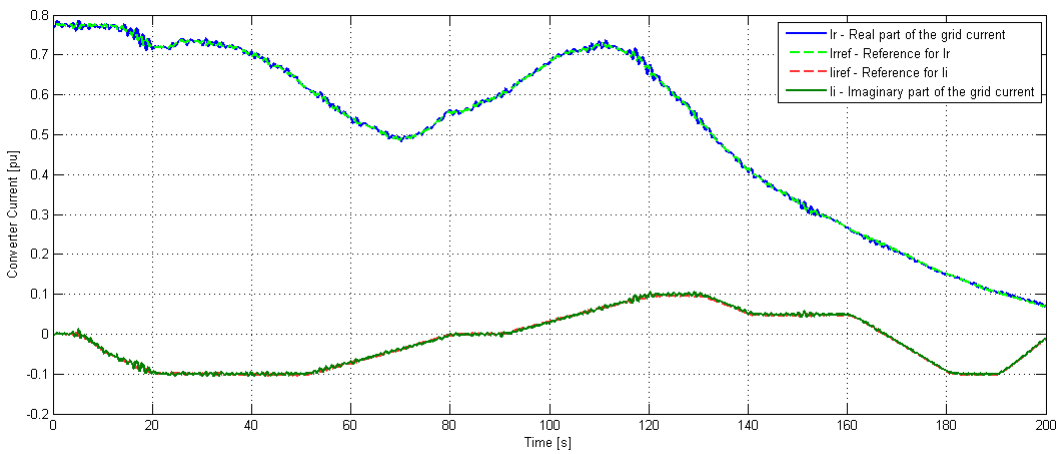

Figure 4.34.: Real and imaginary converter currents

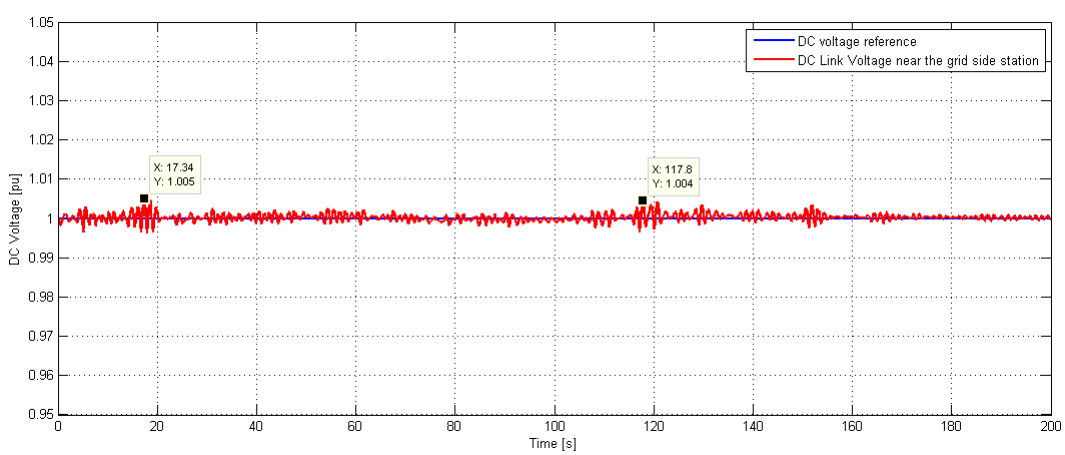

Figure 4.35.: DC bus voltage measured in the grid side station

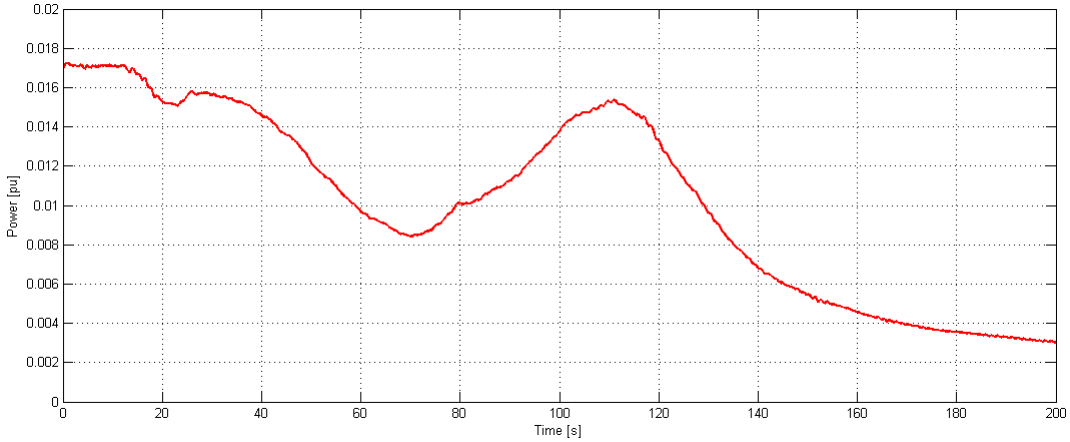

Figure 4.37.: Power losses on the DC link bus

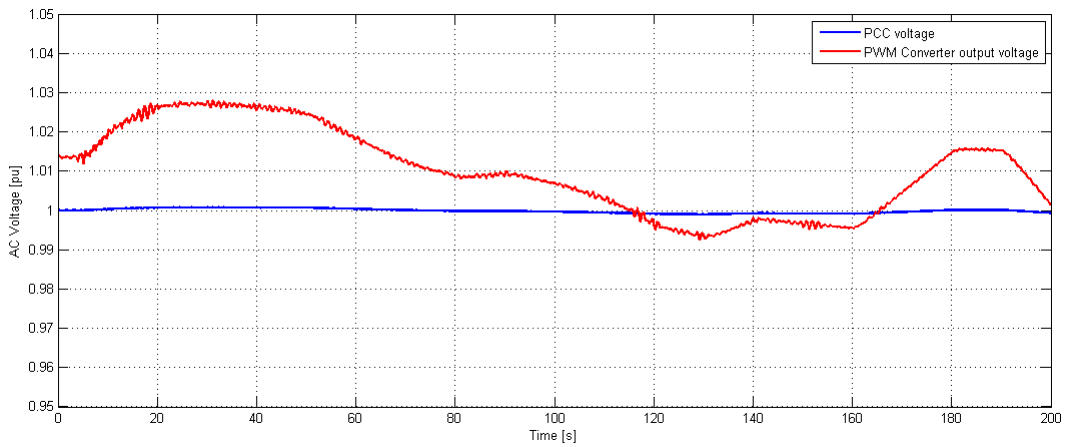

Figure 4.36.: AC voltage level in the PCC and the converter's connection point

4.5. Summary

In this Chapter, the assessment of the WF model for stability analysis has been performed. The most important simulation results have been outlined. A stable operation system is reported through the verification of all the designed WF functions.

The WF model is verified with a typical wind speed characteristic and in normal operating conditions in Section 4.1. All the important parameters of the WF system are analyzed: wind speed, pitch angle variation, AC voltage and current, active and reactive power, WT group output power, AC WF grid frequency, DC bus voltage, power losses in the WF system, AC grid frequency.

The WF controller's active power functions are verified and the advantages of using the proposed system are marked in Section 4.3. Frequency control can participate actively to ensure active power balance in the PCC. Delta production control is setting aside specific amounts of reserve active power for potential use due to imbalances in the power network. Power gradient control is avoiding the occurrence of large active power transients due to fast switching of the power references. Absolute production control can limit the output power

to a user defined value.

Reactive power regulation in the PCC is verified in Section 4.4. A study case verifying the WF grid code compliance of the reactive power exchange in the PCC has been formulated and analyzed. Whether the wind farm is operating at low or full power, the reactive power demand can or cannot be totally fulfilled, depending on the current active power output and implicitly the current wind speed.

One important conclusion is that the WF can greatly improve the power system stability by regulating the active and reactive power, thus resulting in frequency and voltage stability in the PCC.

5. Conclusions

This project deals with RMS dynamic simulation techniques of Wind Power Systems for grid integration studies. The power systems stability topic is addressed throughout the project and all the components are modelled accordingly. Chapter 1 provides an overview of Wind Power Systems from an electrical engineering perspective. Based on the state of the art and the grid code requirements, a generic WF containing 30 WTs forms the basis of the simulation platform developed throughout the project. It offers a practical point of view to the wind power system analysis. It is important to stress that the simulation model is not bound to the particular configuration of the chosen WF but can be further re-dimensioned to specific application cases. A description of the active and reactive power system stability issues being dealt within this project is described in Section 1.4. Basically, there is an increasingly number of grid support requirements for Wind Power Systems that need to be fulfilled in order to connect larger Wind Farms into the main power grid. Also, the WFs must play an active role in the regulation of voltage and frequency, being able to provide full grid support. In Section 1.5 the project objectives and research approach are detailed. The proposed simulation platform for power system stability studies is presented, containing a relatively large WF and an VSC HVDC transmission system.

Chapter 2 describes in detail the components used in the WF and VSC-HVDC model. An overview of the main blocks used in the modelling process, a brief description of the chosen wind farm layout and of the HVDC transmission system have been presented. Two main types of components have been used: build-in and user defined models. The build-in components are models already developed in Power Factory DIgSILENT and require only dimensioning efforts in order to use them. The user defined models, which required the main design efforts are the models that had to be created in order to represent the respective component. The main project contributions are within the latter category. The wind model previously developed in [11] and based on the Risoe Matlab/Simulink wind model [17] has been further adapted for WF models. The smoothing effect of a large number of WTs has been studied on one row of the proposed WF containing 10 WTs. Simulation results are shown in order to provide better understanding on the behaviour of the wind model. A reduced model of the WF based on [18] has been designed, therefore creating a one machine equivalent of each row in the WF. This WF representation highly reduces the computation efforts and still provides valid results for cumulative behaviour of the WF. The WF grid interaction studies can be performed without significant errors due to the previous model simplification. The models defined in Chapter 2 are used throughout the report, the information presented being the knowledge base of the modelling and dimensioning of the proposed WF system. The developed models correspond to a dynamic simulation platform that can be used for stability (RMS) power systems analysis.

Chapter 3 contains the control design of the main components of the WF simulation plat-

form. The Wind Farm controller contains the active power regulation functions: frequency control, delta production, absolute production, power gradient constraints and stop regulation function. The Pitch Controller developed based on [11] is also detailed and a control algorithm is chosen. Control design of the WF Side converter control system comprising voltage and current control loops, frequency and voltage droop characteristic for the converter's reference setpoints. The grid side converter control system is developed with two inner current control loops for the real and imaginary currents (represented as phasors), one DC voltage control loop, and one reactive power control loop. Design considerations for the PIs of the fore mentioned controllers have been performed.

Chapter 4 verifies the developed model of the WF. Specifically, the assessment of the active and reactive power grid support functions of the WF model have been analyzed. A stable WF system is reported through the verification of all the designed WF functions. The WF model is verified with a typical wind speed characteristic and in normal operating conditions in Section 4.1. The WF controller active power functions are verified and the advantages of using the proposed system are marked in Section 4.3. One important conclusion is that the WF can greatly improve the power system stability by regulating the active and reactive power, thus resulting in frequency and voltage stability in the PCC.

As a synthesis of the main contributions in this project, the following aspects are worth mentioning:

- A wind model describing the smoothing effect of WF on power production has been developed in Section 2.2.1. Smaller power variations (caused by wind turbulence) are "seen" at the WF output as the number of WTs increase;
- A reduced model of a WF that is valid for grid integration analyses of WFs (cumulative response of the WF in the power grid) is developed in Section 2.3.1;
- Active power regulation functions implemented in the WF controller model prove stable operation of the WF even if the PCC has a weak main power grid attached as it can be seen in the frequency control section 4.3.3. Furthermore, delta production control characteristic accounts for the reserve power of large power plants, thus creating an energy buffer in the system;
- Reactive power regulation helps maintaining the PCC voltage level in the designed control band. This functionality is verified in Section 4.4, and implemented by the grid side converter control unit of the VSC-HVDC system.
- An RMS dynamic simulation platform of an WF for power system stability studies implemented in Power Factory DIgSILENT is available for practical testing.

6. Future work

This model can be further expanded to allow the analysis of electromechanical RMS transients that may appear due to faults in the electrical network. Therefore, one possible direction of future work is the analysis of the wind farm operation during disturbances e.g. three phase symmetrical faults in the PCC. Different voltage dip characteristics can be defined and the performance of the WF system along with the control system can be studied. Low voltage ride through is thus, one possible topic for analysis.

Island operation of WF in case of power grid outage can be studied with this model. In this scenario, the WF must be kept "on line" even in the case of a power system shutdown and still provide power to the local grid loads. A more detailed grid model is required, with generator and load nodes. Energy storage devices can be also taken into account.

The concept of Virtual Power Plants can be integrated in this simulation model to create a network of distributed renewable energy sources.

Bibliography

[1] Global Wind Energy Council. *"Global Wind 2008 Report"*. Available from http://www.gwec.net/;

[2] The Institute of Electrical and Electronics Engineers, Inc. *"IEEE Standard 1001 - IEEE Guide for Interfacing Dispersed Storage and Generation Facilities with Electric Utility Systems"*. April 3, 1989;

[3] Bharat Singh, S. N. Singh, Demetrios P. Papadopoulos and Panagiotis A. Katsigiannis. *"Grid Code Requirements for Wind Power Interconnection into Power Systems"*. Paper presented at MedPower 2008, 6th Mediterranean Conference and Exhibition on Power Generation, Transmission, Distribution and Energy Conversion;

[4] Elkraft System & Eltra. *"English version of Technical Regulations TF 3.2.6 - Wind Turbines Connected to Grids with Voltages below 100 kV - Technical regulations for the properties and the control of wind turbines"*, May 19, 2004;

[5] Elkraft System & Eltra. *"Regulation TF 3.2.5 - Wind Turbines Connected to Grids with Voltages above 100 kV - Technical regulation for the properties and the regulation of wind turbines"*, Dec. 3, 2004;

[6] E-ON Netz Gmbh, Bayreuth. *"Grid Code - High and Extra High Voltage"*. 1 April 2006;

[7] E-ON Netz Gmbh, Bayreuth. *"Requirements for Offshore Grid Connections in the E.ON Netz Network"*. 1 April 2008;

[8] The Institute of Electrical and Electronics Engineers, Inc. *"1547™ - IEEE Standard for Interconnecting Distributed Resources with Electric Power Systems"*. 28 July 2003. ISBN 0-7381-3720-0;

[9] Jennie Weatherill, Department of Electrical Engineering and Electronics, UMIST. *"Review of First International Workshop on Feasibility of HVDC Transmission Networks for Offshore Wind Farms"*. 30-31 March 2000 KTH, Stockholm, Sweden;

[10] Florin Iov, Department of Energy Technology, Aalborg University. *"Wind Turbine Technologies"*. Wind Power Systems Course Presentation 2007;

[11] Adrian Constantin, Adelina Agap, Madalina Dragan, Borja Markinez Imanol Iurre. *"Modelling, Operation and Control of HVDC Connected Offshore WFs"*. Aalborg University, Department of Energy Technology, Semester Report - Autumn 2008;

[12] Stefan Lundberg. *"Evaluation of wind farm layouts"*. Paper presented at NORPIE 2004, Nordic Workshop on Power and Industrial Electronics 2004 - 009;

[13] Martin Braun. *"Technological Control Capabilities of DER to Provide Future Ancillary Services. International Journal of DER"*, ISSN 1614-7138;

[14] Florin Iov, Frede Blaabjerg. *"Advanced Power Converters for Universal and Flexible Power Management in Future Electricity Network"*. UNIFLEX-PM - 019794, February 2007;

[15] Florin Iov. *"Wind Farm Control"* - Master project proposal, 4th Semester, Department of Energy Technology, AAU Denmark;

[16] Poul Sørensen, Mikael Togeby and Thomas Ackermann. *"Ecogrid.dk Phase 1 WP4 report: New measures for integration of large scale renewable energy"*. Risø National Laboratory and Technical University of Denmark, June 2008. Risø-R-1650(EN);

[17] Florin Iov, Anca Daniela Hansen, Poul Sørensen, Frede Blaabjerg. *"Wind Turbine Blockset in Matlab/Simulink - General Overview and Description of the Models"*. Aalborg University, March 2004. ISBN 87-89179-46-3;

[18] Vladislav Akhmatov. *"Analysis of dynamic behaviour of Electric Power Systems with Large Amount of Wind Power - Phd Thesis"*. Electrical Power Engineering, Ørsted-DTU, April 2003. ISBN 87-91184-18-5/3;

[19] Poul Sørensen, Anca D. Hansen, Pedro Andre Carvalho Rosas. *"Wind models for simulation of power fluctuations from wind farms"*. Journal of Wind Engineering and Industrial Aerodynamics 90, pp. 1381–1402, 2002;

[20] Jørgen Højstrup. *"Spectral coherence in wind turbine wakes"*. Wind Energy and Atmospheric Physics Department, Risø National Library. DK-4000 Roskilde, Denmark;

[21] Poul Sørensen, Anca Hansen, Lorand Janosi, John Bech and Birgitte Bak-Jensen. *"Simulation of Interaction between Wind Farm and Power System"*. Risø National Laboratory, Roskilde, December 2001. Risø-R-1281(EN);

[22] Stefan Marko, Ivan Darul'a, Stanislav Vlcek. *"Development for Wind Farm Models for Power System Studies"*. Journal of Electrical Engineering, Vol. 56, No. 5-6, 2005, 165–168. ISSN 1335-3632;

[23] Poul Sørensen. *"System Integration of Wind Turbines in Denmark - Presentation"*. Wind Energy Department, Risø National Laboratory;

[24] J.G. Slootweg, W.L. Kling. *"Modeling of Large Wind Farms in Power System Simulations"*. Electrical Power Systems Laboratory, Faculty of Information Technology and Systems, Delft University of Technology. IEEE Transactions, 2002;

[25] Poul Sørensen, Anca D. Hansen, Pedro Andre, Carvalho Rosas. *"Wind Models for Simulation of Power Fluctuations from Wind Farms"*. Journal of Wind Engineering and Industrial Aerodynamics 90 (2002) 1381-1402;

[26] J.G. Slootweg, H. Polinder, W.L. Kling. *"Dynamic Modelling of a Wind Turbine with Doubly Fed Induction Generator"*. Electric Power Systems. IEEE Transactions, May 2003;

[27] S. M. Muyeen, Mohammad Abdul Mannan, Mohd. Hasan Ali, Rion Takahashi, Toshiaki Murata, Junji Tamura, Yuichi Tomaki, Atsushi Sakahara, Eiichi Sasano. *"Fault Analysis of WT Generator System Considering Six-Mass Drive Train Model"*. IEEE Transactions. 4th International Conference on Electrical and Computer Engineering. ICECE 2006, 19-21 December 2006, Dhaka, Bangladesh;

[28] S. M. Muyeen, Mohd. Hasan Ali, Rion Takahashi, Toshiaki Murata, Junji Tamura, Yuichi Tomaki, Atsushi Sakahara, Eiichi Sasano. *"Transient Stability Analysis of Wind Generator System with the Consideration of Multi Mass Shaft Model"*. IEEE PEDS 2005;

[29] Stavros A. Papathanassiou and Michael P. Papadopoulos. *"Mechanical Stresses in Fixed-Speed Wind Turbines Due to Network Disturbances"*. IEEE Transactions on Energy Conversion, VOL. 16, NO. 4, December 2001;

[30] M. Martins, A. Perdana, P. Ledesma, E. Agneholm, O. Carlson. *"Validation of fixed speed wind turbine dynamic models with measured data"*. Elsevier, Renewable Energy 32 (2007) 1301–1316;

[31] Anca D. Hansen, Poul Sørensen, Frede Blaabjerg and John Becho. *"Dynamic modelling of wind farm grid interaction"*. Wind Engineering Volume 26, NO. 4 , 2002. PP 191–208;

[32] Markus A. Poeller. *"Doubly-Fed Induction Machine Models for Stability Assessment of Wind Farms"*. DIgSILENT Gmbh, Gomaringen / Germany. Available from: http://www.digsilent.de/?p=Consulting/Publications;

[33] Massimo Valentini, Thordur Ofeigsson, Alin Raducu. *"Control of a Variable Speed Variable Pitch Wind Turbine with Full Scale Power Converter"*. Semester report. Aalborg University, Institute of Energy Technology, Autumn 2007;

[34] Florin Iov. *"VSC based DC Transmission System for Connecting Active Stall Wind Farms to Grid"*. Aalborg University, October 2004;

[35] ABB AB, Grid Systems HVDC. *"It's time to connect - Technical description of HVDC Light® technology"*. Available from www.abb.com/hvdc;

[36] DIgSILENT Gmbh. *"DIgSILENT Technical Documentation - Induction Machine"*. TechRef ElmAsm V1. Build 220 30.03.2007;

[37] DIgSILENT Gmbh. *"DIgSILENT Technical Documentation - PWM Converter"*. TechRef ElmVsc V1. Build 233 30.03.2007;

[38] DIgSILENT Gmbh. *"DIgSILENT Technical Documentation -Two winding transformer (3 Phase)"*. TechRef ElmTr2 V2. Build 331 26.07.2007;

[39] DIgSILENT Gmbh. *"DIgSILENT Technical Documentation - General Load Model"*. TechRef ElmLod V3. Build 337 26.11.2007;

[40] DIgSILENT Gmbh. *"DIgSILENT Technical Documentation - Filter/Shunt"*. TechRef ElmShnt V1. Build 331 30.03.2007;

[41] Myo Thu Aung and Jovica V. Milanovic. *"The Influence of Transformer Winding Connections on the Propagation Voltage Sags"*. IEEE Transactions on Power Delivery, Vol. 21, No. 1, January 2006;

[42] Cuiqing Du. *"VSC-HVDC for Industrial Power Systems"*. Department of Energy and Environment. Phd. Thesis. Chalmers University of Technology. Goteborg, Sweden 2007. ISBN 978-91-7291-913-6;

[43] Per Karlsson. *"DC Distributed Power Systems - Analysis, Design and Control for a Renewable Energy System*", PhD Dissertation, Lund University, Sweden, 2002, ISBN 91-88934-25-X;

[44] Prabha Kundur. *"Power System Stability and Control"*. ISBN 0-070035958-X;

[45] Fernando D. Bianchi, Hernan De Battista, Ricardo J. Mantz. *"Wind Turbine Control Systems. Principles, Modelling and Gain Scheduling Design"*. ISBN-13: 978-1-84628-492-2;

[46] Robert H. Lasseter. *"Microgrids and Distributed Generation"* . Journal of Energy Engineering, American Society of Civil Engineers, Sept. 200

[47] Guibin Zhang, Zheng Xu. *"Steady-State Model for VSC Based HVDC and Its Controller Design"*. Deparment of Electrical Engineering, Zheijiang University. IEEE Transactions 2001.

[48] Guibin Zhang, Zheng Xu, Ye Cai. *"An Equivalent Model for Simulating VSC Based HVDC"*. Deparment of Electrical Engineering, Zheijiang University. IEEE Transactions 2001.

[49] Martyn Durrant, Herbert Werner, Keith Abbot. *"Model of a VSC HVDC Terminal Attached to a Weak AC System"*. IEEE Transactions 2003.

[50] Adel Farag, Martyn Durrant, Herbert Werner, Keith Abbot. *"Robust Control of a VSC HVDC Terminal Attached to a Weak AC System"*. IEEE Transactions 2003.

[51] Guibin Zhang, Zheng Xu, Guan Wang. *"A linear and Decoupled Control Strategy for VSC Based HVDC System"*. IEEE Transactions 2001.

[52] Guibin Zhang, Zheng Xu, Hongtao Liu. *"Supply Passive Networks with VSC-HVDC"*. IEEE Transactions 2001.

[53] Peter Sandeberg, Lars Stendius. *"Large scale Offshore Wind Power Energy evacuation by HVDC Light"*. ABB AB.

[54] Analog Devices. Application note: AN401-24. *"Constant Volts/Hertz Operation for Variable Speed Control of Induction Motors - V/f controller on ADMC401"*. 1999

[55] DIgSILENT Gmbh. *"Power Factory User Manual v. 14"*. PF_Manual_14v0E

[56] Marco Liserre, Antonio Dell'Aquila, Frede Blaabjerg. *"Design and Control of a Three-phase Active Rectifier Under Non-ideal Operating Conditions"*. IEEE Transactions 2002.

[57] George Alin Raducu. *"Control of Grid Side Inverter in a B2B Configuration for WT Applications"* - Master Thesis. Aalborg University, 20

[58] Siemens Wind Turbines - product listing - May 2009. Available from http://www.powergeneration.siemens.com/home

[59] Vestas Wind Turbines - product listing - May 2009. Available from http://www.vestas.com

[60] Emil Ceanga, Cristian Nichita, Ludovic Protin, N. Antonio Cutululis. *"Theorie de la Comande des Systemes"*. Editura Tehnica S.A. 2001. ISBN 973-31-2103-7

Summary

- Chapter 1 represents an introductory chapter describing the state of the art in wind power systems, the current WT technologies and grid code specifications for WFs in Denmark (Energinet.dk) and Germany(EON.Net). A description of the active and reactive power system stability issues being dealt within this project is described in Section 1.4. Basically, there is an increasingly number of grid support requirements for Wind Power Systems that need to be fulfilled in order to connect larger Wind Farms into the main power grid. Also, the WFs must play an active role in the regulation of voltage and frequency, being able to provide full grid support. In Section 1.5 the project objectives and research approach are detailed. The proposed simulation platform for power system stability studies is presented, containing a relatively large WF and an VSC HVDC transmission system.

- Chapter 2 contains most of the project's modelling work. The WT model with its components is presented in Section 2.2. The method for modelling a relatively large WF for grid interaction and cumulative response studies is detailed in Section 2.3.1. The main electrical components (AC and DC) used in the WF, transmission and power grid systems are properly sized for correct operation of the system under study in Section 2.4. The models defined in Chapter 2 are used throughout the report, the information presented being the knowledge base of the modelling and dimensioning of the proposed WF system.

- Chapter 3 is dedicated to the design of the control systems used in the WF and transmission system models. Basically, the control system is split in two hierarchical levels: the user and the equipment control levels. The user control level, described in Section 3.1, is represented by the WF controller. It is responsible with the management the interface between the TSO and the WPS. Also, active and reactive power setpoints are calculated in this block and sent to the specific controllers. The equipment control level presented in Section 3.2, contains all the controllers for their associated equipment e.g. pitch, pwm converters. Control design of the WF and Grid side converters is detailed further on. Control design of the WF Side converter control system comprising voltage and current control loops, frequency and voltage droop characteristic for the converter's reference setpoints. The grid side converter control system is developed with two inner current control loops for the real and imaginary currents (represented as phasors), one DC voltage control loop, and one reactive power control loop. Design considerations for the PIs of the fore mentioned controllers have been performed.

- Chapter 4 describes all the study cases performed on the simulation platform previously developed. It deals with the stability analysis of the proposed WPS. Active and reactive power control capability of the WF is performed in order to analyze the grid support in terms of voltage and frequency. The WF model is verified with a typical wind speed characteristic and in normal operating conditions in Section 4.1. The WF controller active power functions are verified and the advantages of using the proposed system are marked in Section 4.3.

- Chapter 5 draws the conclusions for the entire work performed in this thesis and proposes future developments that may be of interest.

A. Appendix - Grid Code Requirements

A.1. "n-1" Contingency Criterion

The "n-1" Contingency Criterion describes the ability of the power system to maintain its stability and operation in the event of one linkage failure. In other words, in the case of a single contingency event, the power system settles to a new satisfactory operating state without the need to shed non-interruptible loads.

For example, the National Electricity Rules (NER) documentation valid in the state of Queensland have the following definition for the term "satisfactory operation":

"The power system is defined as being in a satisfactory operating state when:

(a) the frequency at all energised busbars of the power system is within the normal operating frequency band, except for brief excursions outside the normal operating frequency band but within the normal operating frequency excursion band;

(b) the voltage magnitudes at all energised busbars at any switchyard or substation of the power system are within the relevant limits set by the relevant Network Service Providers in accordance with Clause S 5.1.4 of schedule 5.1;

(c) the current flows on all transmission lines of the power system are within the ratings (accounting for time dependency in the case of emergency ratings) as defined by the relevant Network Service Providers in accordance with schedule 5.1;

(d) all other plant forming part of or impacting on the power system is being operated within the relevant operating ratings (accounting for time dependency in the case of emergency ratings) as defined by the relevant Network Service Providers in accordance with schedule 5.1;

(e) the configuration of the powe system is such that the severity of any potential fault is within the capability of circuit breakers to disconnect the faulted circuit or equipment; and

(f) the conditions of the power system are stable in accordance with requirements designated in or under clause S5.1.8 of schedule 5.1."

The clause S5.1.8 in schedule 5.1 states the following requirements:

- the power system must remain in synchronism;
- the power system oscillations must be damped adequately;
- voltage stability criteria must be satisfied.

B. Appendix - Wind Farm Modelling

B.1. Wind Turbine Parameters and Ratings

The reference parameters for a generic 2.3 MW WT with squirrel cage induction generator.

Parameter	Value
P_{rated}	2300 kW
Q_{rated}	1200 kVAR
U_{rated}	690 V
$cos(\varphi_n)$	0.89
η_n	96.5 %
$n_{pole-pairs}$	2
R_s	0.00115 Ω
X_s	0.0305 Ω
R_r	0.0015 Ω
X_r	0.01075 Ω
X_m	0.65 Ω
J_{gen}	59 kg·m^2

Table B.1.: Parameters of 2.3 MW SCIG

B.2. Wind model

Wind model histograms

Histograms for power and wind speed for the reduced order wind model in a 1000 seconds simulation time frame are presented in Figures B.1 and B.2.

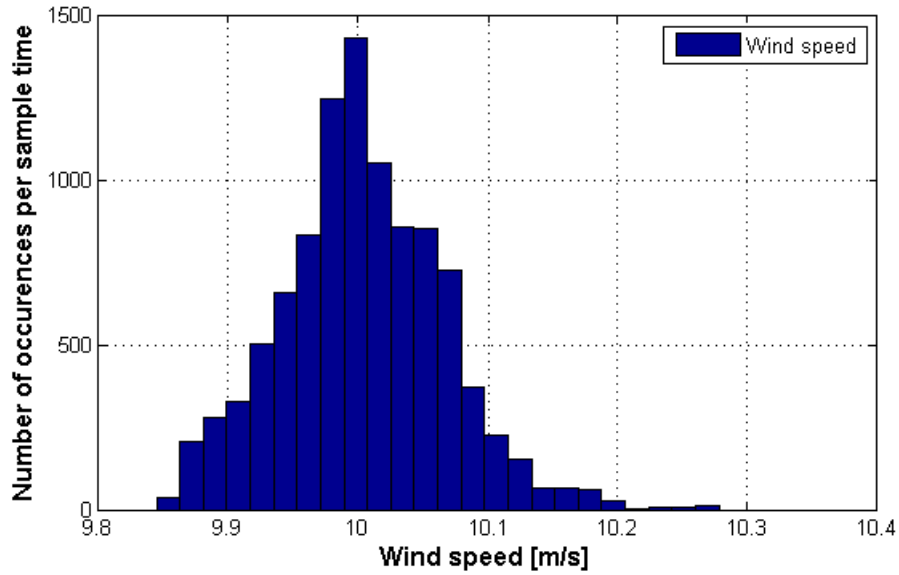

Figure B.1.: Wind speed histogram in 1000 seconds simulation

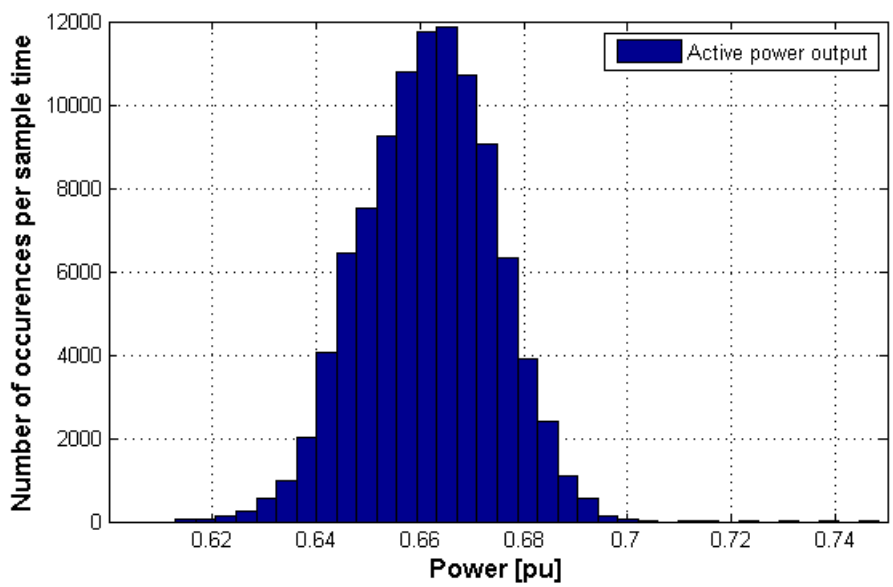

Figure B.2.: Power output histogram in 1000 seconds simulation

B.3. Aerodynamic Model

The Betz' limit is calculated based on [45],and representing the maximum achievable value of the power coefficient of an actuator disc in ideal conditions, is modelled by Equation B.1, and depicted in Figure B.3.

$$C_p = 4 \cdot a(1-a)^2 \tag{B.1}$$

while $a = 0 \div 1$.

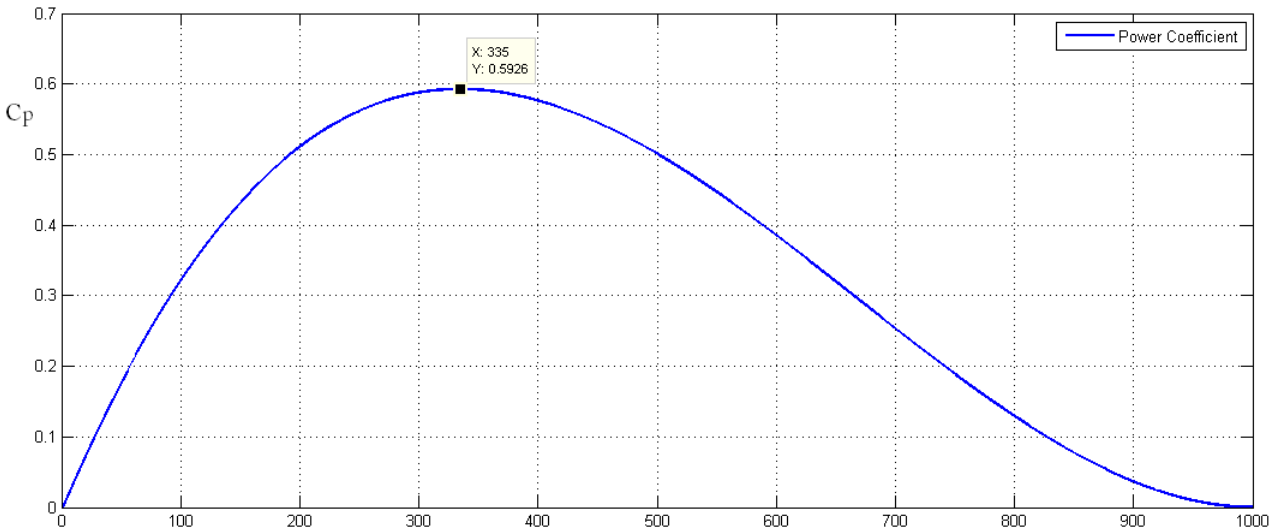

Figure B.3.: Ideal power coefficient for actuator disc, Betz limit

The turbine power expressed in per unit system is shown varying with air density ρ, several wind speeds v_∞, and the rotor speed Ω_r in Figure B.4.

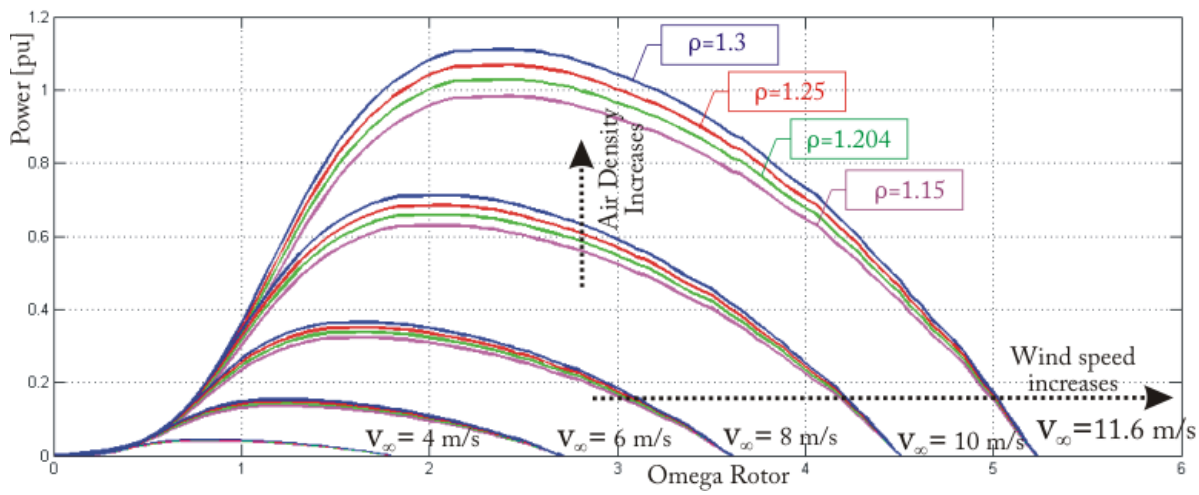

Figure B.4.: Turbine power $P(\Omega_r)$ variation with air density and wind speed

B.4. Asynchronous Machine Buildin Model

Per unit parameter transformation based on datasheet values

Parameter transformation to per unit values starting from datasheet information is detailed below. Typically the datasheet provides values for rated active P_{rated} and reactive power Q_{rated}, rated phase voltage U_{rated}, power factor at nominal operation $cos(\varphi_n)$, efficiency at nominal operation η_n, number of pole pairs $n_{pole-pairs}$, stator resistance R_s in Ω, stator reactance X_s Ω, rotor resistance R_r in Ω, rotor reactance X_r in Ω and mutual reactance X_m in Ω. The previously mentioned parameters measured in absolute values are used to calculate their per unit equivalents with actual value calculus based on the WT generator used in this project (see Table B.1 from Appendix B.1):

$$U_{base} = \frac{U_{rated}}{\sqrt{3}} = \frac{690}{\sqrt{3}} = 398.37V \tag{B.2}$$

$$I_{base} = \frac{S}{3U_{base}} = \frac{2600}{3 \cdot 400} = 2.2kA \tag{B.3}$$

$$Z_{base} = \frac{U_{base}}{I_{base}} = 0.185\Omega \tag{B.4}$$

Using the base impedance Z_{base}, the per unit values of the electrical parameters can be consequently calculated:

$$R_s = \frac{R_s}{Z_{base}} = \frac{0.00117}{0.183} = 0.00640p.u. \tag{B.5}$$

$$X_s = \frac{X_s}{Z_{base}} = \frac{0.03067}{0.183} = 0.165p.u. \tag{B.6}$$

$$R_r = \frac{R_r}{Z_{base}} = \frac{0.0015}{0.183} = 0.0082p.u. \tag{B.7}$$

$$X_r = \frac{X_r}{Z_{base}} = \frac{0.01075}{0.183} = 0.165p.u. \tag{B.8}$$

$$X_m = \frac{X_m}{Z_{base}} = \frac{0.67}{0.183} = 3.65p.u. \tag{B.9}$$

C. Transmission System Model

C.1. PWM converters for WF and grid side stations

The WF and Grid side converters are identical in terms of rated power, AC voltage ratings and the associated line reactors, DC capacitors and AC line filters used in each of the stations.

For choosing the power rating of the converters, a reserve margin of 10 per cent of the total rated power of the WF has been taken into consideration. Therefore,

$$S_{rated} = 110\% \cdot N_{WT} \cdot S_{WT} \tag{C.1}$$

The following results are obtained for the converters transmitting the rated power of the WF described in Section 1.4.

Parameter	Symbol	Value
Rated apparent power	S_{rated}	85 MVA
Rated active power	P_{rated}	69 MW
Rated DC voltage	V_{DC}	80 KV
Rated AC voltage	V_{AC}	44 KV
Phase reactor inductance	L	10.1 mH
Phase reactor resistance	R	0.2278 Ω
DC capacitor capacitance	C_{DC}	600 μF
switching frequency	f_{sw}	1950 Hz
AC rated frequency	f_{rated}	50 Hz
Rated WT apparent power	S_{wt}	2.5989 MW
Number of WTs	N_{wt}	30

Table C.1.: Sending end station parameters

Phase Reactor

The phase reactor is determined by the reactance X_l and resistance R_l, which are calculated as follows.

$$Z_b = 3 \cdot \frac{V_{AC}^2}{S_{rated}} = \frac{44000^2}{85 \cdot 10^6} = 22.77\Omega \tag{C.2}$$

$$\begin{cases} X_l = x_l \cdot Z_b = 0.14 \cdot 22.77 = 3.1887\Omega \\ L_l = \frac{X_l}{2\pi f} = \frac{3.1887}{2\pi 50} = 10.1mH \end{cases} \tag{C.3}$$

$$R_l = r_l \cdot Z_b = 0.01 \cdot 22.77 = 0.2278\Omega \tag{C.4}$$

AC Filters

As described in the report, the AC filters are used to eliminate the harmonic content generated by the VSC switching. In this project three sets of L-C AC filters have been used to eliminate the harmonic currents at the fundamental switching frequency, the second and third order harmonic currents.

$$Z_o = z_o \cdot Z_b = 0.15 \cdot 22.77 = 3.416\Omega \tag{C.5}$$

The fundamental frequency harmonic filter is determined by L_{f1} and C_{f1}:

$$\begin{cases} L_{f1} = \frac{Z_o}{2\pi f_1} = \frac{3.416}{2\pi \cdot 1950Hz} = 278.8\mu H \\ C_{f1} = \frac{L_{f1}}{Z_o^2} = \frac{278.8 \cdot 10^{-6}}{3.416^2} = 23.889\mu F \end{cases} \tag{C.6}$$

The second and third order harmonic filters are defined by:

$$\begin{cases} L_{f2} = \frac{Z_o}{2\pi f_2} = \frac{3.416}{2\pi \cdot 3900Hz} = 139.42\mu H \\ C_{fn} = \frac{L_{fn}}{Z_o^2} = \frac{139.42 \cdot 10^{-6}}{3.416^2} = 11.944\mu F \end{cases} \tag{C.7}$$

$$\begin{cases} L_{f3} = \frac{Z_o}{2\pi f_3} = \frac{3.416}{2\pi \cdot 3900Hz} = 92.94\mu H \\ C_{f3} = \frac{L_{f3}}{Z_o^2} = \frac{92.94 \cdot 10^{-6}}{3.416^2} = 7.963\mu F \end{cases} \tag{C.8}$$

DC Cable

The DC cable has been chosen as a simple Π model as in Figure C.1 with parameters C_s, R_s and L_s.

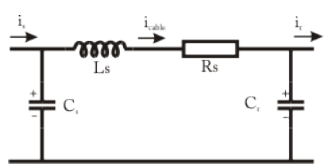

Figure C.1.: DC Cable Π model

The parameters have been selected from datasheet values for 80 KV PEX-AL cables:

$$C_s = \frac{0.39\mu F/m}{2} \tag{C.9}$$

$$R_s = 0.0186\Omega/km \tag{C.10}$$

$$X_s = 0.1\Omega/km \tag{C.11}$$

DC Capacitors

$$\omega_l = 2\pi 30 \tag{C.12}$$

$$\zeta_n = \frac{1}{\sqrt{2}} \tag{C.13}$$

$$\delta n = 0.05 \tag{C.14}$$

$$C_{dctotal} = \frac{P_{rated}}{V_{dc}^2} \cdot \frac{2 \cdot \zeta_n^2}{\omega_l} \cdot \frac{1}{(1 - \delta n) \cdot \delta n} = 1.2mF \tag{C.15}$$

The capacitance on each of the two capacitors, C_{DC}, is equally distributed and defined by:

$$C_{DC} = \frac{C_{dctotal}}{2} = 600\mu F \tag{C.16}$$

D. Control system design

D.1. WF Active power regulation

The frequency control default parameters from [4] are detailed in Table D.1:

	Setting range	Default value
Grid frequency reference point (f_{ref})	49.90 - 50.10 Hz	50.00 Hz
Lower frequency limit for the control range during under-frequency (f_n)	50.00...47.00 Hz	48.70 Hz
Upper frequency range for the control range during over-frequency (f_ϕ)	50.00...52.00 Hz	51.30 Hz
Lower frequency limit for the deadband during under-frequency (f_{d-})	50.00...47.00 Hz	49.85 Hz
Upper frequency limit for the deadband during over-frequency (f_{d+})	50.00...52.00 Hz	50.15 Hz
Control factor for the production applying to frequencies in the range $f_n \ldots f_{d-}$and $f_{d+} \ldots f_u$. (Control factor 1 means that the productionis the maximum possible – or power setpoint if specified)	Over - frequency : $(1 - \frac{f-f_{d+}}{f_\phi - f_{d+}})$ Under - frequency : $(1 + \frac{f-f_{d-}}{f_n - f_{d-}})$	
Regulating speed calculated from exceeding a limit value to completed control action	10 % of the rated power per second	

Table D.1.: Default values applying to frequency control of production

D.2. PI parameters for the control system

The PI current controller has the parameters:

$$\begin{cases} K_i = 0.01 \\ T_i = 0.0446 \end{cases} \tag{D.1}$$

The PI DC voltage and reactive power controller have the parameters:

$$\begin{cases} K_{Vdc} = K_q = 0.00836 \\ T_{Vdc} = T_q = 0.446 \end{cases} \tag{D.2}$$

The PI AC voltage controller has the parameters:

$$\begin{cases} K_{Vac} = 0.01 \\ T_{Vac} = 0.446 \end{cases} \tag{D.3}$$

D.3. Reference frame transformations

Clark Transformation (a,b,c) to (α, β)

Consider the complex AC current vector $\bar{i}$ defined by the three phase components $\bar{i}_a$,$\bar{i}_b$,$\bar{i}_c$:

$$\bar{i} = \bar{i}_a + e^{j\frac{2}{3}\pi}\bar{i}_b + e^{j\frac{4}{3}\pi}\bar{i}_c \tag{D.4}$$

Figure D.1 displays the current complex space vector:

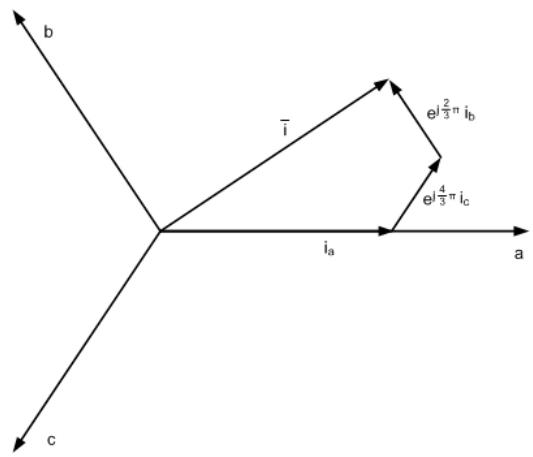

Figure D.1.: Current complex space vector representation

A transformation from the three phase system to a two orthogonal coordinate system can be applied:

$$\begin{cases} i_\alpha = \frac{2}{3}i_a - \frac{1}{3}(i_b - i_c) \\ i_\beta = \frac{2}{\sqrt{3}}(i_b - i_c) \\ i_0 = \frac{2}{3}(i_a + i_b + i_c) \end{cases} \tag{D.5}$$

where i_α and i_β are the orthogonal components and i_0 is the homopolar component. See Figure for a graphical description of the transformation.

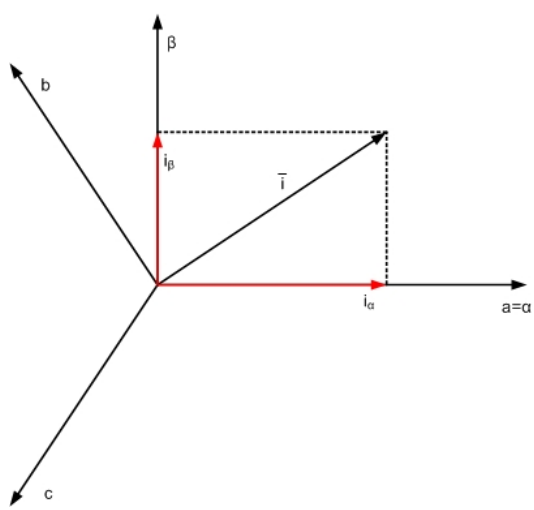

Figure D.2.: Current complex space vector and its α, β components in stationary reference frame

For balanced three phase components, the homopolar component is null. If this is the case, then the following applies:

$$i_a + i_b + i_c = 0 \tag{D.6}$$

Using equation D.6 and introducing it in equation D.5 results the Clark transformation equations for balanced space vectors:

$$\begin{cases} i_\alpha = i_a \\ i_\beta = \frac{1}{\sqrt{3}} i_a + \frac{2}{\sqrt{3}} i_b \end{cases} \tag{D.7}$$

Park Transformation

The process can be continued by transforming the stationary two coordinate system obtained into a rotating synchronous reference frame. For this purpose, an orthogonal coordinate system named dq frame is considered to be rotating synchronously with the complex vector frequency ω. In other words, the angle difference between the d-axis and the α-axis shown in Figure D.3 is equal to θ, where:

$$\theta = \omega t \tag{D.8}$$

Applying the transformation, the following equations results:

$$\begin{cases} i_d = i_\alpha cos(\theta) + i_\beta sin(\theta) \\ i_q = -i_\alpha sin(\theta) + i_\beta cos(\theta) \end{cases} \tag{D.9}$$

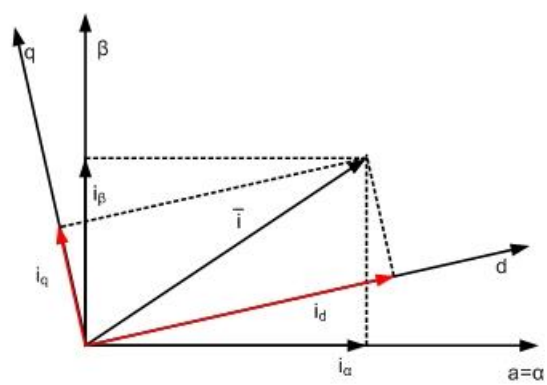

Figure D.3.: Current complex space vector and its d,q components in the rotating reference frame

Inverse Clark and Park transformations

The inverse Park transformation is described by equations D.10.

$$\begin{cases} i_\alpha = i_d cos(\theta) - i_q sin(\theta) \\ i_\beta = i_d sin(\theta) + i_q cos(\theta) \end{cases} \tag{D.10}$$

The inverse Clark transformation is described by equations D.11 .

$$\begin{cases} i_a = i_\alpha \\ i_b = -\frac{1}{2}i_\alpha + \frac{\sqrt{3}}{2}i_\beta \\ i_c = -\frac{1}{2}i_\alpha - \frac{\sqrt{3}}{2}i_\beta \end{cases} \tag{D.11}$$

D.4. Simulation studies

D.4.1. Synchronous generator parameters

- Nominal apparent power - 28.1 MVA;
- Nominal voltage - 11 KV;
- Power factor $cos\varphi = 0.85$;
- Connection YN;
- Acceleration time constant 18 s.